A decoupled, convergent and fully linear algorithm for the Landau–Lifshitz–Gilbert equation with magnetoelastic effects ®

Hywel Normington [a],[ID],[*], Michele Ruggeri [b],[ID]

[a] *Department of Mathematics and Statistics, University of Strathclyde, 26 Richmond Street, Glasgow G1 1XH, United Kingdom*
[b] *Department of Mathematics, University of Bologna, Piazza di Porta San Donato 5, 40126, Bologna Italy*

ARTICLE INFO

ABSTRACT

We consider the coupled system of the Landau–Lifshitz–Gilbert equation and the conservation of linear momentum law to describe magnetic processes in ferromagnetic materials including magnetoelastic effects in the small-strain regime. For this nonlinear system of time-dependent partial differential equations, we present a decoupled integrator based on first-order finite elements in space and an implicit one-step method in time. We prove unconditional convergence of the sequence of discrete approximations towards a weak solution of the system as the mesh size and the time-step size go to zero. Compared to previous numerical works on this problem, for our method, we prove a discrete energy law that mimics that of the continuous problem and, passing to the limit, yields an energy inequality satisfied by weak solutions. Moreover, our method does not employ a nodal projection to impose the unit length constraint on the discrete magnetisation, so that the stability of the method does not require weakly acute meshes. Furthermore, our integrator and its analysis hold for a more general setting, including body forces and traction, as well as a more general representation of the magnetostrain. Numerical experiments underpin the theory and showcase the applicability of the scheme for the simulation of the dynamical processes involving magnetoelastic materials at submicrometer length scales.

1. Introduction

Magnetoelastic (or magnetostrictive) materials are smart materials characterised by a strong interplay between their mechanical and magnetic properties [20]. On the one hand, they change shape when subject to applied magnetic fields (direct magnetostrictive effect), and on the other, they undergo a change in their magnetic state when subject to externally applied mechanical stresses (inverse magnetostrictive effect). Because of these properties, magnetoelastic materials currently find use in many technological applications requiring a magnetomechanical transducer, e.g. actuators or sensors [39].

In this work, we design and analyse a fully discrete numerical scheme for a coupled nonlinear system of partial differential equations (PDEs) modelling the dynamics of magnetisation and displacement in magnetoelastic materials in the small-strain regime. The small-strain assumption is well justified for many ferromagnetic materials, a variety of which experience strains on the order of 10^{-5}; see Table 1 for an example of such a material, and Fig. 1 for an illustration of a ferromagnetic cube with those material parameters.

Table 1

Estimated material parameters for FeCoSiB taken from [26,33,30].

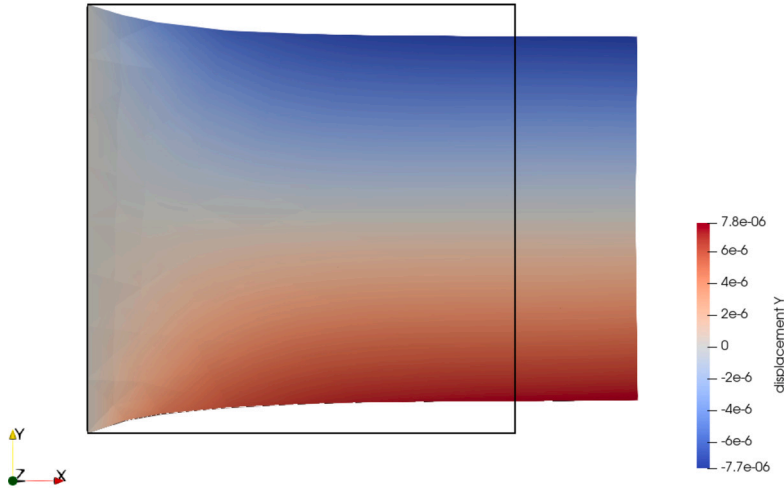| Symbol	Name	Value
A	Exchange constant	$1.5 \cdot 10^{-11}$ Jm^{-1}
α	Gilbert damping parameter	0.005
γ	Gyromagnetic ratio	$1.761 \cdot 10^{11}$ rads^{-1}T^{-1}
μ_0	Permeability of free space	$1.25663706 \cdot 10^{-6}$
M_s	Saturation magnetisation	$1.5 \cdot 10^6$ Am^{-1}
λ_{100}	Saturation magnetostrain	$30 \cdot 10^{-6}$
ρ	Density	7900 kgm^{-3}
g	Gravitational acceleration	9.81 ms^{-2}
μ	First Lamé constant	172 GPa
λ	Second Lamé constant	54 GPa

Fig. 1. Illustration of isotropic, isochoric magnetostriction of a cube shaped ferromagnetic material. The ferromagnetic unit cube is initially uniformly magnetised along the x-direction in the undeformed state the edges of which are shown by the black square. The final state shows the body elongated in the x-direction, and contracted in the y and z directions. The colour indicates the strength of the displacement in the y coordinate. The mesh displacement scaled by a factor of 10^4.

The validity of the small-strain regime for general magnetostrictive materials is the subject of the seminal work [20]. The proposed system consists of the Landau–Lifshitz–Gilbert (LLG) equation for the magnetisation and the conservation of linear momentum law for the displacement (see (4)–(5) below). The two equations are nonlinearly coupled to each other: One of the contributions to the effective field appearing in the LLG equation depends on the mechanical stress in the body (and thus on the displacement) and there is a magnetisation-dependent contribution to the strain (usually referred to as the magnetostrain) in the conservation of momentum law. One additional difficulty is represented by a nonconvex pointwise constraint on the magnetisation, which is a vector field of constant unit length.

Several versions of this PDE system have been used for physical investigations of magnetoelastic materials; see e.g. [46,36,17, 40,43,42,25]. As far as the mathematical literature is concerned, we refer to [50,22], in which existence of weak solutions has been established, and to a series of works by L. Baňas and coauthors [8,6,9,7,15] in numerical analysis. In [8,6,9,7], the focus is on finite element methods for the approximation of strong solutions. More recently, [15] extended the tangent plane scheme proposed in [2] for the LLG equation to this PDE system. The integrator, based on first-order finite elements in space and on an implicit first-order time-stepping method in time, decouples the system and only requires the solution of two linear systems per time-step. Under the assumption that all meshes used for the spatial discretisation are weakly acute (needed to guarantee the stability of the nodal projection used to impose the unit length constraint on the magnetisation [10,2]), the authors proved unconditional convergence of the finite element approximations towards a weak solution of the problem.

In this work, we generalise the PDE system considered in [50,22,15] by including volume and surfaces forces, as well as a more general expression for the magnetostrain [28], which allows the description of a larger class of magnetoelastic materials. For this generalised system, we propose an integrator which resembles the one in [15] (same finite element approximation spaces, same time discretisation method, same decoupled approach). However, following [12,1] (and differently from [15]), we remove the nodal projection from the update of the magnetisation (but we keep it in the discretisation of the elastic contributions). By doing this, we can avoid the requirement of weakly acute meshes at the expense of not maintaining the unit length constraint on the magnetisation at the vertices of the meshes. However, like in [12,1], we can uniformly control the violation of the constraint by the time-step size. Despite the strong nonlinearity of the problem, the resulting integrator is fully linear (in the sense that it involves only linear operations like solving linear systems and updating the approximations using a linear time-stepping). For this generalised and modified integrator, we

show unconditional well-posedness, a discrete energy law satisfied by the approximations, unconditional stability, and unconditional convergence of the approximations towards a weak solution of the problem (here, the adjective 'unconditional' refers to the fact that the analysis does not require any restrictive coupling condition between the time and spatial discretisation parameters). Moreover, assuming a (very restrictive, but artificial) Courant–Friedrichs–Lewy (CFL) condition on the time-step size and the spatial mesh size, we can pass the discrete energy law to the limit and show that the weak solution towards which our finite element approximation is converging satisfies an energy inequality.

Summarising, the contribution of the present paper over the existing literature (and, in particular, over [50,22,15]) is threefold:

- We consider a more general setting than in [50,22,15] including volume/surface forces and a more general magnetoelastic contribution based upon the magnetostriction tensor $\mathbb{Z}$ (see equation (1) below), which allows for more general crystal classes to be considered. In particular, previous papers have described this tensor as fully symmetric and positive definite, e.g. [50,15, 6,7,22], which is not true in general (such as in nickel, which has negative magnetostriction). Since our convergence proof is constructive, a byproduct of our analysis is a proof of existence of weak solutions for a more general model of magnetoelastic materials in the small-strain regime.
- Our integrator is energetically 'mindful', in the sense that our approximations satisfy a discrete energy law which resembles the one satisfied by solutions of the continuous problem (cf. Proposition 4.4 below). Under a restrictive CFL condition on the discretisation parameters, specifically $k = o(h^9)$, we can pass the result to the limit and obtain an energy inequality for weak solutions. This aspect was not considered in [15], where only boundedness of energy was proven.
- The spatial meshes used by our integrator are assumed to be only shape-regular (and do not need to be weakly acute as in [15]). This allows for the use of general mesh generators. This is especially useful in three dimensions, as weakly acute meshes are difficult to generate for arbitrary shapes [18]. Following [12,1], the assumption on the meshes is removed by omitting the nodal projection from the magnetisation update. However, the nodal projection is kept for the magnetisation appearing in the magnetoelastic terms for the sake of unconditional stability. These modifications of the original algorithm of [15] give rise to additional errors that need to be controlled, which makes the analysis more involved (e.g. a more accurate estimate of the projection error is needed; see Lemma 6.6 below). Finally, the discrete variational problems appearing in our integrator are standard and therefore easy to implement in standard finite element packages. For example, in the numerical experiments included in this work, we use Netgen/NGSolve [45].

The remainder of this work is organised as follows: In Section 2, we present the PDE system we are interested in; In Section 3, we introduce the 'ingredients' that are necessary for the definition of our numerical scheme and for its analysis; In Section 4, we present our numerical integrator (Algorithm 4.1) and state the main results of the work; Section 5 is devoted to numerical experiments. In Section 6, we collect the proofs of all results. For the convenience of the reader, we conclude the paper with two appendices, Appendix A, in which we collect several linear algebra definitions and results used throughout the work, and Appendix B, in which we show how to pass from the fully dimensional model considered in the physics literature to the dimensionless setting we study.

2. Model problem

Let $\Omega \subset \mathbb{R}^3$ be a bounded Lipschitz domain representing the volume occupied by a ferromagnetic body. We assume the boundary $\partial\Omega$ is split into two disjoint relatively open parts Γ_D (of positive measure) and Γ_N, i.e. $\partial\Omega = \overline{\Gamma}_D \cup \overline{\Gamma}_N$ and $\Gamma_D \cap \Gamma_N = \emptyset$. Let $T > 0$ denote some final time.

The magnetomechanical state of the material is described by two vector fields: the displacement $\boldsymbol{u} : \Omega \times (0,T) \to \mathbb{R}^3$ and the magnetisation $\boldsymbol{m} : \Omega \times (0,T) \to \mathbb{S}^2$. The total strain $\boldsymbol{\varepsilon}$ is made up of the elastic strain $\boldsymbol{\varepsilon}_{\mathrm{el}}$ and the magnetisation-dependent generally incompatible (in the sense that it does not satisfy the Saint-Venant compatibility conditions [5,36]) magnetostrain $\boldsymbol{\varepsilon}_{\mathrm{m}}$, i.e. $\boldsymbol{\varepsilon} = \boldsymbol{\varepsilon}_{\mathrm{el}} + \boldsymbol{\varepsilon}_{\mathrm{m}}$. The total strain is given by

$$\boldsymbol{\varepsilon}(\boldsymbol{u}) = \frac{1}{2}\left(\boldsymbol{\nabla}\boldsymbol{u} + \boldsymbol{\nabla}\boldsymbol{u}^\top\right)$$

(strain-displacement relation). Following [28], we consider the expression

$$\boldsymbol{\varepsilon}_{\mathrm{m}}(\boldsymbol{m}) = \mathbb{Z} : (\boldsymbol{m} \otimes \boldsymbol{m}), \tag{1}$$

where $\mathbb{Z} \in \mathbb{R}^{3^4}$ is a fourth-order tensor, which we assume to be minorly symmetric (i.e. $\mathbb{Z}_{ij\ell m} = \mathbb{Z}_{ji\ell m} = \mathbb{Z}_{ijm\ell}$ for all $i,j,\ell,m = 1,2,3$, cf. Appendix A). It follows that

$$\boldsymbol{\varepsilon}_{\mathrm{el}}(\boldsymbol{u},\boldsymbol{m}) = \boldsymbol{\varepsilon}(\boldsymbol{u}) - \boldsymbol{\varepsilon}_{\mathrm{m}}(\boldsymbol{m}).$$

The elastic part of the strain compensates for the magnetic part to make the total strain compatible [36]. The elastic strain is related to the stress tensor $\boldsymbol{\sigma}$ by Hooke's law

$$\boldsymbol{\sigma}(\boldsymbol{u},\boldsymbol{m}) = \mathbb{C} : \boldsymbol{\varepsilon}_{\mathrm{el}}(\boldsymbol{u},\boldsymbol{m}),$$

where $\mathbb{C} \in \mathbb{R}^{3^4}$ is the fourth-order, fully symmetric (i.e. $\mathbb{C}_{ij\ell m} = \mathbb{C}_{\ell mij} = \mathbb{C}_{ji\ell m} = \mathbb{C}_{ijm\ell}$ for all $i,j,\ell,m = 1,2,3$, cf. Appendix A), positive definite stiffness tensor. The elastic energy reads as

$$\mathcal{E}_{\mathrm{el}}[\boldsymbol{u}, \boldsymbol{m}] = \frac{1}{2} \int_{\Omega} [\boldsymbol{\varepsilon}(\boldsymbol{u}) - \boldsymbol{\varepsilon}_{\mathrm{m}}(\boldsymbol{m})] : \{\mathbb{C} : [\boldsymbol{\varepsilon}(\boldsymbol{u}) - \boldsymbol{\varepsilon}_{\mathrm{m}}(\boldsymbol{m})]\} - \int_{\Omega} \boldsymbol{f} \cdot \boldsymbol{u} - \int_{\Gamma_N} \boldsymbol{g} \cdot \boldsymbol{u},$$

where the last two terms model the work done by a volume force $\boldsymbol{f} : \Omega \to \mathbb{R}^3$ and a surface force $\boldsymbol{g} : \Gamma_N \to \mathbb{R}^3$ (traction), both assumed to be constant in time. The magnetic energy, for simplicity assumed to comprise only the Heisenberg exchange contribution, is given by

$$\mathcal{E}_{\mathrm{m}}[\boldsymbol{m}] = \frac{1}{2} \int_{\Omega} |\boldsymbol{\nabla} \boldsymbol{m}|^2. \tag{2}$$

The total free energy of the system is defined as the sum of the magnetic and elastic energies, i.e.

$$\mathcal{E}[\boldsymbol{u}, \boldsymbol{m}] = \mathcal{E}_{\mathrm{m}}[\boldsymbol{m}] + \mathcal{E}_{\mathrm{el}}[\boldsymbol{u}, \boldsymbol{m}] = \frac{1}{2} \int_{\Omega} |\boldsymbol{\nabla} \boldsymbol{m}|^2 + \frac{1}{2} \int_{\Omega} [\boldsymbol{\varepsilon}(\boldsymbol{u}) - \boldsymbol{\varepsilon}_{\mathrm{m}}(\boldsymbol{m})] : \{\mathbb{C} : [\boldsymbol{\varepsilon}(\boldsymbol{u}) - \boldsymbol{\varepsilon}_{\mathrm{m}}(\boldsymbol{m})]\} - \int_{\Omega} \boldsymbol{f} \cdot \boldsymbol{u} - \int_{\Gamma_N} \boldsymbol{g} \cdot \boldsymbol{u}. \tag{3}$$

The dynamics of $\boldsymbol{u}$ and $\boldsymbol{m}$ is governed by the coupled system of the conservation of (linear) momentum law and the LLG equation

$$\partial_{tt} \boldsymbol{u} = \nabla \cdot \boldsymbol{\sigma}(\boldsymbol{u}, \boldsymbol{m}) + \boldsymbol{f} \qquad \text{in } \Omega \times (0, T), \tag{4}$$

$$\partial_t \boldsymbol{m} = -\boldsymbol{m} \times \boldsymbol{h}_{\mathrm{eff}}[\boldsymbol{u}, \boldsymbol{m}] + \alpha \, \boldsymbol{m} \times \partial_t \boldsymbol{m} \quad \text{in } \Omega \times (0, T), \tag{5}$$

supplemented with the initial and boundary conditions

$$\boldsymbol{u}(0) = \boldsymbol{u}^0 \quad \text{in } \Omega, \tag{6a}$$

$$\partial_t \boldsymbol{u}(0) = \dot{\boldsymbol{u}}^0 \quad \text{in } \Omega, \tag{6b}$$

$$\boldsymbol{m}(0) = \boldsymbol{m}^0 \quad \text{in } \Omega, \tag{6c}$$

$$\boldsymbol{u} = \boldsymbol{0} \quad \text{on } \Gamma_D \times (0, T), \tag{6d}$$

$$\boldsymbol{\sigma} \boldsymbol{n} = \boldsymbol{g} \quad \text{on } \Gamma_N \times (0, T), \tag{6e}$$

$$\partial_{\boldsymbol{n}} \boldsymbol{m} = \boldsymbol{0} \quad \text{on } \partial\Omega \times (0, T), \tag{6f}$$

where $\boldsymbol{u}^0, \dot{\boldsymbol{u}}^0 : \Omega \to \mathbb{R}^3$ and $\boldsymbol{m}^0 : \Omega \to \mathbb{S}^2$ are suitable initial data, while $\boldsymbol{n} : \partial\Omega \to \mathbb{S}^2$ denotes the outward-pointing unit normal vector to $\partial\Omega$. In (5), $\alpha > 0$ denotes the Gilbert damping parameter, whereas the effective field $\boldsymbol{h}_{\mathrm{eff}}[\boldsymbol{u}, \boldsymbol{m}]$ is the variational derivative of the free energy with respect to the magnetisation, i.e.

$$\boldsymbol{h}_{\mathrm{eff}}[\boldsymbol{u}, \boldsymbol{m}] = -\frac{\delta \mathcal{E}[\boldsymbol{u}, \boldsymbol{m}]}{\delta \boldsymbol{m}} = \Delta \boldsymbol{m} + \boldsymbol{h}_{\mathrm{m}}[\boldsymbol{u}, \boldsymbol{m}],$$

where the elastic field reads as

$$\boldsymbol{h}_{\mathrm{m}}[\boldsymbol{u}, \boldsymbol{m}] = 2 [\mathbb{Z}^\top : \boldsymbol{\sigma}(\boldsymbol{u}, \boldsymbol{m})] \boldsymbol{m} = 2 (\mathbb{Z}^\top : \{\mathbb{C} : [\boldsymbol{\varepsilon}(\boldsymbol{u}) - \boldsymbol{\varepsilon}_{\mathrm{m}}(\boldsymbol{m})]\}) \boldsymbol{m}, \tag{7}$$

with $\mathbb{Z}^\top$ being the transpose of $\mathbb{Z}$ (cf. Appendix A). Note that (4) can be rewritten as

$$\partial_{tt} \boldsymbol{u} = -\frac{\delta \mathcal{E}[\boldsymbol{u}, \boldsymbol{m}]}{\delta \boldsymbol{u}}.$$

A simple formal calculation reveals that sufficiently smooth solutions to (4)–(6) satisfy the energy law

$$\frac{\mathrm{d}}{\mathrm{d}t} \left(\mathcal{E}[\boldsymbol{u}(t), \boldsymbol{m}(t)] + \frac{1}{2} \|\partial_t \boldsymbol{u}(t)\|^2 \right) = -\alpha \|\partial_t \boldsymbol{m}(t)\|^2 \leq 0, \tag{8}$$

i.e. the sum of the total energy (3) (which can be understood as a potential energy) and the kinetic energy $\|\partial_t \boldsymbol{u}\|^2 / 2$ decays over time, with the decay being modulated by α.

For the data of the problem, we assume that $\mathbb{C} \in \boldsymbol{L}^\infty(\Omega)$ is uniformly positive definite, i.e. there exists $C_0 > 0$ such that

$$\boldsymbol{A} : (\mathbb{C} : \boldsymbol{A}) \geq C_0 \|\boldsymbol{A}\|^2 \quad \text{for all } \boldsymbol{A} \in \mathbb{R}^{3 \times 3}, \tag{9}$$

$\mathbb{Z} \in \boldsymbol{L}^\infty(\Omega)$, $\boldsymbol{f} \in \boldsymbol{L}^2(\Omega)$, $\boldsymbol{g} \in \boldsymbol{L}^2(\Gamma_N)$, $\boldsymbol{u}^0 \in \boldsymbol{H}^1(\Omega)$, $\dot{\boldsymbol{u}}^0 \in \boldsymbol{L}^2(\Omega)$, and $\boldsymbol{m}^0 \in \boldsymbol{H}^1(\Omega; \mathbb{S}^2)$. In the following definition, we state the notion of a weak solution of the initial boundary value problem (4)–(6); see [22]. Hereafter, we shall denote L^2-integrals in space over some domain D with $\langle \cdot, \cdot \rangle_D$, omitting the subscript if $D = \Omega$. Moreover, we denote by Ω_T the space-time cylinder $\Omega \times (0, T)$.

Definition 2.1. We say that a pair $(\boldsymbol{u}, \boldsymbol{m}) : \Omega_T \to \mathbb{R}^3 \times \mathbb{R}^3$ is a weak solution to the initial boundary value problem (4)–(6) if the following conditions hold:

(i) $\boldsymbol{u} \in L^\infty(0, T; \boldsymbol{H}_D^1(\Omega))$ with $\partial_t \boldsymbol{u} \in L^\infty(0, T; \boldsymbol{L}^2(\Omega))$ and $\boldsymbol{m} \in L^\infty(0, T; \boldsymbol{H}^1(\Omega; \mathbb{S}^2))$ with $\partial_t \boldsymbol{m} \in L^2(0, T; \boldsymbol{L}^2(\Omega))$;

(ii) for all $\boldsymbol{\xi} \in \boldsymbol{C}_c^\infty([0,T); \boldsymbol{C}^\infty(\overline{\Omega}))$ and $\boldsymbol{\varphi} \in \boldsymbol{C}^\infty(\overline{\Omega_T})$, we have

$$-\int_0^T \langle \partial_t \boldsymbol{u}(t), \partial_t \boldsymbol{\xi}(t) \rangle \mathrm{d}t + \int_0^T \langle \mathbb{C} : [\boldsymbol{\varepsilon}(\boldsymbol{u}(t)) - \boldsymbol{\varepsilon}_\mathrm{m}(\boldsymbol{m}(t))], \boldsymbol{\varepsilon}(\boldsymbol{\xi}(t)) \rangle \mathrm{d}t = \int_0^T \langle \boldsymbol{f}, \boldsymbol{\xi}(t) \rangle \mathrm{d}t + \int_0^T \langle \boldsymbol{g}, \boldsymbol{\xi}(t) \rangle_{\Gamma_N} \mathrm{d}t + \langle \dot{\boldsymbol{u}}^0, \boldsymbol{\xi}(0) \rangle, \tag{10}$$

$$\int_0^T \langle \partial_t \boldsymbol{m}(t), \boldsymbol{\varphi}(t) \rangle \mathrm{d}t - \alpha \int_0^T \langle \boldsymbol{m}(t) \times \partial_t \boldsymbol{m}(t), \boldsymbol{\varphi}(t) \rangle \mathrm{d}t = \int_0^T \langle \boldsymbol{m}(t) \times \boldsymbol{\nabla}\boldsymbol{m}(t), \boldsymbol{\nabla}\boldsymbol{\varphi}(t) \rangle \mathrm{d}t - \int_0^T \langle \boldsymbol{m}(t) \times \boldsymbol{h}_\mathrm{m}[\boldsymbol{u}(t), \boldsymbol{m}(t)], \boldsymbol{\varphi}(t) \rangle \mathrm{d}t; \tag{11}$$

(iii) the initial conditions $\boldsymbol{u}(0) = \boldsymbol{u}^0$ and $\boldsymbol{m}(0) = \boldsymbol{m}^0$ hold in the sense of traces;

(iv) for almost all $t' \in (0,T)$, it holds that

$$\mathcal{E}[\boldsymbol{u}(t'), \boldsymbol{m}(t')] + \frac{1}{2} \left\| \partial_t \boldsymbol{u}(t') \right\|^2 + \alpha \int_0^{t'} \left\| \partial_t \boldsymbol{m}(t) \right\|^2 \mathrm{d}t \le \mathcal{E}[\boldsymbol{u}^0, \boldsymbol{m}^0] + \frac{1}{2} \left\| \dot{\boldsymbol{u}}^0 \right\|^2. \tag{12}$$

Equations (10) and (11) are space-time variational formulations of (4) and (5), respectively. The initial condition (6b) and the boundary conditions (6e) and (6f) are imposed as natural boundary conditions in the variational formulations; The initial conditions (6a) and (6c) are imposed in the sense of traces in (iii); The Dirichlet boundary condition (6d) is imposed as essential boundary condition. Equation (12) is the weak counterpart of the energy law (8) satisfied by strong solutions.

Remark 2.2. Formula (1) is the general expression of the magnetostrain for anisotropic ferromagnets [28] and covers the typical forms of the magnetostrain found in literature. These usually assume that the magnetostrain is *isochoric* [31, Section 3.2.6] (i.e. it has zero trace). In an isochoric material, the magnetic body elongates (contracts) in the magnetisation direction, and contracts (elongates) in the other two for positive (negative) magnetostriction. An example of positive magnetostriction is shown in Fig. 1. Importantly, formula (1) covers the common *cubic* case, considered e.g. in [32,46,36,43,42] and given by

$$\boldsymbol{\varepsilon}_\mathrm{m}(\boldsymbol{m}) = \frac{3}{2} \left\{ \lambda_{100} \left(\boldsymbol{m} \otimes \boldsymbol{m} - \frac{\boldsymbol{I}}{3} \right) + (\lambda_{111} - \lambda_{100}) \sum_{\substack{i,j=1 \\ i \ne j}}^3 (\boldsymbol{m} \cdot \boldsymbol{e}_i^\mathrm{c})(\boldsymbol{m} \cdot \boldsymbol{e}_j^\mathrm{c})(\boldsymbol{e}_i^\mathrm{c} \otimes \boldsymbol{e}_j^\mathrm{c}) \right\},$$

where $I \in \mathbb{R}^{3\times3}$ denotes the 3-by-3 identity matrix, $\lambda_{100}, \lambda_{111} \in \mathbb{R}$ are material constants, and $\{\boldsymbol{e}_1^\mathrm{c}, \boldsymbol{e}_2^\mathrm{c}, \boldsymbol{e}_3^\mathrm{c}\}$ denotes an orthonormal set yielding the crystal basis. When $\lambda_{100} = \lambda_{111}$, the latter reduces to the so-called *isotropic* case

$$\boldsymbol{\varepsilon}_\mathrm{m}(\boldsymbol{m}) = \frac{3}{2} \lambda_{100} \left(\boldsymbol{m} \otimes \boldsymbol{m} - \frac{\boldsymbol{I}}{3} \right), \tag{13}$$

considered e.g. in [17,40,25]. For further details regarding specific crystal classes and their magnetostrain representation, we refer to [28].

Remark 2.3. For the sake of simplicity (and since the focus of this work is on the design of a numerical method for the coupled system (4)–(5)), we neglect from the magnetic energy (2) all lower-order contributions (magnetocrystalline anisotropy, Zeeman energy, magnetostatic energy, Dzyaloshinskii—Moriya interaction). However, we note that their numerical integration is well understood; see e.g. [21,24,29].

3. Preliminaries

In this section, we collect some notation and preliminary results that will be necessary to introduce and analyse the fully discrete algorithm we propose to approximate solutions to the initial boundary value problem (4)–(6). Hereafter, as customary in numerical analysis, given $A, B \in \mathbb{R}$, we shall write $A \lesssim B$ if there exists a constant $c > 0$, clear from the context and always independent of the discretisation parameters, such that $A \le c B$.

3.1. Time discretisation

Let $0 = t_0 < t_1 < \cdots < t_N = T$ be a uniform partition of the time interval into N uniform intervals with constant time-step size $k = T/N$, i.e. $t_i = ik$ for all $i = 0, \dots, N$. Given values $\{\phi^i\}_{0 \le i \le N}$ and $\dot{\phi}^0$, we define the discrete time derivatives by

$$\mathrm{d}_t \phi^i := \begin{cases} \dot{\phi}^0, & \text{if } i = 0, \\ \dfrac{\phi^i - \phi^{i-1}}{k}, & \text{if } 1 \le i \le N, \end{cases} \tag{14}$$

$$\mathrm{d}_t^2 \phi^{i+1} := \frac{\mathrm{d}_t \phi^{i+1} - \mathrm{d}_t \phi^i}{k} = \begin{cases} \dfrac{\phi^1 - \phi^0 - k\dot\phi^0}{k^2}, & \text{if } i = 0, \\[2mm] \dfrac{\phi^{i+1} - 2\phi^i + \phi^{i-1}}{k^2}, & \text{if } 1 \le i \le N-1. \end{cases} \tag{15}$$

Moreover, we define the time reconstructions $\phi_k, \phi_k^-, \phi_k^+, \dot\phi_k, \dot\phi_k^-, \dot\phi_k^+$, defined, for all $0 \le i \le N-1$ and $t \in [t_i, t_{i+1})$, by

$$\phi_k(t) := \frac{t - t_i}{k} \phi^{i+1} + \frac{t_{i+1} - t}{k} \phi^i, \quad \phi_k^-(t) := \phi^i, \quad \phi_k^+(t) := \phi^{i+1}, \tag{16a}$$

$$\dot\phi_k(t) := \mathrm{d}_t \phi^i + (t - t_i)\mathrm{d}_t^2 \phi^{i+1}, \quad \dot\phi_k^-(t) := \mathrm{d}_t \phi^i, \quad \dot\phi_k^+(t) := \mathrm{d}_t \phi^{i+1}. \tag{16b}$$

Note that $\partial_t \phi_k(t) = \dot\phi_k^+(t) = d_t \phi^{i+1}$ for all $t \in [t_i, t_{i+1})$.

3.2. Space discretisation

Let Ω be a polyhedral domain. Let $\{\mathcal{T}_h\}_{h>0}$ be a shape-regular family of meshes of Ω into tetrahedra, where $h = \max_{K \in \mathcal{T}_h} h_K$ denotes the mesh size of $\mathcal{T}_h$ and $h_K = \operatorname{diam} K$ for all $K \in \mathcal{T}_h$. We denote by $\mathcal{N}_h$ the set of nodes in the triangulation $\mathcal{T}_h$. For all $K \in \mathcal{T}_h$, we denote by $\mathcal{P}_1(K)$ the space of polynomials of degree at most 1 over K. We denote by $S^1(\mathcal{T}_h)$ the space of piecewise affine and globally continuous functions from Ω to $\mathbb{R}$, i.e.

$$S^1(\mathcal{T}_h) = \{\phi_h \in C(\overline{\Omega}) : \phi_h|_K \in \mathcal{P}_1(K) \text{ for all } K \in \mathcal{T}_h\} \subset H^1(\Omega).$$

We denote by $\mathcal{I}_h : C(\overline{\Omega}) \to S^1(\mathcal{T}_h)$ the nodal interpolant satisfying $\mathcal{I}_h[\phi](z) = \phi(z)$ for each $z \in \mathcal{N}_h$, where ϕ is a continuous function. Moreover, we consider the space $S_D^1(\mathcal{T}_h) = S^1(\mathcal{T}_h) \cap H_D^1(\Omega)$, where homogeneous Dirichlet boundary conditions on Γ_D are imposed explicitly.

Since the unknowns of the problem in which we are interested are vector fields, we consider the vector-valued finite element space $S^1(\mathcal{T}_h)^3$ and use the same notation adopted in the scalar case to denote the vector-valued nodal interpolant $\mathcal{I}_h : C(\overline{\Omega}) \to S^1(\mathcal{T}_h)^3$. For all $0 \le i \le N$, the approximate displacement at time t_i, $\boldsymbol{u}_h^i \approx \boldsymbol{u}(t_i)$, will be sought in the finite element space $S_D^1(\mathcal{T}_h)^3$, whereas the approximate magnetisation, $\boldsymbol{m}_h^i \approx \boldsymbol{m}(t_i)$, will be sought in the set

$$\mathcal{M}_{h,\delta} = \left\{\boldsymbol{\phi}_h \in S^1(\mathcal{T}_h)^3 : |\boldsymbol{\phi}_h(z)| \ge 1 \text{ for all } z \in \mathcal{N}_h \text{ and } \left\| \mathcal{I}_h\left[|\boldsymbol{\phi}_h|^2\right] - 1 \right\|_{L^1(\Omega)} \le \delta \right\} \tag{17}$$

for some $\delta > 0$. Note that discrete magnetisations in $\mathcal{M}_{h,\delta}$ generally do not satisfy the unit length constraint, not even at the vertices of the mesh, but the error is controlled in the L^1-sense by δ. For the case $\delta = 0$, we obtain the set

$$\mathcal{M}_{h,0} = \{\boldsymbol{\phi}_h \in S^1(\mathcal{T}_h)^3 : |\boldsymbol{\phi}_h(z)| = 1 \text{ for all } z \in \mathcal{N}_h\},$$

in which the constraint holds at the vertices of the mesh. We define the nodal projection operator $\Pi_h : \mathcal{M}_{h,\delta} \to \mathcal{M}_{h,0}$ by $\Pi_h \boldsymbol{\phi}_h(z) = \boldsymbol{\phi}_h(z)/|\boldsymbol{\phi}_h(z)|$ for all $z \in \mathcal{N}_h$ and $\boldsymbol{\phi}_h \in \mathcal{M}_{h,\delta}$.

Another important property of solutions to the LLG equation is the orthogonality $\partial_t \boldsymbol{m} \cdot \boldsymbol{m} = 0$. To realise it at the discrete level, given an approximation $\boldsymbol{m}_h^i \approx \boldsymbol{m}(t_i)$ in $\mathcal{M}_{h,\delta}$, we consider the discrete tangent space

$$\mathcal{K}_h[\boldsymbol{m}_h^i] = \{\boldsymbol{\psi}_h \in S^1(\mathcal{T}_h)^3 : \boldsymbol{m}_h^i(z) \cdot \boldsymbol{\psi}_h(z) = 0 \text{ for all } z \in \mathcal{N}_h\},$$

where approximations $\boldsymbol{v}_h^i \approx \partial_t \boldsymbol{m}(t_i)$ will be sought. Note that the desired orthogonality property is imposed only at the vertices of the mesh.

To conclude, we recall the definition of mass-lumped L^2-product $\langle \cdot, \cdot \rangle_h$, i.e.

$$\langle \boldsymbol{\psi}, \boldsymbol{\phi} \rangle_h = \int_\Omega \mathcal{I}_h[\boldsymbol{\psi} \cdot \boldsymbol{\phi}] \quad \text{for all } \boldsymbol{\psi}, \boldsymbol{\phi} \in C^0(\overline{\Omega}), \tag{18}$$

which is a scalar product on $S^1(\mathcal{T}_h)^3$.

4. Algorithm and main results

In the following algorithm, we state the fully discrete numerical scheme we propose to approximate solutions to the initial boundary value problem (4)–(6).

Algorithm 4.1 (*decoupled algorithm for the LLG equation with magnetostriction*). <u>Discretisation parameters:</u> *Mesh size $h > 0$, time-step size $k > 0$, $\theta \in (1/2, 1]$.*
Input: Approximate initial conditions $\boldsymbol{m}_h^0 \in \mathcal{M}_{h,0}$, $\boldsymbol{u}_h^0 \in S_D^1(\mathcal{T}_h)^3$, $\dot{\boldsymbol{u}}_h^0 \in S^1(\mathcal{T}_h)^3$.
<u>Loop:</u> *For all integers $0 \le i \le N-1$, iterate (i)–(iii):*

(i) *Compute $\boldsymbol{v}_h^i \in \mathcal{K}_h[\boldsymbol{m}_h^i]$ such that, for all $\boldsymbol{\phi}_h \in \mathcal{K}_h[\boldsymbol{m}_h^i]$, it holds that*

$$\alpha \langle \boldsymbol{v}_h^i, \boldsymbol{\phi}_h \rangle_h + \langle \boldsymbol{m}_h^i \times \boldsymbol{v}_h^i, \boldsymbol{\phi}_h \rangle_h + \theta k \langle \nabla \boldsymbol{v}_h^i, \nabla \boldsymbol{\phi}_h \rangle = -\langle \nabla \boldsymbol{m}_h^i, \nabla \boldsymbol{\phi}_h \rangle + \langle \boldsymbol{h}_{\mathrm{m}}[\boldsymbol{u}_h^i, \Pi_h \boldsymbol{m}_h^i], \boldsymbol{\phi}_h \rangle. \tag{19}$$

(ii) *Define*

$$\boldsymbol{m}_h^{i+1} := \boldsymbol{m}_h^i + k \boldsymbol{v}_h^i \in S^1(\mathcal{T}_h)^3. \tag{20}$$

(iii) *Compute $\boldsymbol{u}_h^{i+1} \in S_D^1(\mathcal{T}_h)^3$ such that, for all $\boldsymbol{\psi}_h \in S_D^1(\mathcal{T}_h)^3$, it holds that*

$$\langle \mathrm{d}_t^2 \boldsymbol{u}_h^{i+1}, \boldsymbol{\psi}_h \rangle + \langle \mathbb{C} : \boldsymbol{\varepsilon}(\boldsymbol{u}_h^{i+1}), \boldsymbol{\varepsilon}(\boldsymbol{\psi}_h) \rangle = \langle \mathbb{C} : \boldsymbol{\varepsilon}_{\mathrm{m}}(\Pi_h \boldsymbol{m}_h^{i+1}), \boldsymbol{\varepsilon}(\boldsymbol{\psi}_h) \rangle + \langle \boldsymbol{f}, \boldsymbol{\psi}_h \rangle + \langle \boldsymbol{g}, \boldsymbol{\psi}_h \rangle_{\Gamma_N}. \tag{21}$$

Output: *Approximations $\{(\boldsymbol{u}_h^i, \boldsymbol{m}_h^i)\}_{0 \le i \le N}$.*

Algorithm 4.1 resembles the decoupled algorithm proposed in [15]. The discrete initial data $\boldsymbol{m}_h^0 \in \mathcal{M}_{h,0}$, $\boldsymbol{u}_h^0 \in S_D^1(\mathcal{T}_h)^3$ and $\dot{\boldsymbol{u}}_h^0 \in S^1(\mathcal{T}_h)^3$ denote suitable approximations of the initial conditions $\boldsymbol{m}^0$, $\boldsymbol{u}^0$ and $\dot{\boldsymbol{u}}^0$, respectively. For every time-step, given current approximations of the magnetisation and the displacement, we compute the new magnetisation first, and then the updated displacement using this.

Specifically, to compute the new magnetisation, we use the tangent plane scheme [3,13,2]: In step (i), given $\boldsymbol{u}_h^i$ and $\boldsymbol{m}_h^i$, we compute an approximation $\boldsymbol{v}_h^i \approx \partial_t \boldsymbol{m}(t_i)$ residing in the discrete tangent space $\mathcal{K}_h[\boldsymbol{m}_h^i]$. The variational problem (19) solved by $\boldsymbol{v}_h^i$ is a discretisation of the equivalent formulation of the LLG equation

$$\alpha \, \partial_t \boldsymbol{m} + \boldsymbol{m} \times \partial_t \boldsymbol{m} = \boldsymbol{h}_{\mathrm{eff}}[\boldsymbol{u}, \boldsymbol{m}] - (\boldsymbol{h}_{\mathrm{eff}}[\boldsymbol{u}, \boldsymbol{m}] \cdot \boldsymbol{m})\boldsymbol{m}, \tag{22}$$

which can be obtained from (5) via simple algebraic manipulations; cf. [3]. Looking at (19), we note that the discrete variational formulation of the left-hand side of (22) makes use of the mass-lumped L^2-product (18). The two terms constituting the effective field $\boldsymbol{h}_{\mathrm{eff}}[\boldsymbol{u}, \boldsymbol{m}]$ are treated differently: The exchange contribution is treated implicitly and therefore contributes to the left-hand side of (19). The 'degree of implicitness' is modulated by the parameter $\theta \in (1/2, 1]$. The elastic field is treated explicitly. In step (ii), with $\boldsymbol{v}_h^i$ at hand, we compute the new magnetisation $\boldsymbol{m}_h^{i+1}$ using a first-order time-stepping; cf. (20). Differently from the seminal papers on the tangent plane schemes [3,13,2] and from [15], we follow the approach of [12,1] and in our update we do not use the nodal projection. In particular, it holds that $\mathrm{d}_t \boldsymbol{m}_h^{i+1} = \boldsymbol{v}_h^i$. Finally, in step (iii), we compute the new displacement $\boldsymbol{u}_h^{i+1}$ using a standard finite element discretisation of (4). We use the backward Euler method in time (the second time derivative in (4) is approximated using the different quotient (15)).

In Algorithm 4.1, we apply the nodal projection to all approximate magnetisations arising from the elastic energy, i.e. in the elastic field on the right-hand side of (19) and in the magnetostrain term on the right-hand side of (21), whereas the nodal projection is omitted from the magnetisation in the exchange field on the right-hand side of (19), the cross product on the left hand side of (19), and from the update (20).

Notably, despite the nonlinearity of the LLG equation and its nonlinear coupling with the conservation of momentum law, Algorithm 4.1 is *fully linear* and only requires the solution of two linear systems per time-step.

Remark 4.2. In Algorithm 4.1, the magnesation update is based on the projection-free tangent plane scheme [12,1]. As our analysis below will show, the unit length constraint is imposed inexactly, but the constraint violation error can be controlled by the time-step size. Moreover, passing the estimate to the limit, we can show that the constraint is satisfied by the weak solution towards which the finite element approximations are converging. Other approaches in the literature aim to impose the constraint exactly (at least at the vertices of the underlying finite element mesh). This can be achieved by projecting the magnetisation onto the sphere after each update [3,13,2], using constraint-preserving variational formulation [14] or designing magnetisation updates based on exponential map [35]. In Algorithm 4.1, we refrain from these approaches as they lead to geometric restrictions on the finite element meshes [3,13,2] or lead to the solution of nonlinear systems of equations at each time-step [35,14].

In the following proposition, we show the well-posedness of Algorithm 4.1. The proof, based on standard arguments, is postponed to Section 6.1.

Proposition 4.3. *Algorithm 4.1 is well defined for every $\theta \in (1/2, 1]$, i.e. for every integer $0 \le i \le N-1$, there exists a unique $(\boldsymbol{v}_h^i, \boldsymbol{m}_h^{i+1}, \boldsymbol{u}_h^{i+1}) \in \mathcal{K}_h[\boldsymbol{m}_h^i] \times S^1(\mathcal{T}_h)^3 \times S_D^1(\mathcal{T}_h)^3$ satisfying (19)–(21).*

In the following proposition, we establish a discrete counterpart of the energy law (8) satisfied by smooth solutions of the continuous problem (see also (12) for the corresponding property for weak solutions). Its proof is postponed to Section 6.2.

Proposition 4.4. *For every integer $0 \le i \le N-1$, the iterates of Algorithm 4.1 satisfy the discrete energy law*

$$\mathcal{E}[\boldsymbol{u}_h^{i+1}, \boldsymbol{m}_h^{i+1}] + \frac{1}{2} \left\| \mathrm{d}_t \boldsymbol{u}_h^{i+1} \right\|^2 - \mathcal{E}[\boldsymbol{u}_h^i, \boldsymbol{m}_h^i] - \frac{1}{2} \left\| \mathrm{d}_t \boldsymbol{u}_h^i \right\|^2 = -\alpha k \left\| \boldsymbol{v}_h^i \right\|_h^2 - D_{h,k}^i - E_{h,k}^i, \tag{23}$$

where $D_{h,k}^i$ and $E_{h,k}^i$ are given by

$$D_{h,k}^i = k^2(\theta - 1/2)\left\|\boldsymbol{\nabla}\boldsymbol{v}_h^i\right\|^2 + \frac{1}{2}\left\|\mathrm{d}_t\boldsymbol{u}_h^{i+1} - \mathrm{d}_t\boldsymbol{u}_h^i\right\|^2 + \frac{1}{2}\left\|[\boldsymbol{\varepsilon}(\boldsymbol{u}_h^{i+1}) - \boldsymbol{\varepsilon}_{\mathrm{m}}(\boldsymbol{m}_h^{i+1})] - [\boldsymbol{\varepsilon}(\boldsymbol{u}_h^i) - \boldsymbol{\varepsilon}_{\mathrm{m}}(\boldsymbol{m}_h^i)]\right\|_{\mathbb{C}}^2 \geq 0 \tag{24}$$

and

$$\begin{aligned}
E_{h,k}^i = {} & k^2\langle\mathbb{C} : [\boldsymbol{\varepsilon}(\boldsymbol{u}_h^{i+1}) - \boldsymbol{\varepsilon}_{\mathrm{m}}(\boldsymbol{m}_h^{i+1})], \boldsymbol{\varepsilon}_{\mathrm{m}}(\boldsymbol{v}_h^i)\rangle \\
& + 2k\langle\mathbb{C} : \{[\boldsymbol{\varepsilon}(\boldsymbol{u}_h^{i+1}) - \boldsymbol{\varepsilon}_{\mathrm{m}}(\boldsymbol{m}_h^{i+1})] - [\boldsymbol{\varepsilon}(\boldsymbol{u}_h^i) - \boldsymbol{\varepsilon}_{\mathrm{m}}(\boldsymbol{m}_h^i)]\}, \mathbb{Z}(\boldsymbol{m}_h^i \otimes \boldsymbol{v}_h^i)\rangle \\
& + 2k\langle\mathbb{C} : [\boldsymbol{\varepsilon}(\boldsymbol{u}_h^i) - \boldsymbol{\varepsilon}_{\mathrm{m}}(\boldsymbol{m}_h^i)], \mathbb{Z}[(\boldsymbol{m}_h^i - \Pi_h\boldsymbol{m}_h^i) \otimes \boldsymbol{v}_h^i]\rangle \\
& + \langle\mathbb{C} : [\boldsymbol{\varepsilon}_{\mathrm{m}}(\boldsymbol{m}_h^{i+1}) - \boldsymbol{\varepsilon}_{\mathrm{m}}(\Pi_h\boldsymbol{m}_h^{i+1})], \boldsymbol{\varepsilon}(\boldsymbol{u}_h^{i+1}) - \boldsymbol{\varepsilon}(\boldsymbol{u}_h^i)\rangle.
\end{aligned} \tag{25}$$

respectively.

In (24), we use the norm $\|\cdot\|_{\mathbb{C}}^2 = \langle\mathbb{C} : (\cdot), \cdot\rangle$ for matrix-valued functions in $L^2(\Omega)^{3\times3}$. Thanks to our assumptions on $\mathbb{C}$ (cf. (9)), this norm is equivalent to the standard L^2-norm.

Looking at the right-hand side of (23), we see that the inherent α-modulated energy dissipation of the model (cf. (8)) is spoiled by two terms:

- the artificial damping $D_{h,k}^i$, arising from the implicit treatment of the exchange contribution of the effective field in (19) (the first term) and the use of the backward Euler method in (21) (the last two terms),
- the error $E_{h,k}^i$ due to linearisation (the first term) decoupling (the second term), and use of the nodal projection to impose the unit length constraint on the magnetisations appearing in the elasticity terms (the third and fourth terms).

Remark 4.5. Our argument to show Proposition 4.4 for Algorithm 4.1 can be transferred to the algorithm of [15], hence a by-product of our analysis is a discrete energy law for that algorithm. Due to the use of the nodal projection in [15], the counterpart of (23) is only an inequality (not an identity), its proof requires to assume that the mesh is weakly acute, and the error term $E_{h,k}^i$ does not include the last two terms in (25).

Now, we discuss the stability and the convergence of Algorithm 4.1. To this end, we consider the following convergence assumption on the approximate initial conditions:

$$\boldsymbol{u}_h^0 \to \boldsymbol{u}^0 \text{ in } \boldsymbol{H}^1(\Omega), \quad \dot{\boldsymbol{u}}_h^0 \to \dot{\boldsymbol{u}}^0 \text{ in } \boldsymbol{L}^2(\Omega), \text{ and } \boldsymbol{m}_h^0 \to \boldsymbol{m}^0 \text{ in } \boldsymbol{H}^1(\Omega), \quad \text{as } h \to 0. \tag{26}$$

Firstly, we can show that Algorithm 4.1 is unconditionally stable and that the error in the unit length constraint can be controlled by the time-step size.

Proposition 4.6. Suppose that assumption (26) is satisfied. There exists a threshold $k_0 > 0$ such that, if $k < k_0$, for every integer $1 \leq j \leq N$, the iterates of Algorithm 4.1 satisfy

$$\left\|\mathrm{d}_t\boldsymbol{u}_h^j\right\|^2 + \left\|\boldsymbol{\varepsilon}(\boldsymbol{u}_h^j)\right\|^2 + \sum_{i=0}^{j-1}\left\|\mathrm{d}_t\boldsymbol{u}_h^{i+1} - \mathrm{d}_t\boldsymbol{u}_h^i\right\|^2 + \sum_{i=0}^{j-1}\left\|\boldsymbol{\varepsilon}(\boldsymbol{u}_h^{i+1}) - \boldsymbol{\varepsilon}(\boldsymbol{u}_h^i)\right\|^2 + \left\|\boldsymbol{m}_h^j\right\|_{\boldsymbol{H}^1(\Omega)}^2 + k\sum_{i=0}^{j-1}\left\|\boldsymbol{v}_h^i\right\|^2 + \left(\theta - \frac{1}{2}\right)k^2\sum_{i=0}^{j-1}\left\|\boldsymbol{\nabla}\boldsymbol{v}_h^i\right\|^2 \leq C \tag{27}$$

and

$$\left\|\mathcal{I}_h\left[\left|\boldsymbol{m}_h^j\right|^2\right] - 1\right\|_{L^1(\Omega)} \leq Ck. \tag{28}$$

The threshold $k_0 > 0$ and the constant $C > 0$ depend only on the shape-regularity parameter of $\mathcal{T}_h$, the problem data α, T, Ω, $\mathbb{C}$, $\mathbb{Z}$, $\boldsymbol{f}$ and $\boldsymbol{g}$, and the uniform bounds of the energy of the approximate initial data guaranteed by (26).

For the proof of the result, we refer to Section 6.3. Note that (28) implies that, if the time-step size is sufficiently small, the approximate magnetisations generated by the algorithm belong to the set $\mathcal{M}_{h,\delta}$ from (17) with $\delta = Ck$.

With the approximations generated by Algorithm 4.1, we can construct the piecewise affine time reconstructions $\boldsymbol{u}_{hk} : (0,T) \to S^1(\mathcal{T}_h)^3$ and $\boldsymbol{m}_{hk} : (0,T) \to S^1(\mathcal{T}_h)^3$; see (16). In the following theorem, we show that the sequences $\{\boldsymbol{u}_{hk}\}$ and $\{\boldsymbol{m}_{hk}\}$ converge in a suitable sense towards a weak solution of the initial boundary value problem (4)–(6) as h, k go to 0. Its proof is postponed to Sections 6.4–6.5.

Theorem 4.7. Suppose that assumption (26) is satisfied.

(i) There exist a weak solution $(\boldsymbol{u}, \boldsymbol{m})$ of (4)–(6) in the sense of Definition 2.1(i)–(iii) and a (nonrelabeled) subsequence of $\{(\boldsymbol{u}_{hk}, \boldsymbol{m}_{hk})\}$ which converges towards $(\boldsymbol{u}, \boldsymbol{m})$ as $h, k \to 0$. In particular, as $h, k \to 0$, it holds that $\boldsymbol{u}_{hk} \stackrel{*}{\rightharpoonup} \boldsymbol{u}$ in $L^\infty(0,T; \boldsymbol{H}_D^1(\Omega))$, $\partial_t\boldsymbol{u}_{hk} \stackrel{*}{\rightharpoonup} \partial_t\boldsymbol{u}$ in $L^\infty(0,T; \boldsymbol{L}^2(\Omega))$, $\boldsymbol{m}_{hk} \stackrel{*}{\rightharpoonup} \boldsymbol{m}$ in $L^\infty(0,T; \boldsymbol{H}^1(\Omega; \mathbb{S}^2))$, and $\partial_t\boldsymbol{m}_{hk} \rightharpoonup \partial_t\boldsymbol{m}$ in $\boldsymbol{L}^2(\Omega_T)$.

(ii) *If the discretisation parameters additionally satisfy the CFL condition $k = o(h^9)$, the weak solution from part (i) satisfies the energy inequality* (12) *from Definition 2.1(iv).*

The proof of Theorem 4.7 is constructive and provides also a proof of existence of weak solutions. We recall that, due to the non-convex nature of the problem, uniqueness of weak solutions cannot be expected (cf. the explicit proof of non-uniqueness of weak solutions to the pure LLG equation in [4]). Moreover, if $\theta \in [0, 1/2]$, then Theorem 4.7 still holds, but with an additional CFL condition for part (i), i.e. $k = o(h^2)$ if $\theta \in [0, 1/2]$ and $k = o(h)$ if $\theta = 1/2$; see [2].

Remark 4.8. The application of the nodal projection to all approximate magnetisations arising from the elastic energy is responsible for two of the error terms in (25) and for the severe CFL condition in Theorem 4.7(ii) (cf. the analysis in Section 6.5 below), so one would be tempted to completely remove it. However, we believe that a fully projection-free approach would not lead to an unconditionally stable method. In particular, the use of the nodal projection on the outermost magnetisation in the elastic field (cf. (7)) is non-negotiable as the total strain $\boldsymbol{\varepsilon}(\boldsymbol{u})$ is only in $\boldsymbol{L}^2(\Omega)$. For a stable method, it would be sufficient to take only one projection, not two, within the magnetostrain as this would yield the estimate $\left\| \mathbb{Z} : (\Pi_h \boldsymbol{m}_h \otimes \boldsymbol{m}_h) \right\| \lesssim \left\| \boldsymbol{m}_h \right\|$, which would allow for the stability estimate of Proposition 4.6. However, we prefer not to use this approach as it would introduce some 'unnatural' non-symmetry.

Remark 4.9. The proof of the energy inequality typically requires extra assumptions to be proven. In [21, Appendix A], in the case of the LLG equation (with full effective field), its proof requires higher regularity and stronger convergence assumptions on the applied field and general contribution terms. In [24, Theorem 3.2], in the case of the coupled system of the LLG equation and the eddy current equation, a similar situation arises with a CFL condition $k = o(h^{3/2})$. The very severe CFL condition in Theorem 4.7(ii) is an artifact of the analysis and is due to the nonlinearity of the coupling and the fact that our proof requires explicit estimates of the error associated with the use of the nodal projection in the elastic terms. In particular, we need to estimate this error in a norm that is stronger than the L^1-norm, which leads to a reduced convergence rate with respect to the time-step size k (see Lemma 6.6 below). This, combined with the fact that we need inverse estimates to obtain quantities we are able to control, leads to the CFL condition. For more details, we refer to the proof of the result in Section 6.5 below. However, we stress that this restriction does not show up within the numerics (see, in particular, the experiment Section 5.3.3).

5. Numerical experiments

In this section, to show the applicability of our algorithm, we present a collection of numerical experiments. The implementation of Algorithm 4.1 was written using the Netgen/NGSolve package [45] using version 6.2.2302. The solution of the constrained linear system (19) in Algorithm 4.1 is based on the null-space method given in [41,34]. The resulting system is solved using GMRES with an incomplete LU decomposition preconditioner, with the previous linear update $\boldsymbol{v}_h^{i-1}$ as a starting guess. The elastic equation (21) is solved using a Jacobi preconditioned conjugate gradient method. All computations were made on an i5-9500 CPU with 16 GB of installed memory.

5.1. Material parameters

In the upcoming numerical experiments, we use material parameters estimated for $(Fe_{90}Co_{10})_{78}Si_{12}B_{10}$ (which we shall call FeCoSiB) from [26]. For the mass density and the Gilbert damping parameter (needed in our model, but not in [26]), we take the values used in [33] and [30], respectively. The resulting exchange length is $\ell_{\mathrm{ex}} = \sqrt{2A/(\mu_0 M_s^2)} \approx 3 \cdot 10^{-9}$ m. The stiffness tensor $\mathbb{C}$ is assumed to be isotropic and acts on symmetric matrices $\boldsymbol{\varepsilon}$ (the only type required) as

$$\mathbb{C} : \boldsymbol{\varepsilon} = 2\mu\,\boldsymbol{\varepsilon} + \lambda\,\mathrm{tr}(\boldsymbol{\varepsilon})\,I,$$

where μ and λ are referred to as Lamé constants (for FeCoSiB after non-dimensionalisation we have $\mu \approx 6.89$ and $\lambda \approx 21.96$). For the magnetostrain, we consider the expression in (13). In some experiments, the magnetic energy (2) will be supplemented with the term $-\langle \boldsymbol{h}_{\mathrm{ext}}, \boldsymbol{m} \rangle$ (Zeeman energy), modelling the interaction of the magnetisation with an applied external field $\boldsymbol{h}_{\mathrm{ext}}$. For the sake of reproducibility, the values used are reported in Table 1 (we refer to Appendix B for the relationship between the fully dimensional model and the dimensionless setting of this paper).

5.2. Magnetoelastic coupling

In this section, we present two numerical experiments aimed at showcasing the capability of Algorithm 4.1 to simulate physical processes involving magnetoelastic materials.

The simulation object is a bar of FeCoSiB, clamped at one end ($y = 0$ plane), shown in Fig. 2. The bar has a physical length of $20\ell_{\mathrm{ex}}$ and width/height of $6\ell_{\mathrm{ex}}$. The maximum mesh size is $h_{\max} \approx 0.9\ell_{\mathrm{ex}}$ (thereby being below the exchange length). The initial magneti-sation is uniformly in the x-direction $\boldsymbol{m}_h^0 = (1, 0, 0)$, whereas we set zero initial displacement $\boldsymbol{u}_h^0 = \boldsymbol{0}$ with zero initial velocity $\dot{\boldsymbol{u}}_h^0 = \boldsymbol{0}$. Gravity is enabled and implemented as a volume force $\boldsymbol{f} = (0, 0, -g)$, with a value of $-g = -2.97 \cdot 10^{-14}$ after non-dimensionalisation.

Fig. 2. Experiments of Section 5.2: View from above of the FeCoSiB bar of dimensions $(20\ell_{\text{ex}}, 6\ell_{\text{ex}}, 6\ell_{\text{ex}})$.
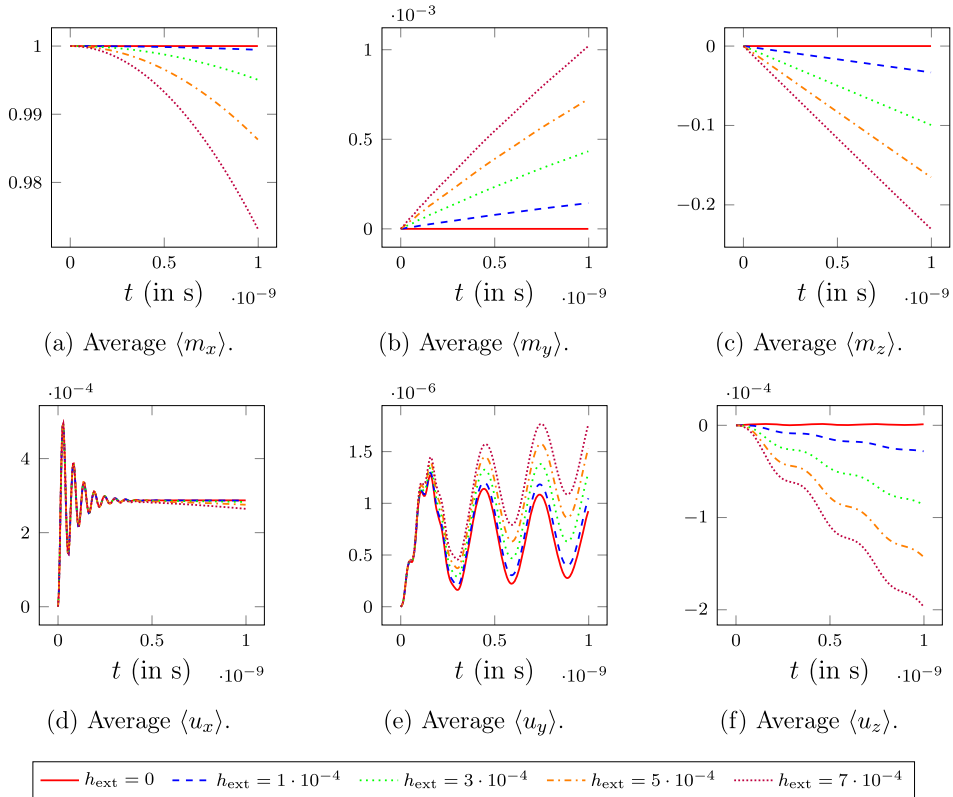

Fig. 3. Experiment of Section 5.2.1: Time evolution of the average magnetisation and displacement components for varied applied magnetic fields.

If enabled, tractions (represented by a surface force $\boldsymbol{g}$ applied on Γ_N) and applied external fields $\boldsymbol{h}_{\text{ext}}$ are applied along the $+y$ direction. Simulations are run for 1 ns, using time-steps of size $2 \cdot 10^{-12}$ s. This corresponds to a non-dimensional time length of $T \approx 330$ and time-step $k \approx 0.66$.

5.2.1. Direct magnetostrictive effect

In this experiment, we show that changes in the magnetisation yield change in the mechanical state of the body. To this end, we neglect traction and apply a uniform applied external field $\boldsymbol{h}_{\text{ext}}$ along the $+y$ direction with low values of $0, 1 \cdot 10^{-4}, 3 \cdot 10^{-4}, 5 \cdot 10^{-4}, 7 \cdot 10^{-4}$, which corresponds to fields of strength 0, 0.2, 0.6, 0.9, 1.3 mT. The fields are weak so that the dynamics is not too fast.

We observe the magnetisation aligning with the applied external field as expected through a precession, yielding an effect on the displacement. The coupling is clearly visible in Fig. 3, where we plot the time evolution of the average magnetisation and displacement components, e.g. $\langle u_x \rangle = (1/|\Omega|) \int_\Omega u_x$. The applied field is pointing in the y-direction, so the y and z components begin to increase in magnitude as seen in Figs. 3b and 3c, taking from the x component. The displacement on the other hand mirrors the magnetisation in the y and z components, with the x component increasing due to magnetostriction, and then changing slowly as the magnetisation changes. Moreover, we see that, with stronger applied magnetic fields, the average magnetisation in the y direction increases, displacing the body in the same direction.

In Fig. 4, we plot the time evolution of the energy for all considered applied external fields. For greater strength applied fields, the energy reaches a lower value at later times. Importantly, we always see the energy decreasing.
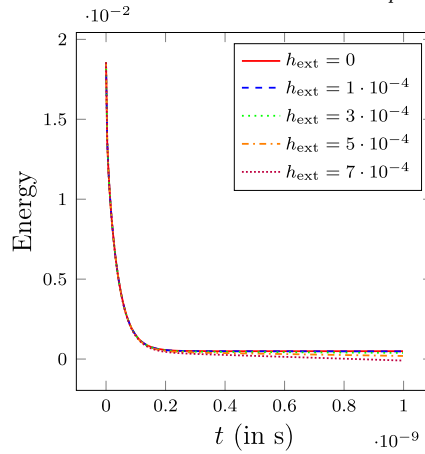
Fig. 4. Experiment of Section 5.2.1: Total energy over time for varied applied magnetic fields.
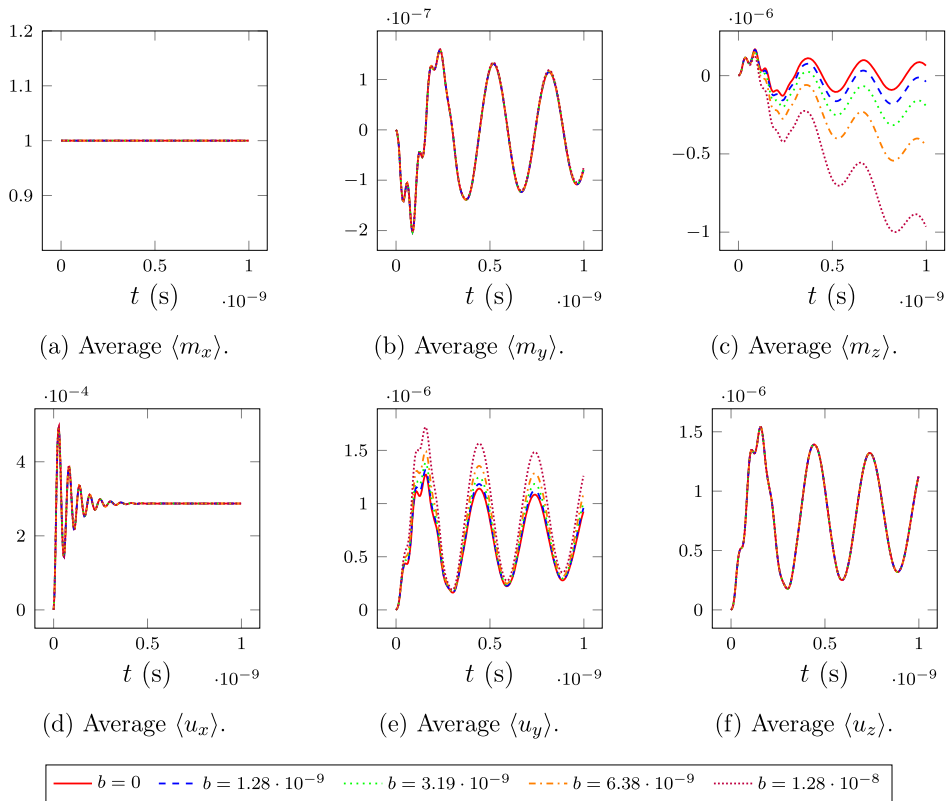
Fig. 5. Experiment of Section 5.2.2: Time evolution of the average magnetisation and displacement components for varied traction strengths.

5.2.2. Inverse magnetostrictive effect

In this experiment, we show that changes in the mechanical state of the body yield change in the magnetisation. To this end, we disable the Zeeman field and apply a traction on the $x = 20\ell_{\mathrm{ex}}$ plane in the $+y$ direction. Specifically, we consider a surface force of the form $\boldsymbol{g} = (0, b, 0)$ for $b \in \{0, 1.28 \cdot 10^{-9}, 3.19 \cdot 10^{-9}, 6.38 \cdot 10^{-9}, 1.28 \cdot 10^{-8}\}$, which corresponds to forces of strength 0, 10, 25, 50, 100 Nm^{-2}.

The time evolution of the average displacement and magnetisation components is shown in Fig. 5. When more traction is applied, the average displacement in the y direction increases. The z component of the magnetisation in Fig. 5c is the most interesting, as it decreases more strongly due to stronger tractions.
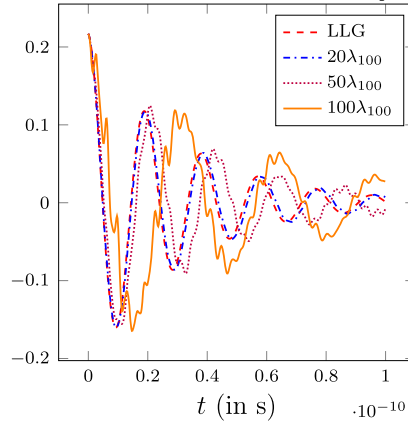
Fig. 6. Experiment of Section 5.2.3: Time evolution of the average $\langle m_y \rangle$ for varying magnetostrain values λ_{100}, compared with purely LLG without magnetoelastic effects.
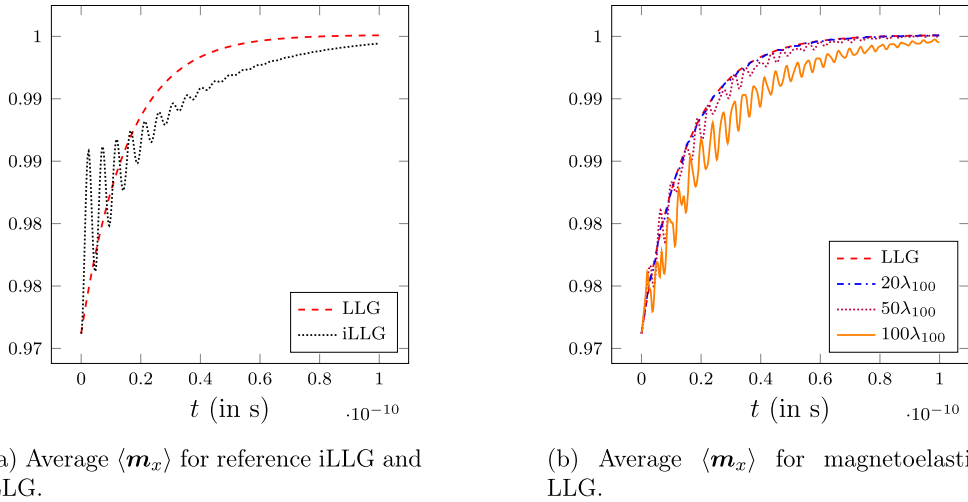
(a) Average $\langle m_x \rangle$ for reference iLLG and LLG.

(b) Average $\langle m_x \rangle$ for magnetoelastic LLG.

Fig. 7. Experiment of Section 5.2.3. Average magnetisation $\langle m_x \rangle$ of (a) reference LLG and iLLG, (b) magnetoelastic LLG with varying magnetostrain.

5.2.3. Nutation dynamics

It has been shown that at extremely short timescales, the LLG equation is inadequate for the ultrafast dynamics that occur [23,51]. At these timescales, the LLG equation (5) should then be replaced by the inertial LLG (iLLG) equation, given by

$$\partial_t \boldsymbol{m} = -\boldsymbol{m} \times \boldsymbol{h}_{\text{eff}}[\boldsymbol{m}] + \alpha\, \boldsymbol{m} \times \partial_t \boldsymbol{m} + \tau\, \boldsymbol{m} \times \partial_{tt} \boldsymbol{m}, \tag{29}$$

where the additional parameter $\tau > 0$ is a relaxation time.

The main difference between iLLG and LLG dynamics is the inclusion of nutation, where the LLG path is not instantly followed due to the inertia of the magnetisation [37]. A preliminary form of the iLLG equation was initially derived using an expansion coming from the magnetoelastic coupling [47,48]. Here the momentum is stored by the displacement instead of the magnetisation. With the experiment in this section, we aim to demonstrate this effect.

We consider the same material parameters as in the previous experiments, except for the Gilbert damping parameter (for which we choose $\alpha = 0.1$). Moreover, as the nutation effects are small, we increase the magnetostriction constant λ_{100} in Table 1. For the ferromagnetic body, we consider a hemisphere of radius ℓ_{ex} with a clamped planar face with outer normal $(-1,0,0)$. We use the values $\{20\lambda_{100}, 50\lambda_{100}, 100\lambda_{100}\}$, and compare this to a reference LLG simulation with no magnetoelastic coupling (computed by the same algorithm with $0\lambda_{100}$). The initial magnetisation is slightly perturbed from the x-direction, specifically $\boldsymbol{m}^0 = (0.9, 0.2, 0)$ (normalised), and subject to a strong Zeeman field $\boldsymbol{h}_{\text{ext}} = (1,0,0) = (3\pi/5, 0, 0)$ T. The initial displacement and velocity are zero. We set $\theta = 0.50000005$, and consider a non-dimensional time-step $k = 0.001 \approx 3 \cdot 10^{-15}$s, for time $T = 1 \cdot 10^{-10}$s. The mesh is made of 210 nodes, 672 elements, and satisfies $h_{\max} \approx 0.6\ell_{\text{ex}}$.

The results can be seen in Fig. 6. It is easily seen that as the magnetostrain parameter is increased, the dissipative effects decrease, seen as a stretching effect to the right. As expected, we see nutation effects perturbing the natural LLG precession behaviour, especially for $50\lambda_{100}$ and $100\lambda_{100}$.
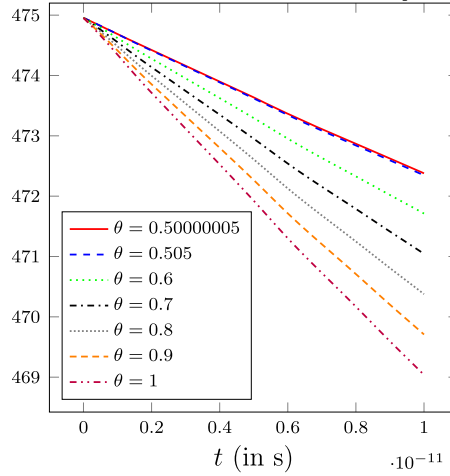
Fig. 8. Experiment of Section 5.3.1: Time evolution of the total energy for different values of θ.

For reference, we also consider this same system without magnetoelastic coupling for the iLLG equation. The modifications required to extend the tangent plane scheme presented in [2] to the iLLG equation are described and analysed in [44]. For consistency, we apply the tangent plane scheme here with the nodal projection step removed. We choose the relaxation time arbitrarily to be $\tau = 0.4 \approx 1.21$ ps. The average x component of the magnetisation for iLLG is shown in Fig. 7a, and the average x components of the magnetisation for the magnetoelastic LLG simulations are shown in Fig. 7b. The qualitative similarities are obvious, with additional oscillations not seen in the pure LLG case, along with lessened damping.

5.3. Properties of Algorithm 4.1

In this section, we present three experiments to numerically investigate the properties of Algorithm 4.1. For all of them, the computational domain will be a cube with edge length equal to $6\ell_{\mathrm{ex}}$.

5.3.1. θ-dependence

In this experiment, we investigate the effect on numerical simulations of the parameter $\theta \in (1/2, 1]$, which controls the 'degree of implicitness' in the treatment of the exchange contribution in (19). We use material parameters for FeCoSiB (cf. Table 1) except for the Gilbert damping parameter, for which we use the smaller value $\alpha = 0.001$. The initial condition for the magnetisation is a 'hot' magnetic state, i.e. the values at the vertices of the mesh (which in this experiment has mesh size $h_{\max} \approx 3\ell_{\mathrm{ex}}$) are assigned randomly to the magnetisation before being normalised. The displacement and its time derivative are initialised by zero.

We run the simulation for $1 \cdot 10^{-11}$ s using a time step size of $1 \cdot 10^{-15}$ s and different values of $\theta \in \{0.50000005, 0.505, 0.6, 0.7, 0.8, 0.9, 1\}$.

The energy-decreasing behaviour can be seen in Fig. 8, with considerably more energy loss associated with greater θ values. So changing the θ-implicitness parameter away from $1/2$ can yield considerable amounts of artificial numerical damping, which can be particularly bad in certain situations (e.g. in the case of long-time simulations).

5.3.2. Unit length constraint violation

An essential property of the LLG equation at constant temperature is the unit length constraint on the magnetisation. Hence, an essential feature of any approximation algorithm must be the capability to achieve the unit length constraint. For Algorithm 4.1, this property is the subject of Proposition 4.6, particularly (28), i.e.

$$\left\| \mathcal{I}_h \left[\left| \boldsymbol{m}_h^j \right|^2 \right] - 1 \right\|_{L^1(\Omega)} \le Ck,$$

which shows that the unit length constraint is violated at most linearly in time (if measured in the L^1-norm).

To see this numerically, we again consider a hot magnet as in Section 5.3.1, a particularly bad case with plenty of rotation by the magnetisation (note that the constant $C > 0$ in (28) depends, among other things, upon the energy of the initial magnetisation and is large for a random configuration), and use various time-steps with $\theta = 0.50000005$.

In Fig. 9a, we plot the constraint violation (measured as the left-hand side of (28)) at the finale iterate $\boldsymbol{m}_h^N$ of Algorithm 4.1 against the time-step size k. We observe that the error decays linearly in k as predicted by (28). The constraint violation is of the order 10^2 for k on the order of $10^{-3/2}$ due to the hot initial state, as the magnetisation at a node may need to rotate several times. Note that these simulations are run for only 0.01 ns as we are only interested in verifying the constraint violation inequalities.

In Fig. 9b, we plot the L^∞-norm of the magnetisation at the final iterate against the time-step size k. We note that while we can control the integral violation with (28), in our projection-free algorithm we cannot directly control the maximum norm $\left\| \boldsymbol{m}_h^j \right\|_{L^\infty(\Omega)}$,
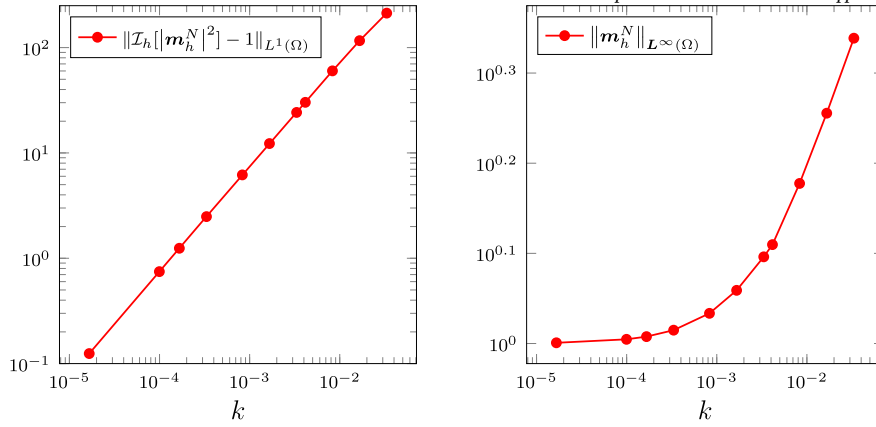
(a) Constraint violation.

(b) Nodal maximum.

Fig. 9. Experiment of Section 5.3.2: (a) Constraint violation at the final iterate against the time-step size. (b) L^∞-norm of the magnetisation at the final iterate against the time-step size.

which with a projection would be 1 for each j. We see that the nodal maximum numerically tends to 1 as desired, but the decay is not linear. Using similar methods to those to prove (28) (see Lemma 6.2 below) and classical inverse estimates [11, Lemma 3.5], one can show that

$$\left\| \boldsymbol{m}_h^j \right\|_{\boldsymbol{L}^\infty}^2 - 1 = \max_{z \in \mathcal{N}_h} |\boldsymbol{m}_h^j(z)|^2 - 1 \le k^2 \sum_{i=0}^{j-1} \max_{z \in \mathcal{N}_h} |\boldsymbol{v}_h^i(z)|^2 = k^2 \sum_{i=0}^{j-1} \left\| \boldsymbol{v}_h^i \right\|_{\boldsymbol{L}^\infty(\Omega)}^2 \lesssim h_{\min}^{-3} k^2 \sum_{i=0}^{j-1} \left\| \boldsymbol{v}_h^i \right\|_{\boldsymbol{L}^2(\Omega)}^2 \lesssim h_{\min}^{-3} k,$$

thus the desired convergence $\left\| \boldsymbol{m}_h^j \right\|_{\boldsymbol{L}^\infty(\Omega)} \to 1$ as $h, k \to 0$ can be obtained assuming the CFL condition $k = o(h^3)$.

5.3.3. Energy law robustness

In this experiment, we investigate the robustness of the evolution of the energy of the approximations generated by Algorithm 4.1 with respect to the discretisation parameters.

We consider a similar setup to the one used in Section 5.3.1. Specifically, we keep $\theta = 0.50000005$ and $\alpha = 0.001$, but we add a Zeeman field $\boldsymbol{h}_{\text{ext}} = (0.001, 0, 0) \approx (1.9, 0, 0)\text{mT}$ to encourage the system to approach the same final state. To give consistency between mesh refinements we change from a purely random initial state to the following initial condition for the magnetisation,

$$\boldsymbol{m}^0(x, y, z) = \frac{1}{\sqrt{5}} (2, \sin(x + y + z), \cos(x + y + z)) \quad \text{for all } (x, y, z) \in \Omega.$$

It is easily shown that the initial condition satisfies $\left\| \nabla \boldsymbol{m}^0 \right\|^2 / 2 = 64.8$ and $\left| \boldsymbol{m}^0 \right| = 1$ in Ω. NGSolve interpolates the initial condition onto the mesh via an Oswald-type interpolation [38], applying an L^2-projection and then averaging for conformity, thus to enforce the condition $\boldsymbol{m}_h^0 \in \mathcal{M}_{h,0}$ we apply the nodal projection to the result of this interpolation. We then ran the simulation for $T \approx 3.32$ with combinations of $k = 0.01, 0.005, 0.0025, 0.00125, 0.000625$ as time-step size and $h = 1.59, 1.09, 0.84, 0.45$ as mesh size.

As can be observed in Fig. 10, the energy decay (and thus stability of the algorithm) occurs for all mesh sizes and time-steps. The initial energy is different for each due to the differing underlying mesh, and the interpolation process mentioned above (which is also different for each mesh), however the initial energies approach the actual energy. The different energy progressions are clustered into the four groups with similar energy decay when the time-step is the same. When the time-step size is smaller, the energy decay is slower, likely due to the error term in the discrete energy law (cf. the term $E_{h,k}^i$ in (23)). With no error term present, the dissipation would always reduce with lower time-step sizes.

These results show that the algorithm behaves energetically well for all combinations of mesh and time-step size considered, including the worst case scenario for a CFL condition (when the finest mesh with $h = 0.45$ and the largest time-step size $k = 0.01$ are used). Clearly, this is not a mathematical proof that the restrictive CFL condition we need to show Theorem 4.7(ii) is not needed, however our numerical experiments seem to corroborate this claim.

6. Proofs

In this section, we collect the proofs of the results presented in Section 4. For the convenience of the reader, we start with recalling some well-known results that will be used multiple times throughout the upcoming analysis.

The norm $\|\cdot\|_h$ induced by the mass-lumped L^2-product (18) satisfies the norm equivalence

$$\|\boldsymbol{\phi}_h\| \le \|\boldsymbol{\phi}_h\|_h \le \sqrt{5} \|\boldsymbol{\phi}_h\| \quad \text{for all } \boldsymbol{\phi}_h \in S^1(\mathcal{T}_h)^3, \tag{30}$$
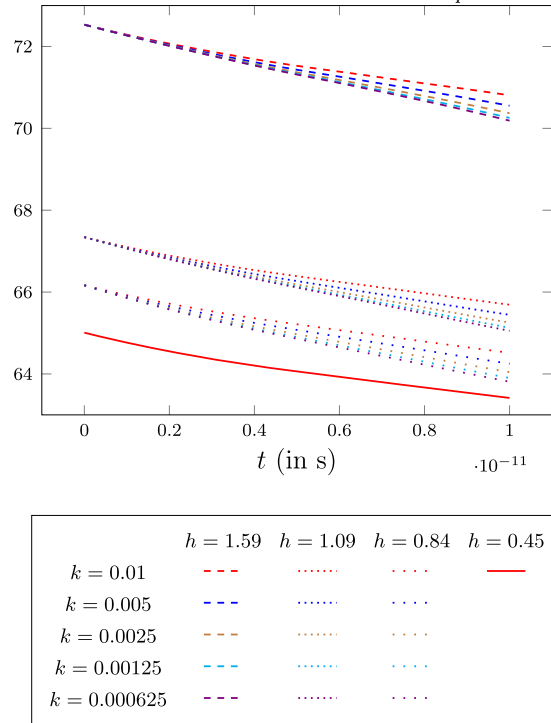
Fig. 10. Time evolution of the total energy of different values of h and k.

and we have the error estimate

$$|\langle \boldsymbol{\phi}_h, \boldsymbol{\psi}_h \rangle - \langle \boldsymbol{\phi}_h, \boldsymbol{\psi}_h \rangle_h| \le C h^2 \|\nabla \boldsymbol{\phi}_h\| \|\nabla \boldsymbol{\psi}_h\| \quad \text{for all } \boldsymbol{\phi}_h, \boldsymbol{\psi}_h \in S^1(\mathcal{T}_h)^3, \tag{31}$$

(cf. [11, Lemma 3.9]). For all $K \in \mathcal{T}_h$ and $1 \le r, p \le \infty$, we have the local inverse estimate

$$\|\boldsymbol{\phi}_h\|_{L^p(K)} \le C h_K^{3(r-p)/(pr)} \|\boldsymbol{\phi}_h\|_{L^r(K)} \quad \text{for all } \boldsymbol{\phi}_h \in S^1(\mathcal{T}_h)^3 \tag{32}$$

(see, e.g. [11, Lemma 3.5]). For all $1 \le p < \infty$, the L^p-norm of functions in $S^1(\mathcal{T}_h)^3$ is equivalent with the ℓ^p-norm of the vector collecting their nodal values, weighted by the local mesh size, i.e.

$$C^{-1} \|\boldsymbol{\phi}_h\|_{L^p(\Omega)} \le \left(\sum_{z \in \mathcal{N}_h} h_z^3 |\boldsymbol{\phi}_h(z)|^p \right)^{1/p} \le C \|\boldsymbol{\phi}_h\|_{L^p(\Omega)} \quad \text{for all } \boldsymbol{\phi}_h \in S^1(\mathcal{T}_h)^3, \tag{33}$$

where $h_z > 0$ denotes the diameter of the node patch of $z \in \mathcal{N}_h$ (cf. [11, Lemma 3.4]). If $p = \infty$, we have that

$$\|\boldsymbol{\phi}_h\|_{L^\infty(\Omega)} = \max_{z \in \mathcal{N}_h} |\boldsymbol{\phi}_h(z)| \quad \text{for all } \boldsymbol{\phi}_h \in S^1(\mathcal{T}_h)^3.$$

Finally, the nodal projection is H^1-stable, i.e., it holds that

$$\|\nabla \Pi_h \boldsymbol{\phi}_h\| \le C \|\nabla \boldsymbol{\phi}_h\| \quad \text{for all } \boldsymbol{\phi} \in S^1(\mathcal{T}_h)^3 \text{ satisfying } |\boldsymbol{\phi}(z)| \ge 1 \text{ for all } z \in \mathcal{N}_h; \tag{34}$$

see [12, Lemma 2.2]. We recall that (34) holds with $C = 1$ if all non-diagonal entries of the stiffness matrix are non-positive (cf. [11, Proposition 3.2]). This assumption, which is satisfied under very restrictive geometric conditions on the mesh in three dimensions, is *not* required by the upcoming analysis. In all these inequalities, the constant $C > 0$ (not the same at each occurrence) depends only on the shape-regularity of $\mathcal{T}_h$.

6.1. Well-posedness

We start by showing an estimate of the L^2-norm of the discrete elastic field.

Lemma 6.1. *For all $\boldsymbol{u}_h, \boldsymbol{m}_h \in S^1(\mathcal{T}_h)^3$ with $|\boldsymbol{m}_h(z)| \ge 1$ for all $z \in \mathcal{N}_h$, it holds that*

$$\left\|\boldsymbol{h}_{\mathrm{m}}[\boldsymbol{u}_h, \Pi_h \boldsymbol{m}_h]\right\|^2 \le 8 \|\mathbb{Z}\|_{L^\infty(\Omega)}^2 \|\mathbb{C}\|_{L^\infty(\Omega)}^2 \left(\|\varepsilon(\boldsymbol{u}_h)\|^2 + \|\mathbb{Z}\|_{L^\infty(\Omega)}^2 |\Omega| \right). \tag{35}$$

Proof. Using the expression of the discrete elastic field, we have

$$\left\| \boldsymbol{h}_{\mathrm{m}}[\boldsymbol{u}_h, \Pi_h \boldsymbol{m}_h] \right\|^2$$
$$\overset{(7)}{=} \left\| 2(\mathbb{Z}^\top : \{\mathbb{C} : [\boldsymbol{\varepsilon}(\boldsymbol{u}_h) - \boldsymbol{\varepsilon}_{\mathrm{m}}(\Pi_h \boldsymbol{m}_h)]\}) \Pi_h \boldsymbol{m}_h \right\|^2$$
$$\leq 4 \left\| \mathbb{Z} \right\|_{\boldsymbol{L}^\infty(\Omega)}^2 \left\| \mathbb{C} \right\|_{\boldsymbol{L}^\infty(\Omega)}^2 \left\| \boldsymbol{\varepsilon}(\boldsymbol{u}_h) - \mathbb{Z} : (\Pi_h \boldsymbol{m}_h \otimes \Pi_h \boldsymbol{m}_h) \right\|^2 \left\| \Pi_h \boldsymbol{m}_h \right\|_{\boldsymbol{L}^\infty(\Omega)}^2$$
$$\leq 8 \left\| \mathbb{Z} \right\|_{\boldsymbol{L}^\infty(\Omega)}^2 \left\| \mathbb{C} \right\|_{\boldsymbol{L}^\infty(\Omega)}^2 \left(\left\| \boldsymbol{\varepsilon}(\boldsymbol{u}_h) \right\|^2 + \left\| \mathbb{Z} \right\|_{\boldsymbol{L}^\infty(\Omega)}^2 |\Omega| \right),$$

where we have used the boundedness of the fourth-order tensors and $\Pi_h \boldsymbol{m}_h$. $\square$

We can now show the well-posedness of Algorithm 4.1.

Proof of Proposition 4.3. The proof is basically identical to the one given in [15] for the algorithm proposed therein. We restate it here including other terms.

For the magnetisation term, define the family of bilinear form $a_1^i(\cdot, \cdot) : \mathcal{K}_h[\boldsymbol{m}_h^i] \times \mathcal{K}_h[\boldsymbol{m}_h^i] \to \mathbb{R}$ for $i = 0, \dots, N-1$, by

$$a_1^i(\boldsymbol{\phi}_h, \boldsymbol{\psi}_h) := \alpha \langle \boldsymbol{\phi}_h, \boldsymbol{\psi}_h \rangle_h + \theta k \langle \nabla \boldsymbol{\phi}_h, \nabla \boldsymbol{\psi}_h \rangle + \langle \boldsymbol{m}_h^i \times \boldsymbol{\phi}_h, \boldsymbol{\psi}_h \rangle$$

and the family of linear (and bounded by Lemma 6.1) functionals L_1^i for $i = 0, \dots, N-1$ by

$$L_1^i(\boldsymbol{\phi}_h) := -\langle \nabla \boldsymbol{m}_h^i, \nabla \boldsymbol{\phi}_h \rangle + \langle \boldsymbol{h}_{\mathrm{m}}[\boldsymbol{u}_h^i, \Pi_h \boldsymbol{m}_h^i], \boldsymbol{\phi}_h \rangle.$$

Then (19) can be rewritten as $a_1^i(\boldsymbol{v}_h^i, \boldsymbol{\psi}_h) = L_1^i(\boldsymbol{\psi}_h)$ for all $\boldsymbol{\psi}_h \in \mathcal{K}_h[\boldsymbol{m}_h^i]$. We can see that $a_1^i(\cdot, \cdot)$ is positive definite (in $\boldsymbol{L}^2(\Omega)$ and $\boldsymbol{H}^1(\Omega)$), as letting $\boldsymbol{\phi}_h = \boldsymbol{\psi}_h$ eliminates the final term, leaving a combination of the L^2-norm and H^1-seminorm. It follows by the finite dimensionality that (19) has a unique solution $\boldsymbol{v}_h^i \in \mathcal{K}_h[\boldsymbol{m}_h^i]$.

For the displacement term, define the bilinear form $a_2 : S_D^1(\mathcal{T}_h)^3 \times S_D^1(\mathcal{T}_h)^3 \to \mathbb{R}$ by

$$a_2(\boldsymbol{\phi}_h, \boldsymbol{\psi}_h) := \langle \boldsymbol{\phi}_h, \boldsymbol{\psi}_h \rangle + k^2 \langle \mathbb{C} : \boldsymbol{\varepsilon}(\boldsymbol{\phi}_h), \boldsymbol{\varepsilon}(\boldsymbol{\psi}_h) \rangle.$$

As $\mathbb{C}$ is positive definite by assumption, applying Korn's inequality (see, e.g. [19, Theorem 11.2.6]) yields positive definiteness of $a_2(\cdot, \cdot)$ in $\boldsymbol{H}^1(\Omega)$. Furthermore, defining the family of linear functionals

$$L_2^i(\boldsymbol{\psi}_h) := k^2 \langle \mathbb{C} : \boldsymbol{\varepsilon}_{\mathrm{m}}(\Pi_h \boldsymbol{m}_h^{i+1}), \boldsymbol{\varepsilon}(\boldsymbol{\psi}_h) \rangle + k \langle \mathrm{d}_t \boldsymbol{u}_h^i, \boldsymbol{\psi}_h \rangle + \langle \boldsymbol{u}_h^i, \boldsymbol{\psi}_h \rangle + k^2 \langle \boldsymbol{f}, \boldsymbol{\psi}_h \rangle + k^2 \langle \boldsymbol{g}, \boldsymbol{\psi}_h \rangle_{\Gamma_N},$$

we have that (21) is equivalent to $a_2(\boldsymbol{u}_h^{i+1}, \boldsymbol{\psi}_h) = L_2^i(\boldsymbol{\psi}_h)$ for all $\boldsymbol{\psi}_h \in S_D^1(\mathcal{T}_h)^3$, for each $i = 0, \dots, N-1$. Again exploiting the finite dimension, we have existence and uniqueness of a solution $\boldsymbol{u}_h^{i+1} \in S_D^1(\mathcal{T}_h)^3$ to (21). $\square$

6.2. Discrete energy law

We now prove the discrete energy law satisfied by the iterates of Algorithm 4.1.

Proof of Proposition 4.4. Let $0 \leq i \leq N-1$ be an arbitrary integer. Choosing the test function $\boldsymbol{\phi}_h = \boldsymbol{v}_h^i \in \mathcal{K}_h[\boldsymbol{m}_h^i]$ in (19), we obtain

$$\alpha \left\| \boldsymbol{v}_h^i \right\|_h^2 + \theta k \left\| \nabla \boldsymbol{v}_h^i \right\|^2 = -\langle \nabla \boldsymbol{m}_h^i, \nabla \boldsymbol{v}_h^i \rangle + \langle \boldsymbol{h}_{\mathrm{m}}[\boldsymbol{u}_h^i, \Pi_h \boldsymbol{m}_h^i], \boldsymbol{v}_h^i \rangle.$$

Moreover, we have

$$\frac{1}{2} \left\| \nabla \boldsymbol{m}_h^{i+1} \right\|^2 = \frac{1}{2} \left\| \nabla \boldsymbol{m}_h^i \right\|^2 + k \langle \nabla \boldsymbol{m}_h^i, \nabla \boldsymbol{v}_h^i \rangle + \frac{k^2}{2} \left\| \nabla \boldsymbol{v}_h^i \right\|^2.$$

Combining the two above equations, we obtain

$$\mathcal{E}_{\mathrm{m}}[\boldsymbol{m}_h^{i+1}] - \mathcal{E}_{\mathrm{m}}[\boldsymbol{m}_h^i] = -\alpha k \left\| \boldsymbol{v}_h^i \right\|_h^2 - k^2(\theta - 1/2) \left\| \nabla \boldsymbol{v}_h^i \right\|^2 + k \langle \boldsymbol{h}_{\mathrm{m}}[\boldsymbol{u}_h^i, \Pi_h \boldsymbol{m}_h^i], \boldsymbol{v}_h^i \rangle. \tag{36}$$

Choosing the test function $\boldsymbol{\psi}_h = \boldsymbol{u}_h^{i+1} - \boldsymbol{u}_h^i = k \, \mathrm{d}_t \boldsymbol{u}_h^{i+1}$ in (21) yields

$$\langle \mathrm{d}_t \boldsymbol{u}_h^{i+1} - \mathrm{d}_t \boldsymbol{u}_h^i, \mathrm{d}_t \boldsymbol{u}_h^{i+1} \rangle + \langle \mathbb{C}[\boldsymbol{\varepsilon}(\boldsymbol{u}_h^{i+1}) - \boldsymbol{\varepsilon}_{\mathrm{m}}(\Pi_h \boldsymbol{m}_h^i)], \boldsymbol{\varepsilon}(\boldsymbol{u}_h^{i+1}) - \boldsymbol{\varepsilon}(\boldsymbol{u}_h^i) \rangle = \langle \boldsymbol{f}, \boldsymbol{u}_h^{i+1} - \boldsymbol{u}_h^i \rangle + \langle \boldsymbol{g}, \boldsymbol{u}_h^{i+1} - \boldsymbol{u}_h^i \rangle_{\Gamma_N}.$$

Using Lemma A.5, the first term on the left-hand side can be reformulated as

$$\langle \mathrm{d}_t \boldsymbol{u}_h^{i+1} - \mathrm{d}_t \boldsymbol{u}_h^i, \mathrm{d}_t \boldsymbol{u}_h^{i+1} \rangle = \frac{1}{2} \left\| \mathrm{d}_t \boldsymbol{u}_h^{i+1} \right\|^2 - \frac{1}{2} \left\| \mathrm{d}_t \boldsymbol{u}_h^i \right\|^2 + \frac{1}{2} \left\| \mathrm{d}_t \boldsymbol{u}_h^{i+1} - \mathrm{d}_t \boldsymbol{u}_h^i \right\|^2$$

which yields

$$\frac{1}{2}\left\|\mathrm{d}_t \boldsymbol{u}_h^{i+1}\right\|^2 - \frac{1}{2}\left\|\mathrm{d}_t \boldsymbol{u}_h^{i}\right\|^2 + \frac{1}{2}\left\|\mathrm{d}_t \boldsymbol{u}_h^{i+1} - \mathrm{d}_t \boldsymbol{u}_h^{i}\right\|^2 + \langle \mathbb{C}[\varepsilon(\boldsymbol{u}_h^{i+1}) - \varepsilon_{\mathrm{m}}(\Pi_h \boldsymbol{m}_h^{i+1})], \varepsilon(\boldsymbol{u}_h^{i+1}) - \varepsilon(\boldsymbol{u}_h^{i})\rangle = \langle \boldsymbol{f}, \boldsymbol{u}_h^{i+1} - \boldsymbol{u}_h^{i}\rangle + \langle \boldsymbol{g}, \boldsymbol{u}_h^{i+1} - \boldsymbol{u}_h^{i}\rangle_{\Gamma_N}.$$

(37)

Similarly, we have

$$\langle \mathbb{C} : [\varepsilon(\boldsymbol{u}_h^{i+1}) - \varepsilon_{\mathrm{m}}(\Pi_h \boldsymbol{m}_h^{i+1})], \varepsilon(\boldsymbol{u}_h^{i+1}) - \varepsilon(\boldsymbol{u}_h^{i})\rangle$$

$$= \langle \mathbb{C} : [\varepsilon(\boldsymbol{u}_h^{i+1}) - \varepsilon_{\mathrm{m}}(\boldsymbol{m}_h^{i+1})], \varepsilon(\boldsymbol{u}_h^{i+1}) - \varepsilon(\boldsymbol{u}_h^{i})\rangle$$

$$\quad + \langle \mathbb{C} : [\varepsilon_{\mathrm{m}}(\boldsymbol{m}_h^{i+1}) - \varepsilon_{\mathrm{m}}(\Pi_h \boldsymbol{m}_h^{i+1})], \varepsilon(\boldsymbol{u}_h^{i+1}) - \varepsilon(\boldsymbol{u}_h^{i})\rangle$$

$$= \langle \mathbb{C} : [\varepsilon(\boldsymbol{u}_h^{i+1}) - \varepsilon_{\mathrm{m}}(\boldsymbol{m}_h^{i+1})], [\varepsilon(\boldsymbol{u}_h^{i+1}) - \varepsilon_{\mathrm{m}}(\boldsymbol{m}_h^{i+1})] - [\varepsilon(\boldsymbol{u}_h^{i}) - \varepsilon_{\mathrm{m}}(\boldsymbol{m}_h^{i})]\rangle$$

$$\quad + \langle \mathbb{C} : [\varepsilon(\boldsymbol{u}_h^{i+1}) - \varepsilon_{\mathrm{m}}(\boldsymbol{m}_h^{i+1})], \varepsilon_{\mathrm{m}}(\boldsymbol{m}_h^{i+1}) - \varepsilon_{\mathrm{m}}(\boldsymbol{m}_h^{i})\rangle$$

$$\quad + \langle \mathbb{C} : [\varepsilon_{\mathrm{m}}(\boldsymbol{m}_h^{i+1}) - \varepsilon_{\mathrm{m}}(\Pi_h \boldsymbol{m}_h^{i+1})], \varepsilon(\boldsymbol{u}_h^{i+1}) - \varepsilon(\boldsymbol{u}_h^{i})\rangle$$

$$\overset{(51)}{=} \frac{1}{2}\left\|\varepsilon(\boldsymbol{u}_h^{i+1}) - \varepsilon_{\mathrm{m}}(\boldsymbol{m}_h^{i+1})\right\|_{\mathbb{C}}^2 - \frac{1}{2}\left\|\varepsilon(\boldsymbol{u}_h^{i}) - \varepsilon_{\mathrm{m}}(\boldsymbol{m}_h^{i})\right\|_{\mathbb{C}}^2$$

$$\quad + \frac{1}{2}\left\|[\varepsilon(\boldsymbol{u}_h^{i+1}) - \varepsilon_{\mathrm{m}}(\boldsymbol{m}_h^{i+1})] - [\varepsilon(\boldsymbol{u}_h^{i}) - \varepsilon_{\mathrm{m}}(\boldsymbol{m}_h^{i})]\right\|_{\mathbb{C}}^2$$

$$\quad + \langle \mathbb{C} : [\varepsilon(\boldsymbol{u}_h^{i+1}) - \varepsilon_{\mathrm{m}}(\boldsymbol{m}_h^{i+1})], \varepsilon_{\mathrm{m}}(\boldsymbol{m}_h^{i+1}) - \varepsilon_{\mathrm{m}}(\boldsymbol{m}_h^{i})\rangle$$

$$\quad + \langle \mathbb{C} : [\varepsilon_{\mathrm{m}}(\boldsymbol{m}_h^{i+1}) - \varepsilon_{\mathrm{m}}(\Pi_h \boldsymbol{m}_h^{i+1})], \varepsilon(\boldsymbol{u}_h^{i+1}) - \varepsilon(\boldsymbol{u}_h^{i})\rangle,$$

respectively. Altogether, we thus obtain

$$\mathcal{E}_{\mathrm{el}}[\boldsymbol{u}_h^{i+1}, \boldsymbol{m}_h^{i+1}] + \frac{1}{2}\left\|\mathrm{d}_t \boldsymbol{u}_h^{i+1}\right\|^2 - \mathcal{E}_{\mathrm{el}}[\boldsymbol{u}_h^{i}, \boldsymbol{m}_h^{i}] - \frac{1}{2}\left\|\mathrm{d}_t \boldsymbol{u}_h^{i}\right\|^2$$

$$= -\frac{1}{2}\left\|\mathrm{d}_t \boldsymbol{u}_h^{i+1} - \mathrm{d}_t \boldsymbol{u}_h^{i}\right\|^2 - \frac{1}{2}\left\|[\varepsilon(\boldsymbol{u}_h^{i+1}) - \varepsilon_{\mathrm{m}}(\boldsymbol{m}_h^{i+1})] - [\varepsilon(\boldsymbol{u}_h^{i}) - \varepsilon_{\mathrm{m}}(\boldsymbol{m}_h^{i})]\right\|_{\mathbb{C}}^2$$

$$\quad - \langle \mathbb{C} : [\varepsilon(\boldsymbol{u}_h^{i+1}) - \varepsilon_{\mathrm{m}}(\boldsymbol{m}_h^{i+1})], \varepsilon_{\mathrm{m}}(\boldsymbol{m}_h^{i+1}) - \varepsilon_{\mathrm{m}}(\boldsymbol{m}_h^{i})\rangle$$

$$\quad - \langle \mathbb{C} : [\varepsilon_{\mathrm{m}}(\boldsymbol{m}_h^{i+1}) - \varepsilon_{\mathrm{m}}(\Pi_h \boldsymbol{m}_h^{i+1})], \varepsilon(\boldsymbol{u}_h^{i+1}) - \varepsilon(\boldsymbol{u}_h^{i})\rangle.$$

(38)

Combining (36) and (38) yields

$$\mathcal{E}[\boldsymbol{u}_h^{i+1}, \boldsymbol{m}_h^{i+1}] + \frac{1}{2}\left\|\mathrm{d}_t \boldsymbol{u}_h^{i+1}\right\|^2 - \mathcal{E}[\boldsymbol{u}_h^{i}, \boldsymbol{m}_h^{i}] - \frac{1}{2}\left\|\mathrm{d}_t \boldsymbol{u}_h^{i}\right\|^2$$

$$= -\alpha k \left\|\boldsymbol{v}_h^{i}\right\|_h^2 - k^2(\theta - 1/2)\left\|\boldsymbol{\nabla}\boldsymbol{v}_h^{i}\right\|^2 + k\langle \boldsymbol{h}_{\mathrm{m}}[\boldsymbol{u}_h^{i}, \Pi_h \boldsymbol{m}_h^{i}], \boldsymbol{v}_h^{i}\rangle$$

$$\quad - \frac{1}{2}\left\|\mathrm{d}_t \boldsymbol{u}_h^{i+1} - \mathrm{d}_t \boldsymbol{u}_h^{i}\right\|^2 - \frac{1}{2}\left\|[\varepsilon(\boldsymbol{u}_h^{i+1}) - \varepsilon_{\mathrm{m}}(\boldsymbol{m}_h^{i+1})] - [\varepsilon(\boldsymbol{u}_h^{i}) - \varepsilon_{\mathrm{m}}(\boldsymbol{m}_h^{i})]\right\|_{\mathbb{C}}^2$$

$$\quad - \langle \mathbb{C} : [\varepsilon(\boldsymbol{u}_h^{i+1}) - \varepsilon_{\mathrm{m}}(\boldsymbol{m}_h^{i+1})], \varepsilon_{\mathrm{m}}(\boldsymbol{m}_h^{i+1}) - \varepsilon_{\mathrm{m}}(\boldsymbol{m}_h^{i})\rangle$$

$$\quad - \langle \mathbb{C} : [\varepsilon(\boldsymbol{m}_h^{i+1}) - \varepsilon_{\mathrm{m}}(\Pi_h \boldsymbol{m}_h^{i+1})], \varepsilon_{\mathrm{m}}(\boldsymbol{u}_h^{i+1}) - \varepsilon(\boldsymbol{u}_h^{i})\rangle$$

$$= -\alpha k \left\|\boldsymbol{v}_h^{i}\right\|_h^2 - D_{h,k}^i - E_{h,k}^i,$$

where, in the last identity, we have used the expression of $D_{h,k}^i$ in (24) and we have defined

$$E_{h,k}^i := \langle \mathbb{C} : [\varepsilon(\boldsymbol{u}_h^{i+1}) - \varepsilon_{\mathrm{m}}(\boldsymbol{m}_h^{i+1})], \varepsilon_{\mathrm{m}}(\boldsymbol{m}_h^{i+1}) - \varepsilon_{\mathrm{m}}(\boldsymbol{m}_h^{i})\rangle$$

$$\quad - k\langle \boldsymbol{h}_{\mathrm{m}}[\boldsymbol{u}_h^{i}, \Pi_h \boldsymbol{m}_h^{i}], \boldsymbol{v}_h^{i}\rangle$$

$$\quad + \langle \mathbb{C} : [\varepsilon_{\mathrm{m}}(\boldsymbol{m}_h^{i+1}) - \varepsilon_{\mathrm{m}}(\Pi_h \boldsymbol{m}_h^{i+1})], \varepsilon(\boldsymbol{u}_h^{i+1}) - \varepsilon(\boldsymbol{u}_h^{i})\rangle$$

To conclude the proof of (23), it remains to show that the latter coincides with (25). To this end, using the expression of the elastic field and Lemma A.4, we obtain

$$k\langle \boldsymbol{h}_{\mathrm{m}}[\boldsymbol{u}_h^{i}, \Pi_h \boldsymbol{m}_h^{i}], \boldsymbol{v}_h^{i}\rangle \overset{(7)}{=} 2k\langle \mathbb{Z}^{\top}\mathbb{C} : [\varepsilon(\boldsymbol{u}_h^{i}) - \varepsilon_{\mathrm{m}}(\Pi_h \boldsymbol{m}_h^{i})]\Pi_h \boldsymbol{m}_h^{i}, \boldsymbol{v}_h^{i}\rangle$$

$$\overset{(50)}{=} 2k\langle \mathbb{C} : [\varepsilon(\boldsymbol{u}_h^{i}) - \varepsilon_{\mathrm{m}}(\Pi_h \boldsymbol{m}_h^{i})], \mathbb{Z}(\Pi_h \boldsymbol{m}_h^{i} \otimes \boldsymbol{v}_h^{i})\rangle.$$

Moreover, from (20) and the minor symmetry of $\mathbb{Z}$, we get the expansion

$$\varepsilon_{\mathrm{m}}(\boldsymbol{m}_h^{i+1}) = \varepsilon_{\mathrm{m}}(\boldsymbol{m}_h^{i}) + 2k\,\mathbb{Z}(\boldsymbol{m}_h^{i} \otimes \boldsymbol{v}_h^{i}) + k^2 \varepsilon_{\mathrm{m}}(\boldsymbol{v}_h^{i}).$$

(39)

Altogether, it follows that

$$
\begin{aligned}
E^i_{h,k} &= k^2 \langle \mathbb{C} : [\boldsymbol{\varepsilon}(\boldsymbol{u}^{i+1}_h) - \boldsymbol{\varepsilon}_{\mathrm{m}}(\boldsymbol{m}^{i+1}_h)], \boldsymbol{\varepsilon}_{\mathrm{m}}(\boldsymbol{v}^i_h) \rangle \\
&\quad + 2k \langle \mathbb{C} : [\boldsymbol{\varepsilon}(\boldsymbol{u}^{i+1}_h) - \boldsymbol{\varepsilon}_{\mathrm{m}}(\boldsymbol{m}^{i+1}_h)], \mathbb{Z}(\boldsymbol{m}^i_h \otimes \boldsymbol{v}^i_h) \rangle \\
&\quad - 2k \langle \mathbb{C} : [\boldsymbol{\varepsilon}(\boldsymbol{u}^{i}_h) - \boldsymbol{\varepsilon}_{\mathrm{m}}(\boldsymbol{m}^{i}_h)], \mathbb{Z}(\Pi_h \boldsymbol{m}^i_h \otimes \boldsymbol{v}^i_h) \rangle \\
&\quad + \langle \mathbb{C} : [\boldsymbol{\varepsilon}_{\mathrm{m}}(\boldsymbol{m}^{i+1}_h) - \boldsymbol{\varepsilon}_{\mathrm{m}}(\Pi_h \boldsymbol{m}^{i+1}_h)], \boldsymbol{\varepsilon}(\boldsymbol{u}^{i+1}_h) - \boldsymbol{\varepsilon}(\boldsymbol{u}^i_h) \rangle \\
&= k^2 \langle \mathbb{C} : [\boldsymbol{\varepsilon}(\boldsymbol{u}^{i+1}_h) - \boldsymbol{\varepsilon}_{\mathrm{m}}(\boldsymbol{m}^{i+1}_h)], \boldsymbol{\varepsilon}_{\mathrm{m}}(\boldsymbol{v}^i_h) \rangle \\
&\quad + 2k \langle \mathbb{C} : \{ [\boldsymbol{\varepsilon}(\boldsymbol{u}^{i+1}_h) - \boldsymbol{\varepsilon}_{\mathrm{m}}(\boldsymbol{m}^{i+1}_h)] - [\boldsymbol{\varepsilon}(\boldsymbol{u}^{i}_h) - \boldsymbol{\varepsilon}_{\mathrm{m}}(\boldsymbol{m}^{i}_h)] \}, \mathbb{Z}(\boldsymbol{m}^i_h \otimes \boldsymbol{v}^i_h) \rangle \\
&\quad + 2k \langle \mathbb{C} : [\boldsymbol{\varepsilon}(\boldsymbol{u}^{i}_h) - \boldsymbol{\varepsilon}_{\mathrm{m}}(\boldsymbol{m}^{i}_h)], \mathbb{Z}[(\boldsymbol{m}^i_h - \Pi_h \boldsymbol{m}^i_h) \otimes \boldsymbol{v}^i_h] \rangle \\
&\quad + \langle \mathbb{C} : [\boldsymbol{\varepsilon}_{\mathrm{m}}(\boldsymbol{m}^{i+1}_h) - \boldsymbol{\varepsilon}_{\mathrm{m}}(\Pi_h \boldsymbol{m}^{i+1}_h)], \boldsymbol{\varepsilon}(\boldsymbol{u}^{i+1}_h) - \boldsymbol{\varepsilon}(\boldsymbol{u}^i_h) \rangle.
\end{aligned}
$$

This shows (25) and concludes the proof. $\quad\square$

6.3. Stability

We now prove Proposition 4.6 showing unconditional stability of Algorithm 4.1 and an estimate of the violation of the unit length constraint. For the sake of clarity, we split the proof into several lemmas.

An immediate consequence of the projection-free update (19) is the following L^2-bound for the approximate magnetisations.

Lemma 6.2. *For every integer $1 \le j \le N$, it holds that*

$$
\left\| \boldsymbol{m}^j_h \right\|^2 \le C_1 \left(1 + k^2 \sum_{i=0}^{j-1} \left\| \boldsymbol{v}^i_h \right\|^2 \right),
\tag{40}
$$

$$
\left\| \mathcal{I}_h \big[\left| \boldsymbol{m}^j_h \right|^2 \big] - 1 \right\|_{L^1(\Omega)} \le C_2 k^2 \sum_{i=0}^{j-1} \left\| \boldsymbol{v}^i_h \right\|^2.
\tag{41}
$$

where $C_1, C_2 > 0$ are constants depending the shape-regularity parameter of $\mathcal{T}_h$ (C_1 depends also on $|\Omega|$).

Proof. We follow [12]. Starting from (20) and noting that $\boldsymbol{v}^i_h \in \boldsymbol{\mathcal{K}}_h[\boldsymbol{m}^i_h]$, we have for each $z \in \mathcal{N}_h$ that for every $0 \le i \le j - 1$

$$
\left| \boldsymbol{m}^{i+1}_h(z) \right|^2 = \left| \boldsymbol{m}^i_h(z) \right|^2 + k^2 \left| \boldsymbol{v}^i_h(z) \right|^2.
$$

Inductively, starting with $|\boldsymbol{m}^0_h(z)| = 1$, we deduce that

$$
|\boldsymbol{m}^j_h(z)|^2 = 1 + k^2 \sum_{i=0}^{j-1} |\boldsymbol{v}^i_h(z)|^2.
$$

Then, noting that $\|1\| = |\Omega|^{1/2}$ and using (33) yields (40) (for a suitable constant $C_1 > 0$ we do not explicitly compute). The same argument shows (41). $\quad\square$

We also have the following estimate of all quantities involving the magnetisation.

Lemma 6.3. *For every integer $1 \le j \le N$, it holds that*

$$
\left\| \nabla \boldsymbol{m}^j_h \right\|^2 + k \sum_{i=0}^{j-1} \left\| \boldsymbol{v}^i_h \right\|^2 + \left(\theta - \frac{1}{2} \right) k^2 \sum_{i=0}^{j-1} \left\| \nabla \boldsymbol{v}^i_h \right\|^2 \le C_3 \left[\left\| \nabla \boldsymbol{m}^0_h \right\|^2 + k \sum_{i=0}^{j-1} \left(1 + \left\| \boldsymbol{\varepsilon}(\boldsymbol{u}^i_h) \right\|^2 \right) \right],
\tag{42}
$$

where $C_3 > 0$ depends only on α, $|\Omega|$, $\|\mathbb{Z}\|_{\boldsymbol{L}^\infty(\Omega)}$, and $\|\mathbb{C}\|_{\boldsymbol{L}^\infty(\Omega)}$.

Proof. Let $1 \le j \le N$ be an integer. Starting from (36) (cf. the proof of Proposition 4.4), we sum up from 0 to $j - 1$ to obtain

$$
\frac{1}{2} \left\| \nabla \boldsymbol{m}^j_h \right\|^2 + \alpha k \sum_{i=0}^{j-1} \left\| \boldsymbol{v}^i_h \right\|^2_h + \left(\theta - \frac{1}{2} \right) k^2 \sum_{i=0}^{j-1} \left\| \nabla \boldsymbol{v}^i_h \right\|^2 = \frac{1}{2} \left\| \nabla \boldsymbol{m}^0_h \right\|^2 + k \sum_{i=0}^{j-1} \langle \boldsymbol{h}_{\mathrm{m}}[\boldsymbol{u}^i_h, \Pi_h \boldsymbol{m}^i_h], \boldsymbol{v}^i_h \rangle.
$$

Using Lemma 6.1, we can estimate the term involving the elastic field for some $v > 0$ by

$$
\left| \langle \boldsymbol{h}_{\mathrm{m}}[\boldsymbol{u}^i_h, \Pi_h \boldsymbol{m}^i_h], \boldsymbol{v}^i_h \rangle \right| \le \frac{1}{4v} \left\| \boldsymbol{h}_{\mathrm{m}}[\boldsymbol{u}^i_h, \Pi_h \boldsymbol{m}^i_h] \right\|^2 + v \left\| \boldsymbol{v}^i_h \right\|^2 \overset{(35)}{\le} \frac{2}{v} \|\mathbb{Z}\|^2_{\boldsymbol{L}^\infty(\Omega)} \|\mathbb{C}\|^2_{\boldsymbol{L}^\infty(\Omega)} \left(\left\| \boldsymbol{\varepsilon}(\boldsymbol{u}^i_h) \right\|^2 + \|\mathbb{Z}\|^2_{\boldsymbol{L}^\infty(\Omega)} |\Omega| \right) + v \left\| \boldsymbol{v}^i_h \right\|^2.
$$

Then we get

$$\frac{1}{2}\left\|\boldsymbol{\nabla m}_h^j\right\|^2 + \alpha k \sum_{i=0}^{j-1}\left\|\boldsymbol{v}_h^i\right\|_h^2 + \left(\theta - \frac{1}{2}\right)k^2\sum_{i=0}^{j-1}\left\|\boldsymbol{\nabla v}_h^i\right\|^2 \le \frac{1}{2}\left\|\boldsymbol{\nabla m}_h^0\right\|^2$$

$$+ \frac{2k}{\nu}\sum_{i=0}^{j-1}\|\mathbb{Z}\|_{\boldsymbol{L}^\infty(\Omega)}^2\|\mathbb{C}\|_{\boldsymbol{L}^\infty(\Omega)}^2\left(\left\|\boldsymbol{\varepsilon}(\boldsymbol{u}_h^i)\right\|^2 + \|\mathbb{Z}\|_{\boldsymbol{L}^\infty(\Omega)}^2|\Omega|\right) + \nu k\sum_{i=0}^{j-1}\left\|\boldsymbol{v}_h^i\right\|^2.$$

Using (30) and choosing $\nu = \alpha/2$ yields (42) (for a suitable constant $C_3 > 0$ which we do not compute explicitly). □

In the following lemma, we show that the magnetostrain is Lipschitz continuous with respect to the magnetisation (the use of the nodal projection is exploited here).

Lemma 6.4. *For all* $\boldsymbol{m}_{h,1}, \boldsymbol{m}_{h,2} \in S^1(\mathcal{T}_h)^3$ *satisfying* $\left|\boldsymbol{m}_{h,\ell}(z)\right| \ge 1$ *for all* $\ell = 1, 2$ *and* $z \in \mathcal{N}_h$, *it holds that*

$$\left\|\boldsymbol{\varepsilon}_{\mathrm{m}}(\Pi_h\boldsymbol{m}_{h,1}) - \boldsymbol{\varepsilon}_{\mathrm{m}}(\Pi_h\boldsymbol{m}_{h,2})\right\| \le C_{\mathrm{m}}\left\|\boldsymbol{m}_{h,1} - \boldsymbol{m}_{h,2}\right\|, \tag{43}$$

where $C_{\mathrm{m}} > 0$ *depends only on* $\|\mathbb{Z}\|_{\boldsymbol{L}^\infty(\Omega)}$ *and the shape-regularity parameter of* $\mathcal{T}_h$.

Proof. Straightforward calculations exploiting the boundedness guaranteed by the nodal projection, i.e. $\left\|\Pi_h\boldsymbol{m}_{h,1}\right\|_{\boldsymbol{L}^\infty(\Omega)} = \left\|\Pi_h\boldsymbol{m}_{h,2}\right\|_{\boldsymbol{L}^\infty(\Omega)} = 1$, show that

$$\left\|\boldsymbol{\varepsilon}_{\mathrm{m}}(\Pi_h\boldsymbol{m}_{h,1}) - \boldsymbol{\varepsilon}_{\mathrm{m}}(\Pi_h\boldsymbol{m}_{h,2})\right\| \lesssim \left\|\Pi_h\boldsymbol{m}_{h,1} - \Pi_h\boldsymbol{m}_{h,2}\right\|,$$

where the hidden constant depends on $\|\mathbb{Z}\|_{\boldsymbol{L}^\infty(\Omega)}$. From the norm equivalence in [11, Lemma 3.4]) and the fact that the projection onto the sphere is non-expanding (i.e. Lipschitz continuous with constant 1), it follows that

$$\left\|\Pi_h\boldsymbol{m}_{h,1} - \Pi_h\boldsymbol{m}_{h,2}\right\| \lesssim \left\|\boldsymbol{m}_{h,1} - \boldsymbol{m}_{h,2}\right\|,$$

where the hidden constant depends on the shape-regularity of the mesh. Combining the above two estimates yields the desired result, where $C_{\mathrm{m}} > 0$ is the product of the two constants hidden above. □

Lemma 6.5. *For every integer* $1 \le j \le N$, *the following estimate holds*

$$\left\|\mathrm{d}_t\boldsymbol{u}_h^j\right\|^2 + \left\|\boldsymbol{\varepsilon}(\boldsymbol{u}_h^j)\right\|^2 + \sum_{i=0}^{j-1}\left\|\mathrm{d}_t\boldsymbol{u}_h^{i+1} - \mathrm{d}_t\boldsymbol{u}_h^i\right\|^2 + \sum_{i=0}^{j-1}\left\|\boldsymbol{\varepsilon}(\boldsymbol{u}_h^{i+1}) - \boldsymbol{\varepsilon}(\boldsymbol{u}_h^i)\right\|^2$$

$$\le C_4\left[1 + \left\|\dot{\boldsymbol{u}}_h^0\right\|^2 + \left\|\boldsymbol{\varepsilon}(\boldsymbol{u}_h^0)\right\|^2 + \left\|\boldsymbol{\nabla m}_h^0\right\|^2 + k\sum_{i=0}^{j-1}\left(1 + \left\|\boldsymbol{\varepsilon}(\boldsymbol{u}_h^i)\right\|^2\right)\right], \tag{44}$$

where $C_4 > 0$ *depends only on the shape-regularity parameter of* $\mathcal{T}_h$ *and the problem data* α, Ω, $\mathbb{C}$, $\mathbb{Z}$, $\boldsymbol{f}$ *and* $\boldsymbol{g}$.

Proof. Let $1 \le j \le N$ be an integer. Starting from (37) (cf. the proof of Proposition 4.4), summing up from 0 to $j - 1$, we have

$$\frac{1}{2}\left\|\mathrm{d}_t\boldsymbol{u}_h^j\right\|^2 - \frac{1}{2}\left\|\mathrm{d}_t\boldsymbol{u}_h^0\right\|^2 + \frac{1}{2}\sum_{i=0}^{j-1}\left\|\mathrm{d}_t\boldsymbol{u}_h^{i+1} - \mathrm{d}_t\boldsymbol{u}_h^i\right\|^2 + \sum_{i=0}^{j-1}\langle\mathbb{C}:\boldsymbol{\varepsilon}(\boldsymbol{u}_h^{i+1}),\boldsymbol{\varepsilon}(\boldsymbol{u}_h^{i+1}) - \boldsymbol{\varepsilon}(\boldsymbol{u}_h^i)\rangle$$

$$= \sum_{i=0}^{j-1}\langle\mathbb{C}:\boldsymbol{\varepsilon}_{\mathrm{m}}(\Pi_h\boldsymbol{m}_h^{i+1}),\boldsymbol{\varepsilon}(\boldsymbol{u}_h^{i+1}) - \boldsymbol{\varepsilon}(\boldsymbol{u}_h^i)\rangle + \langle\boldsymbol{f},\boldsymbol{u}_h^j\rangle - \langle\boldsymbol{f},\boldsymbol{u}_h^0\rangle + \langle\boldsymbol{g},\boldsymbol{u}_h^j\rangle_{\Gamma_N} - \langle\boldsymbol{g},\boldsymbol{u}_h^0\rangle_{\Gamma_N}.$$

Applying Lemma A.5 to the last term on the left-hand side and rearranging we have

$$\frac{1}{2}\left\|\mathrm{d}_t\boldsymbol{u}_h^j\right\|^2 + \frac{1}{2}\left\|\boldsymbol{\varepsilon}(\boldsymbol{u}_h^j)\right\|_{\mathbb{C}}^2 + \frac{1}{2}\sum_{i=0}^{j-1}\left\|\mathrm{d}_t\boldsymbol{u}_h^{i+1} - \mathrm{d}_t\boldsymbol{u}_h^i\right\|^2 + \frac{1}{2}\sum_{i=0}^{j-1}\left\|\boldsymbol{\varepsilon}(\boldsymbol{u}_h^{i+1}) - \boldsymbol{\varepsilon}(\boldsymbol{u}_h^i)\right\|_{\mathbb{C}}^2$$

$$= \frac{1}{2}\left\|\mathrm{d}_t\boldsymbol{u}_h^0\right\|^2 + \frac{1}{2}\left\|\boldsymbol{\varepsilon}(\boldsymbol{u}_h^0)\right\|_{\mathbb{C}}^2 + \sum_{i=0}^{j-1}\langle\mathbb{C}:\boldsymbol{\varepsilon}_{\mathrm{m}}(\Pi_h\boldsymbol{m}_h^{i+1}),\boldsymbol{\varepsilon}(\boldsymbol{u}_h^{i+1}) - \boldsymbol{\varepsilon}(\boldsymbol{u}_h^i)\rangle + \langle\boldsymbol{f},\boldsymbol{u}_h^j\rangle - \langle\boldsymbol{f},\boldsymbol{u}_h^0\rangle + \langle\boldsymbol{g},\boldsymbol{u}_h^j\rangle_{\Gamma_N} - \langle\boldsymbol{g},\boldsymbol{u}_h^0\rangle_{\Gamma_N}.$$

The term involving the magnetostrain can be estimated as

$$\sum_{i=0}^{j-1}\langle \mathbb{C} : \varepsilon_{\mathrm{m}}(\Pi_h \boldsymbol{m}_h^{i+1}), \varepsilon(\boldsymbol{u}_h^{i+1}) - \varepsilon(\boldsymbol{u}_h^i)\rangle$$

$$= \langle \varepsilon_{\mathrm{m}}(\Pi_h \boldsymbol{m}_h^j), \mathbb{C} : \varepsilon(\boldsymbol{u}_h^j)\rangle - \langle \varepsilon_{\mathrm{m}}(\Pi_h \boldsymbol{m}_h^1), \mathbb{C} : \varepsilon(\boldsymbol{u}_h^0)\rangle - k\sum_{i=1}^{j-1}\langle \mathrm{d}_t\varepsilon_{\mathrm{m}}(\Pi_h \boldsymbol{m}_h^{i+1}), \mathbb{C} : \varepsilon(\boldsymbol{u}_h^i)\rangle$$

$$\leq \left\|\varepsilon_{\mathrm{m}}(\Pi_h \boldsymbol{m}_h^j)\right\|^2 + \frac{1}{4}\left\|\varepsilon(\boldsymbol{u}_h^j)\right\|_{\mathbb{C}}^2 + \frac{1}{2}\left\|\varepsilon_{\mathrm{m}}(\Pi_h \boldsymbol{m}_h^1)\right\|_{\mathbb{C}}^2 + \frac{1}{2}\left\|\varepsilon(\boldsymbol{u}_h^0)\right\|_{\mathbb{C}}^2$$

$$+ \frac{k}{2}\sum_{i=1}^{j-1}\left\|\mathrm{d}_t\varepsilon_{\mathrm{m}}(\Pi_h \boldsymbol{m}_h^{i+1})\right\|^2 + \frac{k}{2}\sum_{i=1}^{j-1}\left\|\varepsilon(\boldsymbol{u}_h^i)\right\|_{\mathbb{C}}^2$$

$$\leq \frac{3}{2}\|\mathbb{Z}\|_{\boldsymbol{L}^\infty(\Omega)}^2 |\Omega| + \frac{1}{4}\left\|\varepsilon(\boldsymbol{u}_h^j)\right\|_{\mathbb{C}}^2 + \frac{1}{2}\left\|\varepsilon(\boldsymbol{u}_h^0)\right\|_{\mathbb{C}}^2$$

$$+ \frac{k}{2}\sum_{i=1}^{j-1}\left\|\mathrm{d}_t\varepsilon_{\mathrm{m}}(\Pi_h \boldsymbol{m}_h^{i+1})\right\|^2 + \frac{k}{2}\sum_{i=1}^{j-1}\left\|\varepsilon(\boldsymbol{u}_h^i)\right\|_{\mathbb{C}}^2.$$

Using Lemma 6.4, we get

$$\left\|\mathrm{d}_t\varepsilon_{\mathrm{m}}(\Pi_h \boldsymbol{m}_h^{i+1})\right\| = \frac{1}{k}\left\|\varepsilon_{\mathrm{m}}(\Pi_h \boldsymbol{m}_h^{i+1}) - \varepsilon_{\mathrm{m}}(\Pi_h \boldsymbol{m}_h^i)\right\| \overset{(43)}{\leq} \frac{1}{k}C_{\mathrm{m}}\left\|\boldsymbol{m}_h^{i+1} - \boldsymbol{m}_h^i\right\| = C_{\mathrm{m}}\left\|\boldsymbol{v}_h^i\right\|.$$

It follows that

$$\frac{k}{2}\sum_{i=1}^{j-1}\left\|\mathrm{d}_t\varepsilon_{\mathrm{m}}(\Pi_h \boldsymbol{m}_h^{i+1})\right\|^2 \leq \frac{C_{\mathrm{m}}^2 k}{2}\sum_{i=1}^{j-1}\left\|\boldsymbol{v}_h^i\right\|^2.$$

Moreover, for every $\delta > 0$ we have that

$$\left|\langle \boldsymbol{f}, \boldsymbol{u}_h^j\rangle + \langle \boldsymbol{g}, \boldsymbol{u}_h^j\rangle_{\Gamma_N}\right| \leq C_{\mathrm{KPC}}(\|\boldsymbol{f}\| + \|\boldsymbol{g}\|_{\Gamma_N})\left\|\varepsilon(\boldsymbol{u}_h^j)\right\|_{\mathbb{C}} \leq \frac{C_{\mathrm{KPC}}^2}{4\delta}(\|\boldsymbol{f}\| + \|\boldsymbol{g}\|_{\Gamma_N})^2 + \delta\left\|\varepsilon(\boldsymbol{u}_h^j)\right\|_{\mathbb{C}}^2,$$

where $C_{\mathrm{KPC}} > 0$ is a constant depending only on $|\Omega|$ and $\mathbb{C}$ (a combination of the continuity constant of the trace operator $H^1(\Omega) \to L^2(\Gamma_N)$, the constants appearing in Poincaré's and Korn's inequalities, and the equivalence constant in the norm equivalence $\|\cdot\| \simeq \|\cdot\|_{\mathbb{C}}$). Overall, choosing $\delta = 1/8$ and recalling that $\mathrm{d}_t\boldsymbol{u}_h^0 = \dot{\boldsymbol{u}}_h^0$, we obtain

$$\frac{1}{2}\left\|\mathrm{d}_t\boldsymbol{u}_h^j\right\|^2 + \frac{1}{8}\left\|\varepsilon(\boldsymbol{u}_h^j)\right\|_{\mathbb{C}}^2 + \frac{1}{2}\sum_{i=0}^{j-1}\left\|\mathrm{d}_t\boldsymbol{u}_h^{i+1} - \mathrm{d}_t\boldsymbol{u}_h^i\right\|^2 + \frac{1}{2}\sum_{i=0}^{j-1}\left\|\varepsilon(\boldsymbol{u}_h^{i+1}) - \varepsilon(\boldsymbol{u}_h^i)\right\|_{\mathbb{C}}^2 \leq \frac{3}{2}\|\mathbb{Z}\|_{\boldsymbol{L}^\infty(\Omega)}^2 |\Omega|$$

$$+ 2C_{\mathrm{KPC}}^2(\|\boldsymbol{f}\| + \|\boldsymbol{g}\|_{\Gamma_N})^2 + \frac{1}{2}\left\|\dot{\boldsymbol{u}}_h^0\right\|^2 + \left[1 + C_{\mathrm{KPC}}\left(\|\boldsymbol{f}\| + \|\boldsymbol{g}\|_{\Gamma_N}\right)\right]\left\|\varepsilon(\boldsymbol{u}_h^0)\right\|_{\mathbb{C}}^2 + \frac{k}{2}\sum_{i=1}^{j-1}\left\|\varepsilon(\boldsymbol{u}_h^i)\right\|_{\mathbb{C}}^2 + \frac{C_{\mathrm{m}}^2 k}{2}\sum_{i=1}^{j-1}\left\|\boldsymbol{v}_h^i\right\|^2.$$

Applying Lemma 6.3 to estimate the last term on the right-hand side, we obtain (44) (for a suitable constant $C_4 > 0$ which we do not compute explicitly). $\quad\square$

We are now in a position to prove Proposition 4.6.

Proof of Proposition 4.6. We apply Lemmas 6.2, 6.3 and 6.5. Combining (40), (42) and (44), we obtain

$$\left\|\mathrm{d}_t\boldsymbol{u}_h^j\right\|^2 + \left\|\varepsilon(\boldsymbol{u}_h^j)\right\|^2 + \sum_{i=0}^{j-1}\left\|\mathrm{d}_t\boldsymbol{u}_h^{i+1} - \mathrm{d}_t\boldsymbol{u}_h^i\right\|^2 + \sum_{i=0}^{j-1}\left\|\varepsilon(\boldsymbol{u}_h^{i+1}) - \varepsilon(\boldsymbol{u}_h^i)\right\|^2$$

$$+ \left\|\boldsymbol{m}_h^j\right\|_{\boldsymbol{H}^1(\Omega)}^2 + (1 - C_1 k)k\sum_{i=0}^{j-1}\left\|\boldsymbol{v}_h^i\right\|^2 + \left(\theta - \frac{1}{2}\right)k^2\sum_{i=0}^{j-1}\left\|\nabla\boldsymbol{v}_h^i\right\|^2$$

$$\leq C_1 + C_4 + (C_3 + C_4)\left\|\nabla\boldsymbol{m}_h^0\right\|^2 + C_4\left\|\dot{\boldsymbol{u}}_h^0\right\|^2 + C_4\left\|\varepsilon(\boldsymbol{u}_h^0)\right\|^2$$

$$+ (C_3 + C_4)k\sum_{i=0}^{j-1}\left(1 + \left\|\varepsilon(\boldsymbol{u}_h^i)\right\|^2\right)$$

$$\leq C_1 + C_4 + (C_3 + C_4)\left\|\nabla\boldsymbol{m}_h^0\right\|^2 + C_4\left\|\dot{\boldsymbol{u}}_h^0\right\|^2 + C_4\left\|\varepsilon(\boldsymbol{u}_h^0)\right\|^2$$

$$+ (C_3 + C_4)T + (C_3 + C_4)k\sum_{i=0}^{j-1}\left\|\varepsilon(\boldsymbol{u}_h^i)\right\|^2,$$

where in the last estimate we have used that $kj \leq T$. If the time-step size k is sufficiently small, the coefficients in front of all terms on the left-hand side are strictly positive. Given the boundedness of the approximate initial data guaranteed by assumption (26), the desired stability estimate (27) then follows from the discrete Grönwall lemma; see e.g. [49, Lemma 10.5]. Finally, (28) follows from (27) and (41). This concludes the proof. □

6.4. Convergence

The proof of convergence of Algorithm 4.1 (Theorem 4.7(i)) follows the standard argument to prove existence of weak solutions for parabolic equations (uniform boundedness of Galerkin approximations, extraction of subsequences with suitable convergence properties, identification of the limit with a weak solution of the problem; see, e.g., [27, Section 7.1]) and thus has the same structure as the one which proves the convergence of [15, Algorithm 4.1]. Therefore, in the upcoming analysis, we will provide only a sketch of the steps of the proof that can be found in [15]. However, we will present in detail the (non-obvious) steps that we have to perform to cope with the partial omission of the nodal projection (for which we borrow ideas from [1,12]) and to prove our novel energy estimate.

We start the proof with showing the following lemma, which provides an estimate of the L^p-norm ($p \geq 1$) of the difference between the approximate magnetisations generated by Algorithm 4.1 and their nodal projections.

Lemma 6.6. *Let $p \in [1, \infty)$. For all integers $1 \leq j \leq N$, it holds that*

$$\left\| \boldsymbol{m}_h^j - \Pi_h \boldsymbol{m}_h^j \right\|_{\boldsymbol{L}^p(\Omega)} \leq C \frac{T^{1-1/p}}{2} k^{1+1/p} \sum_{i=0}^{j-1} \left\| \boldsymbol{v}_h^i \right\|_{\boldsymbol{L}^{2p}(\Omega)}^2, \tag{45}$$

where $C > 0$ depends only on the shape-regularity of $\mathcal{T}_h$.

Proof. Let $1 \leq j \leq N$ be an integer. For all $z \in \mathcal{N}_h$, we have that

$$\left| \boldsymbol{m}_h^j(z) - \Pi_h \boldsymbol{m}_h^j(z) \right| = \left| \boldsymbol{m}_h^j(z) - \frac{\boldsymbol{m}_h^j(z)}{\left| \boldsymbol{m}_h^j(z) \right|} \right| = \left| \boldsymbol{m}_h^j(z) \right| - 1 = \frac{\left| \boldsymbol{m}_h^j(z) \right|^2 - 1}{\left| \boldsymbol{m}_h^j(z) \right| + 1} \leq \frac{1}{2} \left(\left| \boldsymbol{m}_h^j(z) \right|^2 - 1 \right) = \frac{k^2}{2} \sum_{i=0}^{j-1} \left| \boldsymbol{v}_h^i(z) \right|^2.$$

If $p = 1$, the norm equivalence (33) immediately yields (45). If $p > 1$, applying (33) twice and using the convexity of x^p for $x > 0$ as well as $jk \leq T$, we obtain

$$\left\| \boldsymbol{m}_h^j - \Pi_h \boldsymbol{m}_h^j \right\|_{\boldsymbol{L}^p(\Omega)}^p \lesssim \sum_{z \in \mathcal{N}_h} h_z^3 \left| \boldsymbol{m}_h^j(z) - \Pi_h \boldsymbol{m}_h^j(z) \right|^p \leq \sum_{z \in \mathcal{N}_h} h_z^3 \left(\frac{k^2}{2} \sum_{i=0}^{j-1} \left| \boldsymbol{v}_h^i(z) \right|^2 \right)^p$$

$$\leq \sum_{z \in \mathcal{N}_h} h_z^3 \frac{k^{2p}}{2^p} j^{p-1} \sum_{i=0}^{j-1} \left| \boldsymbol{v}_h^i(z) \right|^{2p} \leq \sum_{z \in \mathcal{N}_h} h_z^3 \frac{k^{p+1}}{2^p} T^{p-1} \sum_{i=0}^{j-1} \left| \boldsymbol{v}_h^i(z) \right|^{2p}$$

$$\lesssim \frac{k^{p+1}}{2^p} T^{p-1} \sum_{i=0}^{j-1} \left\| \boldsymbol{v}_h^i \right\|_{\boldsymbol{L}^{2p}(\Omega)}^{2p},$$

where the hidden constants depend only on the shape-regularity of $\mathcal{T}_h$. Then, (45) for $p > 1$ follows from the inequality $\|\cdot\|_{\ell^p} \leq \|\cdot\|_{\ell^1}$ satisfied by the p-norms in finite dimensions. This concludes the proof. □

Now, let $\{\boldsymbol{m}_{hk}\}$, $\{\boldsymbol{m}_{hk}^\pm\}$, $\{\boldsymbol{v}_{hk}^-\}$, $\{\boldsymbol{u}_{hk}\}$, $\{\boldsymbol{u}_{hk}^\pm\}$, $\{\dot{\boldsymbol{u}}_{hk}\}$, $\{\dot{\boldsymbol{u}}_{hk}^\pm\}$ be the time reconstructions defined according to (16) using the approximations $\{(\boldsymbol{u}_h^i, \boldsymbol{m}_h^i)\}_{0 \leq i \leq N}$ generated by Algorithm 4.1. In the following lemma, we show that the uniform stability established in Proposition 4.6 allows us to extract convergent subsequences from the sequences of time reconstructions.

Lemma 6.7. *Under the assumptions of Theorem 4.7(i), there exist $\boldsymbol{u} \in L^\infty(0, T; \boldsymbol{H}_D^1(\Omega))$ with $\partial_t \boldsymbol{u} \in L^\infty(0, T; \boldsymbol{L}^2(\Omega))$ and $\boldsymbol{m} \in L^\infty(0, T; \boldsymbol{H}^1(\Omega; \mathbb{S}^2))$ with $\partial_t \boldsymbol{m} \in L^2(0, T; \boldsymbol{L}^2(\Omega))$ such that, upon extraction of (non-relabelled) subsequences, we have the following convergence results:*

$$\boldsymbol{u}_{hk} \rightharpoonup \boldsymbol{u} \quad \text{in } \boldsymbol{H}^1(\Omega_T), \tag{46a}$$

$$\boldsymbol{u}_{hk}, \boldsymbol{u}_{hk}^\pm \overset{*}{\rightharpoonup} \boldsymbol{u} \quad \text{in } L^\infty(0, T; \boldsymbol{H}^1(\Omega)), \tag{46b}$$

$$\boldsymbol{u}_{hk}, \boldsymbol{u}_{hk}^\pm \rightharpoonup \boldsymbol{u} \quad \text{in } L^2(0, T; \boldsymbol{H}^1(\Omega)), \tag{46c}$$

$$\boldsymbol{u}_{hk}, \boldsymbol{u}_{hk}^\pm \to \boldsymbol{u} \quad \text{in } \boldsymbol{L}^2(\Omega_T), \tag{46d}$$

$$\dot{\boldsymbol{u}}_{hk}, \dot{\boldsymbol{u}}_{hk}^\pm \overset{*}{\rightharpoonup} \partial_t \boldsymbol{u} \quad \text{in } L^\infty(0, T; \boldsymbol{L}^2(\Omega)), \tag{46e}$$

$$\dot{u}_{hk}, \dot{u}_{hk}^{\pm} \rightharpoonup \partial_t u \quad \text{in } L^2(\Omega_T), \tag{46f}$$

$$m_{hk} \rightharpoonup m \quad \text{in } H^1(\Omega_T), \tag{46g}$$

$$m_{hk} \rightarrow m \quad \text{in } H^s(\Omega_T) \text{ for all } s \in (0,1), \tag{46h}$$

$$m_{hk}, m_{hk}^{\pm} \overset{*}{\rightharpoonup} m \quad \text{in } L^\infty(0,T; H^1(\Omega)), \tag{46i}$$

$$m_{hk}, m_{hk}^{\pm} \rightharpoonup m \quad \text{in } L^2(0,T; H^1(\Omega)), \tag{46j}$$

$$m_{hk}, m_{hk}^{\pm} \rightarrow m \quad \text{in } L^2(0,T; H^s(\Omega)) \text{ for all } s \in (0,1), \tag{46k}$$

$$m_{hk}, m_{hk}^{\pm} \rightarrow m \quad \text{in } L^2(\Omega_T), \tag{46l}$$

$$m_{hk}, m_{hk}^{\pm} \rightarrow m \quad \text{pointwise a.e. in } \Omega_T, \tag{46m}$$

$$v_{hk}^{-} \rightharpoonup \partial_t m \quad \text{in } L^2(\Omega_T), \tag{46n}$$

as $h, k \to 0$.

Proof. Using the boundedness expressed in Proposition 4.6, we can successively extract weakly (-star) convergent subsequences (non-relabelled, with possibly different limits) from $\{u_{hk}\}$ and $\{u_{hk}^{\pm}\}$, from $\{\dot{u}_{hk}\}$ and $\{\dot{u}_{hk}^{\pm}\}$, from $\{m_{hk}\}$ and $\{m_{hk}^{\pm}\}$, and from $\{v_{hk}^{-}\}$.

Let $u \in H^1(\Omega_T)$ satisfy the weak convergence (46a). Owing to the continuous inclusions $H^1(\Omega_T) \subset L^2(0,T; H^1(\Omega)) \subset L^2(\Omega_T)$ and the compact inclusion $H^1(\Omega_T) \Subset L^2(\Omega_T)$, we obtain convergences (46c) and (46d). Moreover, from the continuous inclusion $L^\infty(0,T; H^1(\Omega)) \subset L^2(0,T; H^1(\Omega))$, we can identify the weak-star limit of $\{u_{hk}\}$ in $L^\infty(0,T; H^1(\Omega))$ with the weak limit in $L^2(0,T; H^1(\Omega))$, which shows (46b) for $\{u_{hk}\}$.

Let $m \in H^1(\Omega_T)$ satisfy the weak convergence (46g). Arguing as above and using a well-known result for convergence in L^p-spaces, we obtain convergences (46j), (46l) and (upon extraction of a further subsequence) (46m) for $\{m_{hk}\}$. The continuous inclusion $L^\infty(0,T; H^1(\Omega)) \subset L^2(0,T; H^1(\Omega))$, shows (46i) for $\{m_{hk}\}$.

Let $0 < s < 1$ be arbitrary. Since $H^s(\Omega_T) = [L^2(\Omega_T), H^1(\Omega_T)]_s$ and $L^2(0,T; H^s(\Omega)) = [L^2(\Omega_T), L^2(0,T; H^1(\Omega))]_s$, well-known results from interpolation theory (see, e.g., [16, Theorem 6.4.5 and Theorem 3.8.1] and [16, Theorem 5.1.2]) yield the compact embedding $H^1(\Omega_T) \Subset H^s(\Omega_T)$ and the continuous inclusion $H^s(\Omega_T) \subset L^2(0,T; H^s(\Omega))$. These in turn show convergences (46h) and (46k) for $\{m_{hk}\}$. Furthermore, (46n) follows directly from $\partial_t m_{hk} = v_{hk}^{-}$.

Overall, this shows the convergence results (46a)–(46d) and (46g)–(46n) for the sequences $\{u_{hk}\}$, $\{m_{hk}\}$ and $\{v_{hk}^{-}\}$. Using the same argument, one can obtain the same results for $\{u_{hk}^{\pm}\}$ and $\{m_{hk}^{\pm}\}$. Since the quantity

$$\sum_{i=0}^{j-1} \left\| m_h^{i+1} - m_h^i \right\|^2 + \sum_{i=0}^{j-1} \left\| u_h^{i+1} - u_h^i \right\|^2 + \sum_{i=0}^{j-1} \left\| d_t u_h^{i+1} - d_t u_h^i \right\| \tag{47}$$

is uniformly bounded, arguing as in [15, Lemma 5.7] we can show that the limits of $\{u_{hk}\}$ and $\{u_{hk}^{\pm}\}$ (resp. $\{m_{hk}\}$ and $\{m_{hk}^{\pm}\}$) coincide. The continuous inclusion $L^\infty(0,T; L^2(\Omega)) \subset L^2(0,T; L^2(\Omega)) = L^2(\Omega_T)$, the boundedness of the third term in (47) and the identity $\partial_t u_{hk} = \dot{u}_{hk}^{+}$ imply (46e)–(46f). Finally, the fact that m satisfies $|m| = 1$ a.e. in Ω follows from the available convergence results and (28). For the details, we refer to Step 3 of the proof of [29, Proposition 6]. This concludes the proof. $\square$

Let $\{\hat{m}_{hk}^{\pm}\}$ be the piecewise constant time reconstructions defined using the projection of the approximate magnetisations, i.e., $\hat{m}_{hk}^{-}(t) := \Pi_h m_h^i$ and $\hat{m}_{hk}^{+}(t) := \Pi_h m_h^{i+1}$ for all $i = 0, \dots, N_1$ and $t \in [t_i, t_{i+1})$ (cf. (16)).

In the following lemma, we establish further convergence results that will be needed to identify the limit (u, m) constructed in Lemma 6.7 with a weak solution of (4)–(6).

Lemma 6.8 (auxiliary convergences). *Under the assumptions of Theorem 4.7(i), upon extraction of a further (non-relabelled) subsequence, we have the following convergence results:*

$$\hat{m}_{hk}^{\pm} \overset{*}{\rightharpoonup} m \quad \text{in } L^\infty(0,T; H^1(\Omega)), \tag{48a}$$

$$\hat{m}_{hk}^{\pm} \rightharpoonup m \quad \text{in } L^2(0,T; H^1(\Omega)), \tag{48b}$$

$$\hat{m}_{hk}^{\pm} \rightarrow m \quad \text{in } L^2(\Omega_T), \tag{48c}$$

$$m_{hk}^{\pm} \otimes m_{hk}^{\pm} \rightarrow m \otimes m \quad \text{in } L^2(\Omega_T), \tag{48d}$$

$$\hat{m}_{hk}^{\pm} \otimes \hat{m}_{hk}^{\pm} \rightarrow m \otimes m \quad \text{in } L^2(\Omega_T), \tag{48e}$$

as $h, k \to 0$.

Proof. Firstly, we note that $\left\| \Pi_h m_h^i \right\|_{L^\infty(\Omega)} = 1$ and $\left\| \nabla \Pi_h m_h^i \right\| \lesssim \left\| \nabla m_h^i \right\| \lesssim 1$ for all $i = 0, \dots, N$ (the estimate of the gradient follows from (27) and (34)). We infer that the sequences $\{\hat{m}_{hk}^{\pm}\}$ are uniformly bounded in $L^\infty(0,T; H^1(\Omega))$ and arguing as in the proof of

Lemma 6.7, we can extract subsequences satisfying the convergence properties in (48a)–(48c). The fact that the limit is exactly the function $\boldsymbol{m} \in L^\infty(0,T;\boldsymbol{H}^1(\Omega;\mathbb{S}^2))$ constructed in Lemma 6.7 follows from Lemma 6.6 (applied $p = 1$), which guarantee that $\hat{\boldsymbol{m}}_{hk}^\pm \to \boldsymbol{m}$ in $\boldsymbol{L}^1(\Omega_T)$, which in turn implies that the limit functions in $\boldsymbol{L}^2(\Omega_T)$, $\boldsymbol{L}^2(0,T;\boldsymbol{H}^1(\Omega))$ and $\boldsymbol{L}^\infty(0,T;\boldsymbol{H}^1(\Omega))$ must necessarily be the same.

To show (48d)–(48e), we note that for $\boldsymbol{x}, \boldsymbol{y} \in \mathbb{R}^3$ we have

$$\boldsymbol{x} \otimes \boldsymbol{x} - \boldsymbol{y} \otimes \boldsymbol{y} = \frac{1}{2}[(\boldsymbol{x} + \boldsymbol{y}) \otimes (\boldsymbol{x} - \boldsymbol{y}) + (\boldsymbol{x} - \boldsymbol{y}) \otimes (\boldsymbol{x} + \boldsymbol{y})].$$

Let $3/4 \leq s < 1$. Using the above identity and the continuous inclusion $\boldsymbol{H}^s(\Omega) \subset \boldsymbol{L}^4(\Omega)$ for all $s \geq 3/4$, for arbitrary $t \in (0,T)$, we have

$$\left\| \boldsymbol{m}_{hk}^\pm(t) \otimes \boldsymbol{m}_{hk}^\pm(t) - \boldsymbol{m}(t) \otimes \boldsymbol{m}(t) \right\| \leq \left\| \boldsymbol{m}_{hk}^\pm(t) + \boldsymbol{m}(t) \right\|_{\boldsymbol{L}^4(\Omega)} \left\| \boldsymbol{m}(t) - \boldsymbol{m}_{hk}^\pm(t) \right\|_{\boldsymbol{L}^4(\Omega)}$$
$$\lesssim \left\| \boldsymbol{m}_{hk}^\pm(t) + \boldsymbol{m}(t) \right\|_{\boldsymbol{H}^1(\Omega)} \left\| \boldsymbol{m}(t) - \boldsymbol{m}_{hk}^\pm(t) \right\|_{\boldsymbol{H}^s(\Omega)}.$$

It follows that

$$\left\| \boldsymbol{m}_{hk}^\pm \otimes \boldsymbol{m}_{hk}^\pm - \boldsymbol{m} \otimes \boldsymbol{m} \right\|_{\boldsymbol{L}^2(\Omega_T)} \lesssim \left\| \boldsymbol{m}_{hk}^\pm + \boldsymbol{m} \right\|_{\boldsymbol{L}^\infty(0,T;\boldsymbol{H}^1(\Omega))} \left\| \boldsymbol{m} - \boldsymbol{m}_{hk}^\pm \right\|_{\boldsymbol{L}^2(0,T;\boldsymbol{H}^s(\Omega))}.$$

Convergence (48d) then follows from the uniform boundedness of both $\boldsymbol{m}_{hk}^\pm$ and $\boldsymbol{m}$ in $\boldsymbol{L}^\infty(0,T;\boldsymbol{H}^1(\Omega))$ and the strong convergence (46k) from Lemma 6.7. The proof of (48e) is identical (due to the use of the nodal projection, one can use the Hölder inequality $\|\cdot\|_{L^2} \leq \|\cdot\|_{L^\infty} \|\cdot\|_{L^2}$). This concludes the proof. $\quad\square$

Now, we are in a position to prove Theorem 4.7(i).

Proof of Theorem 4.7(i). We apply Lemma 6.7, which yields $\boldsymbol{u} \in L^\infty(0,T;\boldsymbol{H}_D^1(\Omega))$ with $\partial_t \boldsymbol{u} \in L^\infty(0,T;\boldsymbol{L}^2(\Omega))$ and $\boldsymbol{m} \in L^\infty(0,T;\boldsymbol{H}^1(\Omega;\mathbb{S}^2))$ with $\partial_t \boldsymbol{m} \in L^2(0,T;\boldsymbol{L}^2(\Omega))$ as well as subsequences of $\{\boldsymbol{u}_{hk}\}$ and $\{\boldsymbol{m}_{hk}\}$ satisfying the desired convergence properties. This already shows that $\boldsymbol{u}$ and $\boldsymbol{m}$ satisfy property (i) of Definition 2.1. Property (iii) follows from the available convergence results, the continuity of the trace operator $\boldsymbol{H}^1(\Omega_T) \to \boldsymbol{H}^{1/2}(\Omega)$, and assumption (26) on the discrete initial data. To conclude the proof, it remains to show that property (ii) holds, i.e., that $\boldsymbol{u}$ and $\boldsymbol{m}$ satisfy the variational formulations (10) and (11), respectively. The result follows from the convergence properties established in Lemmas 6.7–6.8. We omit the details, because

- the proof that $\boldsymbol{u}$ satisfies (10) is identical to the one presented in [15, page 1378], which is a consequence of the fact that in the displacement update (21) we employ the nodal projection for the magnetisation appearing on the right-hand side (our generalised setting involving a more general expression for the magnetostrain, body forces and traction does not pose further mathematical challenges here).
- the proof that $\boldsymbol{m}$ satisfies (11) can be obtained combining the argument of [15, pages 1376–1378] (which show convergence of the method with nodal projection towards a variational formulation of the LLG equation with magnetoelastic term) with the one of [29, page 1363] (where the modifications due to the omission of the nodal projection are presented).

This concludes the proof. $\quad\square$

6.5. Energy inequality

In this section, we use the compact notation $\hat{\boldsymbol{m}}_h = \Pi_h \boldsymbol{m}_h$ to denote the nodal projection of a general magnetisation approximation $\boldsymbol{m}_h$.

To start with, in the following proposition, we state a variant of Proposition 4.4 for the discrete energy

$$\hat{\mathcal{E}}_h[\boldsymbol{u}_h, \boldsymbol{m}_h] = \frac{1}{2} \left\| \boldsymbol{\nabla} \boldsymbol{m}_h \right\|^2 + \frac{1}{2} \left\| \boldsymbol{\varepsilon}(\boldsymbol{u}_h) - \boldsymbol{\varepsilon}_{\mathrm{m}}(\hat{\boldsymbol{m}}_h) \right\|_{\mathbb{C}}^2 - \langle \boldsymbol{f}, \boldsymbol{u}_h \rangle - \langle \boldsymbol{g}, \boldsymbol{u}_h \rangle_{\Gamma_N},$$

which is obtained from (3) by applying the nodal projection to the discrete magnetisation appearing in the elastic energy. We omit the proof since it is very similar to the one of Proposition 4.4.

Proposition 6.9. *For every integer $0 \leq i \leq N - 1$, the iterates of Algorithm 4.1 satisfy the discrete energy law*

$$\hat{\mathcal{E}}_h[\boldsymbol{u}_h^{i+1}, \boldsymbol{m}_h^{i+1}] + \frac{1}{2} \left\| \mathrm{d}_t \boldsymbol{u}_h^{i+1} \right\|^2 - \hat{\mathcal{E}}_h[\boldsymbol{u}_h^i, \boldsymbol{m}_h^i] - \frac{1}{2} \left\| \mathrm{d}_t \boldsymbol{u}_h^i \right\|^2 = -\alpha k \left\| \boldsymbol{v}_h^i \right\|_h^2 - \hat{D}_{h,k}^i - \hat{E}_{h,k}^i, \tag{49}$$

where $\hat{D}_{h,k}^i$ and $\hat{E}_{h,k}^i$ are given by

$$\hat{D}_{h,k}^i := k^2(\theta - 1/2) \left\| \boldsymbol{\nabla} \boldsymbol{v}_h^i \right\|^2 + \frac{1}{2} \left\| \mathrm{d}_t \boldsymbol{u}_h^{i+1} - \mathrm{d}_t \boldsymbol{u}_h^i \right\|^2 + \frac{1}{2} \left\| [\boldsymbol{\varepsilon}(\boldsymbol{u}_h^{i+1}) - \boldsymbol{\varepsilon}_{\mathrm{m}}(\hat{\boldsymbol{m}}_h^{i+1})] - [\boldsymbol{\varepsilon}(\boldsymbol{u}_h^i) - \boldsymbol{\varepsilon}_{\mathrm{m}}(\hat{\boldsymbol{m}}_h^i)] \right\|_{\mathbb{C}}^2 \geq 0$$

and

$$\hat{E}^i_{h,k} := \sum_{\ell=1}^{5} \hat{E}^i_{h,k,\ell}$$

$$:= \langle \sigma(\boldsymbol{u}^{i+1}_h, \hat{\boldsymbol{m}}^{i+1}_h) - \sigma(\boldsymbol{u}^i_h, \hat{\boldsymbol{m}}^i_h), \varepsilon_{\mathrm{m}}(\hat{\boldsymbol{m}}^{i+1}_h) - \varepsilon_{\mathrm{m}}(\hat{\boldsymbol{m}}^i_h) \rangle$$

$$+ \langle \sigma(\boldsymbol{u}^i_h, \hat{\boldsymbol{m}}^i_h), \varepsilon_{\mathrm{m}}(\hat{\boldsymbol{m}}^{i+1}_h) - \varepsilon_{\mathrm{m}}(\boldsymbol{m}^{i+1}_h) \rangle + \langle \sigma(\boldsymbol{u}^i_h, \hat{\boldsymbol{m}}^i_h), \varepsilon_{\mathrm{m}}(\boldsymbol{m}^i_h) - \varepsilon_{\mathrm{m}}(\hat{\boldsymbol{m}}^i_h) \rangle$$

$$+ 2k \langle \sigma(\boldsymbol{u}^i_h, \hat{\boldsymbol{m}}^i_h), \mathbb{Z} : [(\hat{\boldsymbol{m}}^i_h - \boldsymbol{m}^i_h) \otimes \boldsymbol{v}^i_h] \rangle + k^2 \langle \sigma(\boldsymbol{u}^i_h, \hat{\boldsymbol{m}}^i_h), \varepsilon_{\mathrm{m}}(\boldsymbol{v}^i_h) \rangle.$$

respectively.

Now, we are in a position to prove Theorem 4.7(ii).

Proof of Theorem 4.7(ii). Let $t' \in (0, T)$. Let $1 \le j \le N$ such that $t' \in (t_{j-1}, t_j)$. Summing (49) for $i = 0, \dots, j-1$ yields

$$\hat{\mathcal{E}}_h[\boldsymbol{u}^j_h, \boldsymbol{m}^j_h] + \frac{1}{2} \left\| \mathrm{d}_t \boldsymbol{u}^j_h \right\|^2 - \hat{\mathcal{E}}_h[\boldsymbol{u}^0_h, \boldsymbol{m}^0_h] - \frac{1}{2} \left\| \mathrm{d}_t \boldsymbol{u}^0_h \right\|^2 + \alpha k \sum_{i=0}^{j-1} \left\| \boldsymbol{v}^i_h \right\|^2_h + \sum_{i=0}^{j-1} \hat{D}^i_{h,k} = -\sum_{i=0}^{j-1} \hat{E}^i_{h,k}.$$

Using the Cauchy–Schwarz inequality, the weighted Young inequality, and Lemma 6.4, we obtain the estimate

$$|E^i_{h,k,1}| = |\langle \sigma(\boldsymbol{u}^{i+1}_h, \hat{\boldsymbol{m}}^{i+1}_h) - \sigma(\boldsymbol{u}^i_h, \hat{\boldsymbol{m}}^i_h), \varepsilon_{\mathrm{m}}(\hat{\boldsymbol{m}}^{i+1}_h) - \varepsilon_{\mathrm{m}}(\hat{\boldsymbol{m}}^i_h) \rangle|$$

$$\le \left\| [\varepsilon(\boldsymbol{u}^{i+1}_h) - \varepsilon_{\mathrm{m}}(\hat{\boldsymbol{m}}^{i+1}_h)] - [\varepsilon(\boldsymbol{u}^i_h) - \varepsilon_{\mathrm{m}}(\hat{\boldsymbol{m}}^i_h)] \right\|_{\mathbb{C}} \left\| \varepsilon_{\mathrm{m}}(\hat{\boldsymbol{m}}^{i+1}_h) - \varepsilon_{\mathrm{m}}(\hat{\boldsymbol{m}}^i_h) \right\|_{\mathbb{C}}$$

$$\le \frac{1}{4} \left\| [\varepsilon(\boldsymbol{u}^{i+1}_h) - \varepsilon_{\mathrm{m}}(\hat{\boldsymbol{m}}^{i+1}_h)] - [\varepsilon(\boldsymbol{u}^i_h) - \varepsilon_{\mathrm{m}}(\hat{\boldsymbol{m}}^i_h)] \right\|^2_{\mathbb{C}}$$

$$+ C^2_{\mathrm{m}} \| \mathbb{C} \|_{\boldsymbol{L}^{\infty}(\Omega)} k^2 \left\| \boldsymbol{v}^i_h \right\|^2.$$

We now estimate $E^i_{h,k,4}$ (assuming $i \ge 1$, because $E^0_{h,k,4} = 0$ as $\hat{\boldsymbol{m}}^0_h = \boldsymbol{m}^0_h$ by assumption). Using the Cauchy–Schwarz inequality, the Hölder inequality (for $p = 2/(1 - 2\varepsilon)$ and $p' = 2p/(p-2)$ with $0 < \varepsilon \ll 1/2$ arbitrary), Lemma 6.6, and classical inverse estimates (see, e.g. [11, Lemma 3.5]), we obtain

$$|E^i_{h,k,4}| = 2k |\langle \sigma(\boldsymbol{u}^i_h, \hat{\boldsymbol{m}}^i_h), \mathbb{Z} : [(\hat{\boldsymbol{m}}^i_h - \boldsymbol{m}^i_h) \otimes \boldsymbol{v}^i_h] \rangle|$$

$$\le 2 \| \mathbb{Z} \|_{\boldsymbol{L}^{\infty}(\Omega)} k \left\| \sigma(\boldsymbol{u}^i_h, \hat{\boldsymbol{m}}^i_h) \right\| \left\| \hat{\boldsymbol{m}}^i_h - \boldsymbol{m}^i_h \right\|_{\boldsymbol{L}^p(\Omega)} \left\| \boldsymbol{v}^i_h \right\|_{\boldsymbol{L}^{p'}(\Omega)}$$

$$\lesssim k \left\| \sigma(\boldsymbol{u}^i_h, \hat{\boldsymbol{m}}^i_h) \right\| k^{(p+1)/p} \left(\sum_{\ell=0}^{i-1} \left\| \boldsymbol{v}^{\ell}_h \right\|^2_{\boldsymbol{L}^{2p}(\Omega)} \right) \left\| \boldsymbol{v}^i_h \right\|_{\boldsymbol{L}^{p'}(\Omega)}$$

$$\lesssim k^{2+1/p} \left\| \sigma(\boldsymbol{u}^i_h, \hat{\boldsymbol{m}}^i_h) \right\| h^{3(1-p)/p}_{\min} \left(\sum_{\ell=0}^{i-1} \left\| \boldsymbol{v}^{\ell}_h \right\|^2 \right) h^{3(2-p')/(2p')}_{\min} \left\| \boldsymbol{v}^i_h \right\|$$

$$\lesssim h^{-3}_{\min} k^{5/2-\varepsilon} \left\| \sigma(\boldsymbol{u}^i_h, \hat{\boldsymbol{m}}^i_h) \right\| \left(\sum_{\ell=0}^{i-1} \left\| \boldsymbol{v}^{\ell}_h \right\|^2 \right) \left\| \boldsymbol{v}^i_h \right\|.$$

Similarly, we obtain

$$|E^i_{h,k,5}| = |k^2 \langle \sigma(\boldsymbol{u}^i_h, \hat{\boldsymbol{m}}^i_h), \varepsilon_{\mathrm{m}}(\boldsymbol{v}^i_h) \rangle| \lesssim h^{-3/2}_{\min} k^2 \left\| \sigma(\boldsymbol{u}^i_h, \hat{\boldsymbol{m}}^i_h) \right\| \left\| \boldsymbol{v}^i_h \right\|^2.$$

Moreover, noting $\boldsymbol{m}^0_h = \hat{\boldsymbol{m}}^0_h$ we have that

$$\sum_{i=0}^{j-1} \left(\hat{E}^i_{h,k,2} + \hat{E}^i_{h,k,3} \right)$$

$$= \sum_{i=0}^{j-1} \langle \sigma(\boldsymbol{u}^i_h, \hat{\boldsymbol{m}}^i_h), \varepsilon_{\mathrm{m}}(\hat{\boldsymbol{m}}^{i+1}_h) - \varepsilon_{\mathrm{m}}(\boldsymbol{m}^{i+1}_h) \rangle + \sum_{i=0}^{j-1} \langle \sigma(\boldsymbol{u}^i_h, \hat{\boldsymbol{m}}^i_h), \varepsilon_{\mathrm{m}}(\boldsymbol{m}^i_h) - \varepsilon_{\mathrm{m}}(\hat{\boldsymbol{m}}^i_h) \rangle$$

$$= \langle \sigma(\boldsymbol{u}^0_h, \hat{\boldsymbol{m}}^0_h), \varepsilon_{\mathrm{m}}(\boldsymbol{m}^0_h) - \varepsilon_{\mathrm{m}}(\hat{\boldsymbol{m}}^0_h) \rangle - \langle \sigma(\boldsymbol{u}^{j-1}_h, \hat{\boldsymbol{m}}^{j-1}_h), \varepsilon_{\mathrm{m}}(\boldsymbol{m}^j_h) - \varepsilon_{\mathrm{m}}(\hat{\boldsymbol{m}}^j_h) \rangle$$

$$+ \sum_{i=0}^{j-2} \langle \sigma(\boldsymbol{u}^{i+1}_h, \hat{\boldsymbol{m}}^{i+1}_h) - \sigma(\boldsymbol{u}^i_h, \hat{\boldsymbol{m}}^i_h), \varepsilon_{\mathrm{m}}(\boldsymbol{m}^i_h) - \varepsilon_{\mathrm{m}}(\hat{\boldsymbol{m}}^i_h) \rangle.$$

$$= - \langle \sigma(\boldsymbol{u}^{j-1}_h, \hat{\boldsymbol{m}}^{j-1}_h), \varepsilon_{\mathrm{m}}(\boldsymbol{m}^j_h) - \varepsilon_{\mathrm{m}}(\hat{\boldsymbol{m}}^j_h) \rangle$$

$$+ \sum_{i=0}^{j-2} \langle \sigma(\boldsymbol{u}^{i+1}_h, \hat{\boldsymbol{m}}^{i+1}_h) - \sigma(\boldsymbol{u}^i_h, \hat{\boldsymbol{m}}^i_h), \varepsilon_{\mathrm{m}}(\boldsymbol{m}^i_h) - \varepsilon_{\mathrm{m}}(\hat{\boldsymbol{m}}^i_h) \rangle$$

Using inverse estimates, Lemma 6.4 and Lemma 6.6, we obtain the estimate

$$
\begin{aligned}
&|\langle \boldsymbol{\sigma}(\boldsymbol{u}_h^{i+1}, \hat{\boldsymbol{m}}_h^{i+1}) - \boldsymbol{\sigma}(\boldsymbol{u}_h^i, \hat{\boldsymbol{m}}_h^i), \boldsymbol{\varepsilon}_{\mathrm{m}}(\boldsymbol{m}_h^i) - \boldsymbol{\varepsilon}_{\mathrm{m}}(\hat{\boldsymbol{m}}_h^i)\rangle| \\
&\quad \lesssim \left(\left\| \boldsymbol{\varepsilon}(\boldsymbol{u}_h^{i+1}) - \boldsymbol{\varepsilon}(\boldsymbol{u}_h^i) \right\| + \left\| \boldsymbol{\varepsilon}_{\mathrm{m}}(\hat{\boldsymbol{m}}_h^{i+1}) - \boldsymbol{\varepsilon}_{\mathrm{m}}(\hat{\boldsymbol{m}}_h^i) \right\| \right) \left\| \boldsymbol{\varepsilon}_{\mathrm{m}}(\boldsymbol{m}_h^i) - \boldsymbol{\varepsilon}_{\mathrm{m}}(\hat{\boldsymbol{m}}_h^i) \right\| \\
&\quad \lesssim \left(h_{\min}^{-1} k \left\| \mathrm{d}_t \boldsymbol{u}_h^{i+1} \right\| + k^2 \left\| \boldsymbol{v}_h^i \right\|^2 \right) \left\| \boldsymbol{m}_h^i + \hat{\boldsymbol{m}}_h^i \right\|_{\boldsymbol{H}^1(\Omega)} k^{4/3} h_{\min}^{-2} \sum_{\ell=0}^{i-1} \left\| \boldsymbol{v}_h^\ell \right\|^2.
\end{aligned}
$$

Altogether, omitting all non-negative dissipative terms and using the stability from Proposition 4.6, we thus obtain

$$
\begin{aligned}
&\hat{\mathcal{E}}_h[\boldsymbol{u}_h^j, \boldsymbol{m}_h^j] + \frac{1}{2} \left\| \mathrm{d}_t \boldsymbol{u}_h^j \right\|^2 - \hat{\mathcal{E}}_h[\boldsymbol{u}_h^0, \boldsymbol{m}_h^0] - \frac{1}{2} \left\| \mathrm{d}_t \boldsymbol{u}_h^0 \right\|^2 + \alpha k \sum_{i=0}^{j-1} \left\| \boldsymbol{v}_h^i \right\|_h^2 \\
&\qquad - \langle \boldsymbol{\sigma}(\boldsymbol{u}_h^{j-1}, \hat{\boldsymbol{m}}_h^{j-1}), \boldsymbol{\varepsilon}_{\mathrm{m}}(\boldsymbol{m}_h^j) - \boldsymbol{\varepsilon}_{\mathrm{m}}(\hat{\boldsymbol{m}}_h^j)\rangle \\
&\quad \lesssim \sum_{i=0}^{j-1} \left(k^2 \left\| \boldsymbol{v}_h^i \right\|^2 + h_{\min}^{-3} k^{4/3} \left\| \mathrm{d}_t \boldsymbol{u}_h^{i+1} \right\| \left\| \boldsymbol{m}_h^i + \hat{\boldsymbol{m}}_h^i \right\|_{\boldsymbol{H}^1(\Omega)} + h_{\min}^{-2} k^{7/3} \left\| \boldsymbol{v}_h^i \right\|^2 \right. \\
&\qquad \left. + h_{\min}^{-3} k^{3/2 - \epsilon} \left\| \boldsymbol{\sigma}(\boldsymbol{u}_h^i, \hat{\boldsymbol{m}}_h^i) \right\| \left\| \boldsymbol{v}_h^i \right\| + h_{\min}^{-3/2} k^2 \left\| \boldsymbol{v}_h^i \right\|^2 \right) \\
&\quad \lesssim k + h_{\min}^{-3} k^{1/3} + h_{\min}^{-2} k^{4/3} + h_{\min}^{-3} k^{1/2 - \epsilon} + h_{\min}^{-3/2} k.
\end{aligned}
$$

Using (30), rewriting the above using the time reconstructions (16) and integrating in time over an arbitrary measurable set $\mathfrak{T} \subset [0, T]$, we obtain

$$
\begin{aligned}
&\int_{\mathfrak{T}} \left(\mathcal{E}[\boldsymbol{u}_{hk}^+(t'), \boldsymbol{m}_{hk}^+(t')] + \frac{1}{2} \left\| \dot{\boldsymbol{u}}_{hk}^+(t') \right\|^2 - \hat{\mathcal{E}}_h[\boldsymbol{u}_{hk}^-(0), \boldsymbol{m}_{hk}^-(0)] - \frac{1}{2} \left\| \dot{\boldsymbol{u}}_{hk}^-(0) \right\|^2 \right) \mathrm{d}t' \\
&\qquad + \int_{\mathfrak{T}} \left(\alpha \int_0^{t'} \left\| \boldsymbol{v}_{hk}^-(t) \right\|^2 \mathrm{d}t \right) \mathrm{d}t' + \int_{\mathfrak{T}} \left(\alpha \int_{t'}^{t_j} \left\| \boldsymbol{v}_{hk}^-(t) \right\|^2 \mathrm{d}t \right) \mathrm{d}t' \\
&\qquad - \int_{\mathfrak{T}} \langle \boldsymbol{\sigma}(\boldsymbol{u}_{hk}^-(t'), \hat{\boldsymbol{m}}_{hk}^-(t')), \boldsymbol{\varepsilon}_{\mathrm{m}}(\boldsymbol{m}_{hk}^+(t')) - \boldsymbol{\varepsilon}_{\mathrm{m}}(\hat{\boldsymbol{m}}_{hk}^+(t'))\rangle \mathrm{d}t' \\
&\quad \lesssim k + h_{\min}^{-3} k^{1/3} + h_{\min}^{-2} k^{4/3} + h_{\min}^{-3} k^{1/2 - \epsilon} + h_{\min}^{-3/2} k.
\end{aligned}
$$

We now consider the limit of this inequality as $h, k \to 0$. The assumed CFL condition $k = o(h^9)$ implies that the right-hand side converges to 0 in the limit as $h, k \to 0$. The last two terms on the left-hand side converge to 0: the first one by no concentration of Lebesgue functions, the other thanks to the available convergence results (cf. the convergences guaranteed by Lemmas 6.7–6.8). Weak lower semicontinuity guarantees

$$
\int_{\mathfrak{T}} \left(\mathcal{E}[\boldsymbol{u}(t'), \boldsymbol{m}(t')] + \frac{1}{2} \left\| \partial_t \boldsymbol{u}(t') \right\|^2 + \alpha \int_0^{t'} \left\| \partial_t \boldsymbol{m}(t) \right\|^2 \mathrm{d}t \right) \mathrm{d}t' \leq \liminf_{h, k \to 0} \int_{\mathfrak{T}} \left(\hat{\mathcal{E}}_h[\boldsymbol{u}_{hk}^+(t'), \boldsymbol{m}_{hk}^+(t')] + \frac{1}{2} \left\| \dot{\boldsymbol{u}}_{hk}^+(t') \right\|^2 + \alpha \int_0^{t'} \left\| \boldsymbol{v}_{hk}^-(t) \right\|^2 \mathrm{d}t \right) \mathrm{d}t'.
$$

Assumption (26) yields

$$
\lim_{h, k \to 0} \left(\hat{\mathcal{E}}_h[\boldsymbol{u}_{hk}^-(0), \boldsymbol{m}_{hk}^-(0)] + \frac{1}{2} \left\| \dot{\boldsymbol{u}}_{hk}^-(0) \right\|^2 \right) = \mathcal{E}[\boldsymbol{u}^0, \boldsymbol{m}^0] + \frac{1}{2} \left\| \dot{\boldsymbol{u}}^0 \right\|^2.
$$

Since $\mathfrak{T} \subset [0, T]$ was arbitrary, this shows that the energy inequality (12) holds a.e. in $(0, T)$ and concludes the proof. $\square$

Code availability statement

The code used to generate the findings of this study is openly available in Zenodo at https://doi.org/10.5281/zenodo.14641594.

Acknowledgements

Appendix A. Linear algebra definitions and identities

In this section, for the convenience of the reader, we collect some definitions and vector/matrix/tensor identities from linear algebra that are used throughout the work.

Definition A.1. Let $\mathbb{A} \in \mathbb{R}^{3^4}$ be a fourth-order tensor (4-tensor) with components $\mathbb{A}_{ij\ell m}$, where $i, j, \ell, m = 1, 2, 3$. We say that

(1) $\mathbb{A}$ is minorly symmetric if $\mathbb{A}_{ij\ell m} = \mathbb{A}_{ji\ell m} = \mathbb{A}_{ijm\ell}$,
(2) $\mathbb{A}$ is majorly symmetric if $\mathbb{A}_{ij\ell m} = \mathbb{A}_{\ell mji}$,
(3) and $\mathbb{A}$ is (fully) symmetric if the aforementioned two conditions hold together.

The transpose of $\mathbb{A}$ is the 4-tensor $\mathbb{A}^\top \in \mathbb{R}^{3^4}$ given by $(\mathbb{A}^\top)_{ij\ell m} = \mathbb{A}_{\ell mji}$. In particular, $\mathbb{A}$ is majorly symmetric if $\mathbb{A}^\top = \mathbb{A}$.

Remark A.2. In three dimensions, 4-tensors have $3^4 = 81$ components. Minorly symmetric 4-tensors have 36 independent components, majorly symmetric 4-tensors have 45 independent components, and fully symmetric 4-tensors have 21 independent components. Throughout this work the stiffness tensor $\mathbb{C}$ is assumed to be fully symmetric, whereas the magnetostriction tensor $\mathbb{Z}$ is assumed to be only minorly symmetric. In the numerical experiments of Section 5, we consider the isotropic case, in which $\mathbb{C}$ and $\mathbb{Z}$ have only two (the so-called Lamé constants) and one (the so-called saturation magnetostriction) independent components, respectively.

In the following definition, we recall some operations between tensors.

Definition A.3. Let $\mathbb{A}, \mathbb{B} \in \mathbb{R}^{3^4}$ be 4-tensors, let $\nu, \mu \in \mathbb{R}^{3 \times 3}$ be 2-tensors (matrices), and let $\boldsymbol{m}, \boldsymbol{w} \in \mathbb{R}^3$ be 1-tensors (vectors).

- We denote the double contraction between $\mathbb{A}$ and $\mathbb{B}$ as the 4-tensor $\mathbb{A} : \mathbb{B} \in \mathbb{R}^{3^4}$ given by

$$(\mathbb{A} : \mathbb{B})_{ij\ell m} = \sum_{p,q} \mathbb{A}_{ijpq} \mathbb{B}_{pq\ell m}.$$

- We denote the double contraction between $\mathbb{A}$ and ν as the 2-tensor $\mathbb{A} : \nu \in \mathbb{R}^{3 \times 3}$ given by

$$(\mathbb{A} : \nu)_{ij} = \sum_{\ell,m} \mathbb{A}_{ij\ell m} \nu_{\ell m}.$$

- We denote the Frobenius product of μ and ν as the scalar $\mu : \nu \in \mathbb{R}$ given by

$$\mu : \nu = \sum_{i,j} \mu_{ij} \nu_{ij}.$$

- We denote the tensor product of $\boldsymbol{m}$ and $\boldsymbol{w}$ as the 2-tensor $\boldsymbol{m} \otimes \boldsymbol{w} \in \mathbb{R}^{3 \times 3}$ given by

$$(\boldsymbol{m} \otimes \boldsymbol{w})_{ij} = m_i w_j.$$

The following result is useful for manipulation of the magnetostrain terms.

Lemma A.4. *Let $\mathbb{Z} \in \mathbb{R}^{3^4}$ be a minorly symmetric 4-tensor, let $\sigma \in \mathbb{R}^{3 \times 3}$ be a symmetric 2-tensor, and let $\boldsymbol{m}, \boldsymbol{w} \in \mathbb{R}^3$ be two 1-tensors. We have the identity*

$$[(\mathbb{Z}^\top : \sigma)\boldsymbol{w}] \cdot \boldsymbol{m} = [\mathbb{Z}^\top : \sigma)\boldsymbol{m}] \cdot \boldsymbol{w} = \sigma : [\mathbb{Z} : (\boldsymbol{m} \otimes \boldsymbol{w})]. \tag{50}$$

Proof. We have by the minor symmetry of $\mathbb{Z}$ that

$$
\begin{aligned}
(\mathbb{Z}^\top : \sigma)\boldsymbol{m} \cdot \boldsymbol{w} &= \sum_{i,j,\ell,m} \mathbb{Z}^\top_{ijk\ell} \sigma_{\ell m} m_j w_i \\
&= \sum_{i,j,\ell,m} \mathbb{Z}^\top_{jik\ell} \sigma_{\ell m} m_i w_j \quad \text{by relabelling} \\
&= \sum_{i,j,\ell,m} \mathbb{Z}^\top_{ijk\ell} \sigma_{\ell m} w_j m_i \quad \text{via minor symmetry} \\
&= (\mathbb{Z}^\top : \sigma)\boldsymbol{w} \cdot \boldsymbol{m}.
\end{aligned}
$$

Furthermore, we have that

$$(\mathbb{Z}^\top : \boldsymbol{\sigma})\boldsymbol{m} \cdot \boldsymbol{w} = \sum_{i,j,\ell,m} \mathbb{Z}^\top_{ij\ell m}\sigma_{\ell m}m_j w_i = \sum_{i,j,\ell,m} \sigma_{\ell m}\mathbb{Z}^\top_{ij\ell m}m_j w_i$$

$$= \sum_{i,j,\ell,m} \sigma_{\ell m}\mathbb{Z}_{\ell mji}m_j w_i \quad \text{via minor symmetry}$$

$$= \sum_{\ell,m} \sigma_{\ell m}[\mathbb{Z} : (\boldsymbol{m} \otimes \boldsymbol{w})]_{\ell m} = \boldsymbol{\sigma} : [\mathbb{Z} : (\boldsymbol{m} \otimes \boldsymbol{w})].$$

This show both identities in (50). □

The following identity is useful to show the stability of numerical schemes.

Lemma A.5. *Let $\{v_i\}$ be a sequence in an inner product space with inner product $\langle \cdot, \cdot \rangle$ and associated norm $\|\cdot\|$. We have the identity*

$$\langle v_{i+1} - v_i, v_{i+1} \rangle = \frac{1}{2}\|v_{i+1}\|^2 - \frac{1}{2}\|v_i\|^2 + \frac{1}{2}\|v_{i+1} - v_i\|^2. \tag{51}$$

Appendix B. Nondimensionalisation

Let $\Omega \subset \mathbb{R}^3$ denote the volume occupied by a ferromagnetic body (with the spatial variable $x \in \Omega$ measured in meter). Consider the magnetisation $\boldsymbol{M}$ (measured in A/m), which satisfies the length constraint $|\boldsymbol{M}| = M_s$, where the saturation magnetisation $M_s > 0$ is also measured in A/m, and the displacement $\boldsymbol{U}$ (measured in m). We denote by $\boldsymbol{\varepsilon}(\boldsymbol{U})$ the total strain given by

$$\boldsymbol{\varepsilon}(\boldsymbol{U}) = (\boldsymbol{\nabla}\boldsymbol{U} + \boldsymbol{\nabla}\boldsymbol{U}^\top)/2$$

and by $\boldsymbol{\varepsilon}_{\mathrm{m}}(\boldsymbol{M})$ the magnetostrain given by

$$\boldsymbol{\varepsilon}_{\mathrm{m}}(\boldsymbol{M}) = \mathbb{Z} : (\boldsymbol{M} \otimes \boldsymbol{M}/M_s^2),$$

where $\mathbb{Z}$ is a dimensionless fourth-order tensor.

The total energy of the system (measured in J) is given by

$$\mathcal{E}[\boldsymbol{U}, \boldsymbol{M}] = \frac{A}{M_s^2}\int_\Omega |\boldsymbol{\nabla}\boldsymbol{M}|^2 - \mu_0 \int_\Omega \boldsymbol{H}_{\mathrm{ext}} \cdot \boldsymbol{M} + \frac{1}{2}\int_\Omega [\boldsymbol{\varepsilon}(\boldsymbol{U}) - \boldsymbol{\varepsilon}_{\mathrm{m}}(\boldsymbol{M})] : \{\boldsymbol{C} : [\boldsymbol{\varepsilon}(\boldsymbol{U}) - \boldsymbol{\varepsilon}_{\mathrm{m}}(\boldsymbol{M})]\} - \int_\Omega \boldsymbol{F} \cdot \boldsymbol{U} - \int_{\Gamma_N} \boldsymbol{G} \cdot \boldsymbol{U},$$

where A is the exchange constant (measured in Jm^{-1}), μ_0 is the permeability of free space (measured in NA^{-2}), $\boldsymbol{H}_{\mathrm{ext}}$ is an applied external field (measured in A m), $\boldsymbol{C}$ is the fourth-order stiffness tensor (measured in Nm^{-2}), $\boldsymbol{F}$ is a body force (measured in Nm^{-3}), and $\boldsymbol{G}$ is a surface force (measured in Nm^{-2}).

The dynamics of $\boldsymbol{M}$ are described by the LLG equation:

$$\partial_t \boldsymbol{M} = -\gamma\mu_0 \boldsymbol{M} \times \boldsymbol{H}_{\mathrm{eff}}[\boldsymbol{U}, \boldsymbol{M}] + \frac{\alpha}{M_s}\boldsymbol{M} \times \partial_t\boldsymbol{M},$$

where γ is the gyromagnetic ratio (measured in $\mathrm{rads}^{-1}\mathrm{T}^{-1}$), $\alpha > 0$ is the dimensionless Gilbert damping parameter, and the effective field $\boldsymbol{H}_{\mathrm{eff}}$ (measured in A/m) reads as

$$\boldsymbol{H}_{\mathrm{eff}}[\boldsymbol{U}, \boldsymbol{M}] = -\frac{1}{\mu_0}\frac{\delta\mathcal{E}[\boldsymbol{U}, \boldsymbol{M}]}{\delta\boldsymbol{M}} = \frac{2A}{\mu_0 M_s^2}\boldsymbol{\Delta}\boldsymbol{M} + \boldsymbol{H}_{\mathrm{ext}} + \frac{2}{\mu_0 M_s^2}[\mathbb{Z}^\top : \boldsymbol{\Sigma}(\boldsymbol{U}, \boldsymbol{M})]\boldsymbol{M},$$

where $\boldsymbol{\Sigma}(\boldsymbol{U}, \boldsymbol{M}) = \boldsymbol{C} : [\boldsymbol{\varepsilon}(\boldsymbol{U}) - \boldsymbol{\varepsilon}_{\mathrm{m}}(\boldsymbol{M})]$ is the stress (measured in Nm^{-2}). The LLG equation is coupled with the conservation of momentum equation satisfied by the displacement:

$$\rho\,\partial_{tt}\boldsymbol{U} = \boldsymbol{\nabla} \cdot \boldsymbol{\Sigma}(\boldsymbol{U}, \boldsymbol{M}) + \boldsymbol{F},$$

where ρ is the mass density (measured in kgm^{-3}).

Let $\boldsymbol{m} = \boldsymbol{M}/M_s$ denote the normalised magnetisation. We define the exchange length $\ell_{\mathrm{ex}}^2 = 2A/\mu_0 M_s^2$ (measured in m) and use it to rescale the spatial variable and the displacement according to $x' = x/\ell_{\mathrm{ex}}$ and $\boldsymbol{u} = \boldsymbol{U}/\ell_{\mathrm{ex}}$, respectively. Additionally we introduce the dimensionless domain $\Omega' = \Omega/\ell_{\mathrm{ex}}$, the dimensionless time $t' = \gamma\mu_0 M_s t$, the dimensionless coupling parameter $\kappa = \rho\ell_{\mathrm{ex}}^2\gamma^2\mu_0$, as well as the dimensionless differential operators $\boldsymbol{\nabla} = \boldsymbol{\nabla}'/\ell_{\mathrm{ex}}$ and $\boldsymbol{\Delta} = \boldsymbol{\Delta}'/\ell_{\mathrm{ex}}^2$. Further we define the dimensionless energy as

$$\mathcal{E}'[\boldsymbol{u}, \boldsymbol{m}] = \frac{\mathcal{E}[\ell_{\mathrm{ex}}\boldsymbol{u}, M_s\boldsymbol{m}]}{\mu_0 M_s^2\ell_{\mathrm{ex}}^3} = \frac{1}{2}\int_{\Omega'} |\boldsymbol{\nabla}'\boldsymbol{m}|^2 - \int_{\Omega'} \boldsymbol{h}_{\mathrm{ext}} \cdot \boldsymbol{m} + \frac{\kappa}{2}\int_{\Omega'} [\boldsymbol{\varepsilon}(\boldsymbol{u}) - \boldsymbol{\varepsilon}'_{\mathrm{m}}(\boldsymbol{m})] : \{\mathbb{C} : [\boldsymbol{\varepsilon}(\boldsymbol{u}) - \boldsymbol{\varepsilon}'_{\mathrm{m}}(\boldsymbol{m})] - \kappa\int_{\Omega'} \boldsymbol{f} \cdot \boldsymbol{u} - \kappa\int_{\Gamma'_N} \boldsymbol{g} \cdot \boldsymbol{u},$$

where $\boldsymbol{h}_{\mathrm{ext}} = \boldsymbol{H}_{\mathrm{ext}}/M_s$, $\boldsymbol{\varepsilon}_{\mathrm{m}}(\boldsymbol{m}) = \mathbb{Z} : (\boldsymbol{m} \otimes \boldsymbol{m})$, $\boldsymbol{\Sigma} = \kappa\mu_0 M_s^2\boldsymbol{\sigma}$, $\boldsymbol{G} = \kappa\mu_0 M_s^2\boldsymbol{g}$, $\boldsymbol{F} = \kappa(\mu_0 M_s^2/\ell_{\mathrm{ex}})\boldsymbol{f}$, and $\boldsymbol{C} = \kappa\mu_0 M_s^2\mathbb{C}$ (all dimensionless). The dimensionless effective field, defined by $\boldsymbol{h}_{\mathrm{eff}}[\boldsymbol{u}, \boldsymbol{m}] = \boldsymbol{H}_{\mathrm{eff}}[\ell_{\mathrm{ex}}\boldsymbol{u}, M_s\boldsymbol{m}]/M_s$, satisfies the relation

$$\boldsymbol{h}_{\mathrm{eff}}[\boldsymbol{u}, \boldsymbol{m}] = -\frac{\delta\mathcal{E}'[\boldsymbol{u}, \boldsymbol{m}]}{\delta\boldsymbol{m}} = \boldsymbol{\Delta}'\boldsymbol{m} + 2\kappa[\mathbb{Z}^\top : \boldsymbol{\sigma}(\boldsymbol{u}, \boldsymbol{m})]\boldsymbol{m} + \boldsymbol{h}_{\mathrm{ext}}.$$

With all these definitions, we retrieve the coupled system

$$\partial_{t't'} \boldsymbol{u} = \boldsymbol{\nabla}' \cdot \boldsymbol{\sigma}(\boldsymbol{u}, \boldsymbol{m}) + \boldsymbol{f},$$

$$\partial_{t'} \boldsymbol{m} = -\boldsymbol{m} \times \boldsymbol{h}_{\text{eff}}[\boldsymbol{u}, \boldsymbol{m}] + \alpha\, \boldsymbol{m} \times \partial_{t'} \boldsymbol{m}.$$

Altogether, we thus obtain the dimensionless model problem discussed throughout this work. Note that, to simplify the notation, in Sections 2–6 we omit all 'primes' from the dimensionless quantities, we assume $\kappa = 1$, and we neglect the applied external field (unless otherwise mentioned).

Data availability

Data will be made available on request.

References

[1] C. Abert, G. Hrkac, M. Page, D. Praetorius, M. Ruggeri, D. Suess, Spin-polarized transport in ferromagnetic multilayers: an unconditionally convergent FEM integrator, Comput. Math. Appl. 68 (6) (2014) 639–654, https://doi.org/10.1016/j.camwa.2014.07.010.

[2] F. Alouges, A new finite element scheme for Landau–Lifchitz equations, Discrete Contin. Dyn. Syst., Ser. S 1 (2) (2008) 187–196, https://doi.org/10.3934/dcdss.2008.1.187.

[3] F. Alouges, P. Jaisson, Convergence of a finite element discretization for the Landau–Lifshitz equation in micromagnetism, Math. Models Methods Appl. Sci. 16 (2) (2006) 299–316, https://doi.org/10.1142/S0218202506001169.

[4] F. Alouges, A. Soyeur, On global weak solutions for Landau–Lifshitz equations: existence and nonuniqueness, Nonlinear Anal. 18 (11) (1992) 1071–1084, https://doi.org/10.1016/0362-546X(92)90196-L.

[5] C. Amrouche, P.G. Ciarlet, L. Gratie, S. Kesavan, On saint Venant's compatibility conditions and Poincaré's lemma, C. R. Acad. Sci., Sér. I 342 (11) (2006) 887–891, https://doi.org/10.1016/j.crma.2006.03.026.

[6] L. Baňas, A numerical method for the Landau–Lifshitz equation with magnetostriction, Math. Methods Appl. Sci. 28 (16) (2005) 1939–1954, https://doi.org/10.1002/mma.651.

[7] L. Baňas, Adaptive techniques for Landau–Lifshitz–Gilbert equation with magnetostriction, J. Comput. Appl. Math. 215 (2) (2008) 304–310, https://doi.org/10.1016/j.cam.2006.03.043.

[8] L. Baňas, M. Slodička, Space discretization for the Landau–Lifshitz–Gilbert equation with magnetostriction, Comput. Methods Appl. Mech. Eng. 194 (2–5) (2005) 467–477, https://doi.org/10.1016/j.cma.2004.06.021.

[9] L. Baňas, M. Slodička, Error estimates for Landau–Lifshitz–Gilbert equation with magnetostriction, Appl. Numer. Math. 56 (8) (2006) 1019–1039, https://doi.org/10.1016/j.apnum.2005.09.003.

[10] S. Bartels, Stability and convergence of finite-element approximation schemes for harmonic maps, SIAM J. Numer. Anal. 43 (1) (2005) 220–238, https://doi.org/10.1137/040606594.

[11] S. Bartels, Numerical Methods for Nonlinear Partial Differential Equations, Springer Series in Computational Mathematics, vol. 47, Springer, 2015.

[12] S. Bartels, Projection-free approximation of geometrically constrained partial differential equations, Math. Compet. 85 (299) (2016) 1033–1049, https://doi.org/10.1090/mcom/3008.

[13] S. Bartels, J. Ko, A. Prohl, Numerical analysis of an explicit approximation scheme for the Landau–Lifshitz–Gilbert equation, Math. Compet. 77 (262) (2008) 773–788, https://doi.org/10.1090/S0025-5718-07-02079-0.

[14] S. Bartels, A. Prohl, Convergence of an implicit finite element method for the Landau-Lifshitz-Gilbert equation, SIAM J. Numer. Anal. 44 (4) (2006) 1405–1419, https://doi.org/10.1137/050631070.

[15] L. Baňas, M. Page, D. Praetorius, J. Rochat, A decoupled and unconditionally convergent linear FEM integrator for the Landau-Lifshitz-Gilbert equation with magnetostriction, IMA J. Numer. Anal. 34 (4) (2014) 1361–1385, https://doi.org/10.1093/imanum/drt050.

[16] J. Bergh, J. Löfström, Interpolation Spaces: An Introduction, Grundlehren der Mathematischen Wissenschaften., vol. 223, Springer, 1976.

[17] B. Bergmair, T. Huber, F. Bruckner, C. Vogler, M. Fuger, D. Suess, Fully coupled, dynamic model of a magnetostrictive amorphous ribbon and its validation, J. Appl. Phys. 115 (2) (2014) 023905, https://doi.org/10.1063/1.4861735.

[18] J. Brandts, S. Korotov, M. Křížek, et al., Simplicial Partitions with Applications to the Finite Element Method, Springer Monographs in Mathematics, Springer, 2020.

[19] S.C. Brenner, L.R. Scott, The Mathematical Theory of Finite Element Methods, third edition, Texts in Applied Mathematics, vol. 15, Springer, New York, 2008.

[20] W.F. Brown, Magnetoelastic Interactions, Springer Tracts in Nat. Phil., vol. 9, Springer, Berlin, Heidelberg, 1966.

[21] F. Bruckner, M. Feischl, T. Führer, P. Goldenits, M. Page, D. Praetorius, M. Ruggeri, D. Suess, Multiscale modeling in micromagnetics: existence of solutions and numerical integration, Math. Models Methods Appl. Sci. 24 (13) (2014) 2627–2662, https://doi.org/10.1142/S0218202514500328.

[22] G. Carbou, M.A. Efendiev, P. Fabrie, Global weak solutions for the Landau–Lifshitz equation with magnetostriction, Math. Methods Appl. Sci. 34 (10) (2011) 1274–1288, https://doi.org/10.1002/mma.1440.

[23] M.-C. Ciornei, J. Rubí, J.-E. Wegrowe, Magnetization dynamics in the inertial regime: nutation predicted at short time scales, Phys. Rev. B 83 (2) (2011) 020410, https://doi.org/10.1103/PhysRevB.83.020410.

[24] G. Di Fratta, C.-M. Pfeiler, D. Praetorius, M. Ruggeri, B. Stiftner, Linear second order IMEX-type integrator for the (eddy current) Landau–Lifshitz–Gilbert equation, IMA J. Numer. Anal. 40 (4) (2020) 2802–2838, https://doi.org/10.1093/imanum/drz046.

[25] C. Dorn, S. Wulfinghoff, Computing magnetic noise with micro-magneto-mechanical simulations, IEEE Trans. Magn. 59 (2) (2023) 1–4, https://doi.org/10.1109/TMAG.2022.3212764.

[26] C. Dorn, S. Wulfinghoff, A magneto-mechanically coupled material model for magnetic sensor investigation, PAMM 22 (1) (2023) e202200008, https://doi.org/10.1002/pamm.202200008.

[27] L.C. Evans, Partial Differential Equations, second edition, Graduate Studies in Mathematics, vol. 19, American Mathematical Society, Providence, RI, 2010.

[28] S. Federico, G. Consolo, G. Valenti, Tensor representation of magnetostriction for all crystal classes, Math. Mech. Solids 24 (9) (2019) 2814–2843, https://doi.org/10.1177/1081286518810741.

[29] G. Hrkac, C.-M. Pfeiler, D. Praetorius, M. Ruggeri, A. Segatti, B. Stiftner, Convergent tangent plane integrators for the simulation of chiral magnetic skyrmion dynamics, Adv. Comput. Math. 45 (3) (2019) 1329–1368, https://doi.org/10.1007/s10444-019-09667-z.

[30] W. Hu, L. Zhang, L. Jin, F. Bai, Temperature dependent intrinsic Gilbert damping in magnetostrictive FeCoSiB thin film, AIP Adv. 13 (2) (2023), https://doi.org/10.1063/9.0000418.

[31] A. Hubert, R. Schäfer, Magnetic Domains: The Analysis of Magnetic Microstructures, Springer, Berlin, Heidelberg, 1998.

[32] R.D. James, M. Wuttig, Magnetostriction of martensite, Philos. Mag. A 77 (5) (1998) 1273–1299, https://doi.org/10.1080/01418619808214252.

[33] O. Kohmoto, K. Ohya, Mass densities of amorphous Co-rich FeCo-SiB alloys, J. Appl. Phys. 57 (2) (1985) 626–627, https://doi.org/10.1063/1.334752.

[34] J. Kraus, C.-M. Pfeiler, D. Praetorius, M. Ruggeri, B. Stiftner, Iterative solution and preconditioning for the tangent plane scheme in computational micromagnetics, J. Comput. Phys. 398 (2019) 108866, https://doi.org/10.1016/j.jcp.2019.108866.

[35] D. Lewis, N. Nigam, Geometric integration on spheres and some interesting applications, J. Comput. Appl. Math. 151 (1) (2003) 141–170, https://doi.org/10.1016/S0377-0427(02)00743-4.

[36] F.S. Mballa-Mballa, O. Hubert, S. He, S. Depeyre, P. Meilland, Micromagnetic modeling of magneto-mechanical behavior, IEEE Trans. Magn. 50 (4) (2014) 1–4, https://doi.org/10.1109/TMAG.2013.2288911.

[37] K. Neeraj, N. Awari, S. Kovalev, D. Polley, N.Z. Hagström, S.S. Arekapudi, A. Semisalova, K. Lenz, B. Green, J.-C. Deinert, I. Ilyakov, M. Chen, M. Bawatna, V. Scalera, M. d'Aquino, C. Serpico, O. Hellwig, J.-E. Wegrowe, M. Gensch, S. Bonetti, Inertial spin dynamics in ferromagnets, Nat. Phys. 17 (2021) 245–250, https://doi.org/10.1038/s41567-020-01040-y.

[38] P. Oswald, On a BPX-preconditioner for P1 elements, Computing 51 (2) (1993) 125–133, https://doi.org/10.1007/BF02243847.

[39] M. Pasquale, Mechanical sensors and actuators, Sens. Actuators A, Phys. 106 (1) (2003) 142–148, https://doi.org/10.1016/S0924-4247(03)00153-5.

[40] R.-C. Peng, J.J. Wang, J.-M. Hu, L.-Q. Chen, C.-W. Nan, Electric-field-driven magnetization reversal in square-shaped nanomagnet-based multiferroic heterostructure, Appl. Phys. Lett. 106 (14) (2015) 142901, https://doi.org/10.1063/1.4917228.

[41] A. Ramage, E.C. Gartland Jr., A preconditioned nullspace method for liquid crystal director modeling, SIAM J. Sci. Comput. 35 (1) (2013) B226–B247, https://doi.org/10.1137/120870219.

[42] A. Renuka Balakrishna, R.D. James, A solution to the permalloy problem – a micromagnetic analysis with magnetostriction, Appl. Phys. Lett. 118 (21) (2021) 212404, https://doi.org/10.1063/5.0051360.

[43] A. Renuka Balakrishna, R.D. James, A tool to predict coercivity in magnetic materials, Acta Mater. 208 (2021) 116697, https://doi.org/10.1016/j.actamat.2021.116697.

[44] M. Ruggeri, Numerical analysis of the Landau–Lifshitz–Gilbert equation with inertial effects, ESAIM: Math. Model. Numer. Anal. 56 (4) (2022) 1199–1222, https://doi.org/10.1051/m2an/2022043.

[45] J. Schöberl, Netgen/NGSolve, https://ngsolve.org.v6.2.2301, 2023.

[46] Y.C. Shu, M.P. Lin, K.C. Wu, Micromagnetic modeling of magnetostrictive materials under intrinsic stress, Mech. Mater. 36 (10) (2004) 975–997, https://doi.org/10.1016/j.mechmat.2003.04.004.

[47] H. Suhl, Theory of the magnetic damping constant, IEEE Trans. Magn. 34 (4) (1998) 1834–1838, https://doi.org/10.1109/20.706720.

[48] H. Suhl, Relaxation Processes in Micromagnetics, vol. 133, OUP, Oxford, 2007.

[49] V. Thomée, Galerkin Finite Element Methods for Parabolic Problems, second edition, Springer Series in Computational Mathematics, vol. 25, Springer, 2006.

[50] A. Visintin, On Landau–Lifshitz' equations for ferromagnetism, Jpn. J. Appl. Math. 2 (1) (1985) 69–84, https://doi.org/10.1007/BF03167039.

[51] J.-E. Wegrowe, M.-C. Ciornei, Magnetization dynamics, gyromagnetic relation, and inertial effects, Am. J. Phys. 80 (7) (2012) 607–611, https://doi.org/10.1119/1.4709188.